NTNU
Norwegian University of
Science and Technology

Ship hulls exposed to ice-induced loads and resistance

Stian Rørvik Johansen

Marine Technology
Submission date: June 2018
Supervisor: Bernt Johan Leira, IMT

Norwegian University of Science and Technology
Department of Marine Technology

Problem description

In this master thesis, the following subjects are presented:

1. A presentation of ice covered areas, with the main focus on the Arctic region.

2. Different types of sea ice and their physical and mechanical properties are described.

3. Ship-ice interactions

4. A presentation of KV Svalbard and its measurement systems.

5. A review of ice classifications for polar going ships, with an focus on the regulation for the Arctic region.

6. An introduction to finite element analysis, both linear and non-linear.

7. Empirical models for calculation of ice-induced resistance are presented and compared.

8. A parameter study for the empirical formulations

9. Resistance for KV Svalbard

10. A finite element analysis of a hull section using Abaqus, with a parameter study of the parameters involved.

NORWEGIAN UNIVERSITY OF SCIENCE AND TECHNOLOGY

Abstract

Institute of Marine Techonolgy
Department of Marine Techology

Master Thesis

Ship hulls exposed to ice-induced loads and resistance

by Stian Rørvik JOHANSEN

Marine activities in the Arctic have always been difficult. In recent year there have been a significant increase in activities in this region. This is a combined result of both global warming and a strong development in the design and the technology for ice-classified vessels. Arctic transportation routes, exploration of hydrocarbons and tourism are all exiting opportunities related this development.

This master thesis contains a theoretical study sea ice. In addition to a introduction to ice covered areas, both different types of sea ice and their mechanical and physical properties are presented.

In this master thesis, KV Svalbard will be used as a reference. This is a Norwegian coast guard vessel, specialized for operations in Arctic waters.

To operate in ice-infested waters, the right classifications are necessary. In these areas the vessels are exposed to conditions they would not experience in other regions, and special classifications for navigation in ice are therefore developed. This thesis contains a review of the classifications presented in DNV GL's "Ship for navigation in ice". Here, both Baltic, Arctic and Polar classes are described. Since the Arctic region has been in focus for this thesis, a particular emphasis has been placed on the Arctic rules by DNV GL and the Polar rules by IACS.

An introduction to finite element analysis is presented. Linear and non-linear analysis are described and compared. In the event of ship-ice interaction, large displacements and deformations may occur. Here, linear elastic theory may no longer be valid, and non-linear theory must be applied.

To estimate the ice resistance for a vessel, analytical formulations may be used. In this master thesis, three models are presented and compared. All of the formulations are meant to give an early estimation of resistance for ice and power requirements. By using the main parameters from Norwegian coast guard vessel KV Svalbard, the three models are compared to each other. In addition, a parameter study for the models was conducted to see how each of the parameters involved influenced the final results.

Using the measured power from KV Svalbard, the total resistance was calculated utilizing Newton's second law and conservation of energy. This resistance was then compared by calculating the ratios between estimated and empirical resistance. From the results one can see a big variation in the ratios. The most stable results were found for higher vessel speeds.

To see how ice loads affect local parts of a hull, a plate model was created and analyzed using Abaqus. As for the resistance, KV Svalbard was used as a reference. This vessel has ice classification Icebreaker Polar 10, and using this classification, values for stiffener dimensions, load height and ice pressure were obtained. In addition to the ice pressure from DNV GL, an empirical ice pressure was used in the analysis. Not all parameters involved in the analyzes were defined according to regulations, but chosen arbitrary. As a consequence, there are some uncertainty connected to the results. To see how modifying different values would affect the final response of the panel, a parameter study was conduced. The parameters modified were contact area, stiffener spacings and dimensions, and load angles. From the results, one can see a clear difference between the results for the different ice pressures. Using the DNV GL ice pressure, stresses above the yield strength of the material will occur, leading to plasticity.

Sammendrag

Marine aktiviteter i arktiske områder har alltid vanskelig. I nyere tid har det derimot vært en kraftig utvikling i disse aktivitetene. Dette er et resultat av både global oppvarming, og en sterk utvikling i design og teknologi for is-klassifiserte skip. Nye transportruter, utvinning av olje og gass, i tillegg til arktisk turisme er alle spennende muligheter relatert til denne utviklingen.

Denne masteroppgaven inneholder en teoretisk studie av sjø-is. I tillegg til en introduksjon til islagte områder, er både forskjellige typer sjø-is, samt dens fysiske og mekaniske egenskaper presentert.

I denne oppgaven vil KV Svalbard bli brukt som en referanse. Dette er et norsk kystvaktskip, som er spesialisert for operasjoner i arktiske områder.

For å kunne operere i islagte strøk er det viktig at skipene er riktig klassifisert. I disse områdene er skip utsatt for påkjenninger de ikke ville opplevd i andre farvann, og på grunn at dette er spesialiserte regler utviklet. Denne masteroppgaven presenterer klassifikasjonene fremstilt i DNV GL sin "Ships for ice navigation". Her er både baltiske, arktiske og polare klasser presentert. Siden det arktiske området har vært i fokus i denne oppgaven, har det blitt spesiell vekt på de arktiske reglene fra DNV GL og de polare reglene fra IACS.

En introduksjon til FEM-analyse er presentert. Både lineær og ikke-lineær analyse er forklart og sammenlignet. Ved kollisjoner mellom skip og is kan store deformasjoner komme som en konsekvens. Her vil lineær elastisk teori ikke lenger være gyldig, og ikke-lineær teori må bli brukt.

For å beregne is-motstanden for et skip kan analytiske modeller bli brukt. I denne masteroppgaven er tre slike modeller presentert og sammenlignet. Alle disse modellene har som formål å kunne gi et tidlig anslag av motstand og nødvendig motorkapasitet. Ved å bruke hovedparameter fra KV Svalbard har en sammenligning av de tre modellene blitt gjennomført. I tillegg har et parameterstudie blitt utført, der det er mulig å se hvordan de ulike parametrene påvirker det endelige resultatet.

Ved å bruke den målte motorkraften fra KV Svalbard, ble den totale motstanden funnet. Her ble Newtons andre lov og prinsippet om energibevaring brukt. Denne motstanden ble deretter sammenlignet med resultatene fra dei analytiske modellene. Fra de endelige resultatene kan man se en stor variasjon i den målte motstanden, med de mest stabile resultatene funnet for høyere hastigheter.

For å se hvordan is-laster påvirket lokale deler av skroget, ble en platemodell laget og analysert ved bruk av Abaqus. Også her ble KV Svalbard brukt som referanse. Dette

skipet har is-klassifisering "Icebreaker Polar 10", og ved å bruke denne klassifiseringen ble verdier for stiverdimensjoner, lasthøyde og istrykk funnet. I tillegg til istrykket fra DNV GL ble også et empirisk trykk brukt i denne analysen. Ikke alle parameter brukt ble valgt ut i fra klassifiseringen, men valgt mer tilfeldig. På grunn av dette er det noen usikkerheter knyttet til resultatene. For å se hvordan de ulike parameterne påvirket utfallet av analysene, har en parameterstudie blitt gjennomført. De undersøkte parameterne er kontaktareal, stiveravstand, stiverdimensjoner og lastvinkler. Fra resultatene kan man se en store forskjell mellom de to brukte istrykkene. Ved å bruke trykket fra DNV GL vil spenninger over flytegrensen oppstå, som leder til plastisitet i materialet.

Preface

This is an individual master thesis carried out during the spring semester of 2018 at the Norwegian University of Technology and Science, Department of Marine Technology. Professor Bernt J. Leira has been my supervisor for this master thesis. The scope of this thesis has been written by me and my supervisor, in cooperation.

The topic of this thesis has been interesting and rewarding. I have learned a lot about ice properties, resistance, loads and classifications. I have also learned a lot about finite element analysis using Abaqus and data processing in MATLAB.

I would like to thank my supervisor Bernt J. Leira for for helpful guidance during the semester. Through meetings and email correspondence he has provided vital feedback.

Stian Rørvik Johansen
Trondheim, 2018

Contents

Problem description iii

Abstract v

Sammendrag vii

Preface ix

List of Symbols xxi

1 Introduction 1
- 1.1 Objective . . . 2
- 1.2 Scope and Limitations . . . 2

2 Ice Covered Areas 3
- 2.1 Introduction . . . 3
- 2.2 Baltic region . . . 3
- 2.3 Arctic region . . . 3

3 Sea ice 7
- 3.1 Types of sea ice . . . 7
- 3.2 Physical and mechanical properties . . . 10
  - 3.2.1 Growth and microstructure . . . 10
  - 3.2.2 Ice thickness . . . 10
  - 3.2.3 Ice density, salinity and temperature . . . 12
  - 3.2.4 Ice porosity . . . 13
  - 3.2.5 Tensile strength . . . 13
  - 3.2.6 Flexural strength . . . 14
  - 3.2.7 Compressive strength . . . 16
  - 3.2.8 Young's modulus . . . 16
  - 3.2.9 Selected values in further calculations . . . 17

4 Ship-ice interaction 19
- 4.1 Load Patch . . . 20
- 4.2 Ice pressure . . . 21

5 KV Svalbard 23
- 5.1 Main parameters . . . 23
- 5.2 Ice load monitoring system . . . 24
- 5.3 H-V curve . . . 25

6 Classifications of ships **27**
6.1 Introduction . . . 27
6.2 Baltic region . . . 28
6.3 Arctic region . . . 29
6.3.1 Design Loads . . . 29
Vertical design force . . . 29
Total design force normal to the shell plating . . . 30
Compression loads midships . . . 30
Local ice pressure . . . 30
6.3.2 Local strength . . . 31
6.4 Polar class . . . 33
6.4.1 Design Ice Loads . . . 33
6.4.2 Local strength . . . 37
6.5 Comparison . . . 38

7 Finite Element Analysis **39**
7.1 Linear Finite Element Analysis . . . 39
7.2 Non-linear Finite Element Analysis . . . 42
7.2.1 Geometrical non-linear behavior . . . 42
7.2.2 Non-linear material behavior . . . 43
7.2.3 Non-linear boundaries . . . 43
7.2.4 Solution techniques . . . 44

8 Models for calculation of ice-induced resistance **45**
8.1 Introduction . . . 45
8.2 Lindqvist . . . 46
8.2.1 Crushing . . . 46
8.2.2 Breaking by bending . . . 47
8.2.3 Submersion . . . 48
8.2.4 Vessel speed . . . 48
8.2.5 Verification . . . 48
8.3 Riska . . . 49
8.4 Keinonen . . . 51
8.5 Comparing the models . . . 53
8.5.1 Plots . . . 53

9 Parameter study - Empirical models **61**
9.1 Length of bow . . . 62
9.2 Length of parallel mid-body . . . 62
9.3 Water line entrance angle . . . 63
9.4 Buttock angle . . . 64
9.5 Stem angle . . . 64
9.6 Flexural strength . . . 65
9.7 Hull-ice friction coefficient . . . 66
9.8 Temperature . . . 66
9.9 Parameter study conclusion . . . 67

10 Estimation of resistance from measurements **69**
10.1 The work-kinetic energy theorem . . . 69
10.2 Propeller thrust . . . 70
10.3 Resistance . . . 71

11 Data selection **73**
11.1 H-V curve for KV Svalbard . . . 74

12 Open water resistance **75**

13 Resistance KV Svalbard **77**
13.1 Introduction . . . 77
13.2 Ratios . . . 78
13.3 Higher quality data . . . 80
13.3.1 Lindqvist ratios . . . 80
13.3.2 Riska ratios . . . 81
13.3.3 Keinonen ratios . . . 81
13.4 Propeller efficiency . . . 82
13.5 Discussion . . . 83

14 Plate model and ice pressures **85**
14.1 Hull section . . . 85
14.1.1 Plate . . . 86
14.1.2 Stiffeners . . . 86
14.1.3 Material properties . . . 87
14.1.4 Model . . . 88
14.2 Ice pressures . . . 89
14.2.1 Ice pressure according to DNVGL . . . 89
14.2.2 Ice pressure from empirical calculations . . . 89
14.2.3 Selected values . . . 90

15 Ice Pressure Analysis **91**
15.1 Parameter study . . . 94
15.1.1 Load patch . . . 94
15.1.2 Stiffener dimensions . . . 97
15.1.3 Stiffener spacing . . . 99
15.1.4 Load angles . . . 102
15.1.5 Summary . . . 105
15.2 Discussion . . . 106

16 Conclusion **109**

17 Further work **111**
17.1 Resistance . . . 111
17.2 Finite element analysis . . . 111

A Empirical model comparison **115**

B Sensitivity plots - combinations of ice thickness and vessel speed **119**
B.1 Length of bow . . . 119
B.2 Length of parallel mid-body . . . 120
B.3 Water line entrance angle . . . 122
B.4 Buttock angle . . . 123
B.5 Stem angle . . . 124
B.6 Flexural strength . . . 126
B.7 Hull-ice friction coefficient . . . 127
B.8 Temperature . . . 128

C Ice resistance **131**
C.1 Additional figures . . . 131
C.2 Data from Suyuthi . . . 134
C.3 100% propeller efficiency using data from Skaar . . . 136
C.4 80% propeller efficiency using data from Skaar . . . 137
C.5 70% propeller efficiency using data from Skaar . . . 138

D Finite Element Analysis **139**
D.1 Original analysis . . . 139
D.2 Load patch area . . . 141
D.3 Stiffener dimensions . . . 143
D.4 Stiffener spacing . . . 144

List of Figures

2.1 Different definitions of the Arctic area (AMAP 1997). 4
2.2 Arctic sea ice extent (Portal 2017) 5
2.3 The Northwest Passage and the Northern Sea Route (AMAP 2011) . . . 5

3.1 Organizing of ice based on distance to shore (Riska 2011) 8
3.2 Ice thickness profile (Riska 2017) 12
3.3 Density vs temperature for different salinities (Timco and Weeks 2010). . 13
3.4 Flexural strength relative to brine volume (Timco and Weeks 2010) . . . 15
3.5 Flexural strength 15
3.6 E-modulus relative to brine volume 17

4.1 Forces present in interactions between ship and ice (Riska 2017) 19
4.2 Load patches for local ice pressure (Riska 2017) 20
4.3 Load height (Riska 2017) 20
4.4 Forces acting during ship-ice interaction (Riska 2017) 21

5.1 Picture of KV Svalbard (ACCESS 2012) 23
5.2 Measured frames at KV Svalbard (B. Leira et al. 2009) 24

6.1 Angels needed to determine β from DNVGL 2016 32
6.2 Hull angles (DNVGL 2016) 34

7.1 Linear relation between stress and strain (Solidworks 2013) 40
7.2 Non-linear relation between stress and strain (Moan 2003) 43
7.3 Typical non-linear behavior due to boundaries (Moan 2003) 44

8.1 Ship hull angles (Riska 2011) 45
8.2 Bending by breaking (Lindqvist 1989) 47
8.3 Plot of resistance from Lindqvist model 54
8.4 Plot of resistance from Riska model 55
8.5 Plot of resistance from Keinonen model 56
8.6 Riska vs Lindqvist vs Keinonen for ice thickness of 0.2 meter 57
8.7 Riska vs Lindqvist vs Keinonen for ice thickness of 1.6 meter 57
8.8 Riska vs Lindqvist vs Keinonen for vessel speed 0.4 m/s 58
8.9 Riska vs Lindqvist vs Keinonen for vessel speed 3 m/s 58
8.10 Riska vs Lindqvist vs Keinonen for vessel speed 1.4 m/s - New parameters 59
8.11 Riska vs Lindqvist vs Keinonen for ice thickness 0.8 m - New parameters 60

9.1 Sensitivity when changing the length of bow 62
9.2 Sensitivity when changing the length of parallel mid-body 63
9.3 Sensitivity when changing the water line entrance angle 63

9.4 Sensitivity when changing the buttock angle . . . 64
9.5 Sensitivity when changing the stem angle . . . 65
9.6 Sensitivity when changing the flexural strength . . . 65
9.7 Sensitivity when changing the friction coefficient . . . 66
9.8 Sensitivity when changing the temperature . . . 66

10.1 For a specific speed, total resistance experienced by the ship is balanced by thrust force (Suyuthi, B. J. Leira, and Riska 2011) . . . 70

11.1 Net thurst of KV Svalbard and resistance for different ice thicknesses . . . 74
11.2 H-V curve for KV Svalbard . . . 74

12.1 Open water resistance as a function of speed (Skår 2011) . . . 75

13.1 Ratios between measured and Lindqvist for varying thickness . . . 78
13.2 Ratios between measured and Riska for varying ice thickness . . . 79
13.3 Ratios between measured and Keinonen for varying ice thickness . . . 79
13.4 Varying vessel speed . . . 80
13.5 Varying ice thickness . . . 80
13.6 Varying vessel speed . . . 81
13.7 Varying ice thickness . . . 81
13.8 Varying vessel speed . . . 81
13.9 Varying ice thickness . . . 81

14.1 Plate model used in analysis . . . 88

15.1 Displacement with ice pressure according to DNVGL . . . 91
15.2 Von Mises stresses with ice pressure according to DNVGL . . . 92
15.3 Displacement with ice pressure according to empiric calculations . . . 92
15.4 Von Mises stresses with ice pressure according to empiric calculations . . . 93
15.5 Displacement for a contact area of 0.32 m^2 . . . 94
15.6 Stresses for a contact area of 0.32 m^2 . . . 95
15.7 Displacement for a contact area of 0.64 m^2 . . . 95
15.8 Stresses for a contact area of 0.64 m^2 . . . 96
15.9 Displacements without flanges . . . 97
15.10 Stresses without flanges . . . 98
15.11 Displacement for a stiffener spacing of 0.2 m . . . 99
15.12 Stresses for a stiffener spacing of 0.2 m . . . 100
15.13 Displacement for a stiffener spacing of 0.6 m . . . 100
15.14 Stresses for a stiffener spacing of 0.6 m . . . 101
15.15 Displacement for load angles of 45 degrees . . . 103
15.16 Stresses for load angles of 45 degrees . . . 103
15.17 Displacement for load angles of 75 degrees . . . 104
15.18 Stresses for load angles of 75 degrees . . . 104

C.1 Lindqvist vs measured resistance for varying vessel speed . . . 131
C.2 Riska vs measured resistance for varying vessel speed . . . 132
C.3 Keinonen vs measured resistance for varying vessel speed . . . 132
C.4 Varying vessel speed . . . 133

C.5 Varying ice thickness . . . 133
C.6 Varying vessel speed . . . 133
C.7 Varying ice thickness . . . 133
C.8 Varying vessel speed . . . 133
C.9 Varying ice thickness . . . 133
C.10 default . . . 134
C.11 default . . . 135
C.12 default . . . 135
C.13 Varying vessel speed . . . 136
C.14 Varying ice thickness . . . 136
C.15 Varying vessel speed . . . 136
C.16 Varying ice thickness . . . 136
C.17 Varying vessel speed . . . 136
C.18 Varying ice thickness . . . 136
C.19 Varying vessel speed . . . 137
C.20 Varying ice thickness . . . 137
C.21 Varying vessel speed . . . 137
C.22 Varying ice thickness . . . 137
C.23 Varying vessel speed . . . 137
C.24 Varying ice thickness . . . 137
C.25 Varying vessel speed . . . 138
C.26 Varying ice thickness . . . 138
C.27 Varying vessel speed . . . 138
C.28 Varying ice thickness . . . 138
C.29 Varying vessel speed . . . 138
C.30 Varying ice thickness . . . 138

D.1 Stresses in x-direction with ice pressure according to DNV GL regulations 139
D.2 Stresses in z-direction with ice pressure according to DNV GL regulations 140
D.3 Stresses in x-direction with ice pressure according to empiric calculations 140
D.4 Stresses in z-direction with ice pressure according to empiric calculations 141
D.5 Displacement for a contact area of 0.32 m^2 . . . 141
D.6 Stresses for a contact area of 0.32 m^2 . . . 142
D.7 Displacement for a contact area of 0.64 m^2 . . . 142
D.8 Stresses for a contact area of 0.64 m^2 . . . 143
D.9 Displacements without flanges . . . 143
D.10 Stresses without flanges . . . 144
D.11 Displacement for a stiffener spacing of 0.2 m . . . 144
D.12 Stresses for a stiffener spacing of 0.2 m . . . 145
D.13 Displacement for a stiffener spacing of 0.6 m . . . 145
D.14 Stresses for a stiffener spacing of 0.6 m . . . 146

List of Tables

3.1 Types of sea ice organized by age . . . 7
3.2 Forms of sea ice . . . 8
3.3 Selected input parameters for further calculations . . . 17

5.1 Main parameters for KV Svalbard (Thorsen 2012) . . . 24
5.2 Parameters for H-V curve for KV Svalbard (Teien 2014) . . . 25

6.1 DNV GL ice classes and the equivalent Finnish-Swedish ice classes and the description of these classes . . . 28
6.2 DNV GL ice classes and the corresponding heights . . . 28
6.3 Vessels in Arctic waters . . . 29
6.4 Types of sea ice organized by age . . . 33
6.5 Parameters for glancing load . . . 34

8.1 Range of accuracy . . . 52
8.2 Parameters from Riska . . . 59

9.1 Comparison of involved parameters . . . 61
9.2 A summary of resistance changes when modifying parameters . . . 67

11.1 Variables of interest and max values for CV . . . 73

13.1 Mean ratio for different propeller efficiencies . . . 82
13.2 Standard deviations for different mean ratios . . . 82
13.3 Mean ratio for different propeller efficiencies using higher quality data . 82
13.4 Standard deviation for different mean ratios using higher quality data . 83

14.1 Plate field dimensions . . . 86
14.2 Stiffener dimensions . . . 87
14.3 Material properties . . . 87
14.4 Stress/strain from CAE 2013 . . . 87
14.5 Values used to find ice pressure from empirical calculations . . . 90
14.6 Values used to find ice pressure from empirical calculations . . . 90

15.1 Stiffener parameters when removing the flange . . . 97
15.2 Stiffener parameters for a stiffener spacing of 0.2 m . . . 99
15.3 New ice pressures and minimum section modulus . . . 102
15.4 New stiffener dimensions . . . 102
15.5 Displacements and Von Mises stresses found in the parameter study . . 105
15.6 Comparing new results versus original results . . . 105

List of Symbols

Symbol	Description	Unit
A_c	Load patch area	m^2
α	Water line entrance angle	deg
B	Breadth	m
β	Angle of web with shell plating	deg
β'	Normal frame angle	deg
β_n	Frame angle	deg
C	Ice concentration	
C	Constant dependent on horizontal boundary geometry of ice floe	
δ	The difference in density between ice and water	t/kg^3
E	Young's modulus	MPa
ϵ_p	Residual plastic strain	
F_{B}	Correction factor for design contact area	
F_{v}	Crushing force	kN
F_μ	Frictional force	kN
$F_{\mathrm{resistance}}$	Resistance force	kN
g	Gravitational constant	m/s^2
γ	Buttock angle	deg
h	Ice thickness	m
h_{eq}	Equivalent ice thickness	m

H_{R}	Average ridge thickness	m
k	Thermal conductivity	W/m*K
t_{freeze}	Total freezing time	t
l	Span of stiffeners	m
L	Length	m
L_{wl}	Length of water line	m
L_{par}	Length of parallel sides	m
L_{bow}	Length of bow section	m
μ	Friction coefficient	
m	mass of the ship	ton
p_c	Ice pressure	MPa
ϕ	Stem angle	deg
ψ	Angle between the normal of the surface and a vertical vector	deg
$\rho_{\mathrm{saltwater}}$	Density of salt water	t/kg^3
ρ_{ice}	Density of ice	t/kg^3
R_{v}	Resistance force in crushing	kN
R_{b}	Resistance force from breaking by bending	kN
R_{s}	Resistance from submersion	kN
$R_{\mathrm{Lindqvist}}$	Total ice resistance from the Lindqvist model	kN
R_{ice}	Ice resistance	kN
$R_{\mathrm{openwater}}$	Open water resistance	kN
R_{Riska}	Total ice resistance from the Riska model	kN
σ_{b}	Bending strength of ice	MPa

σ_{f}	Flexural strength of ice	MPa
σ_{ice}	Nominal strength of ice	MPa
σ_{y}	Yield stress level	MPa
S_i	Average salinity	ppt
s	Stiffener spacing	m
t	Plate thickness	m
T	Fraught	m
V	Vessel speed	m/s
V_{RAM}	Design speed when ramming may occur	m/s
v_{T}	Total porosity	
w_k	Section modulus correction factor	
W_{net}	Net work done by the forces	J
W_{thrust}	Propeller thrust	J
$W_{resistance}$	Total work done by resistance	J
ν	Poisson's ratio	
Z	Section modulus	cm^3

Chapter 1

Introduction

Marine activities in the Arctic have always been difficult, with the presence of sea ice as the main problem. Designing ships capable of operation is these geographical areas are challenging, and as a consequence, this have lead to limited activity in these areas. In recent years there have been a significant increase in activities. This is a combined result of both global warming and a strong development in the design and the technology for ice-classified vessels. This makes it possible to operate in larger parts, longer periods of the year.

The new opportunities in the Arctic region opens a lot of doors. Using the Arctic as a route of transportation in longer periods of the year, without assistance from icebreakers, can strongly decrease transportation times and therefore also the costs. Another opportunity is the possibility of exploring hydrocarbons and the other natural resources available in these regions. In addition to this, there is a huge potential in Arctic tourism. With the global warming and cruise ships increasing capability to travel in ice and more challenging weather, it is now feasible to have tourism in areas where this never have been possible.

To operate safe in ice-infested waters, vessels need to be able to face rough ice conditions and extreme weather. As a consequence of this, there have over the years been developed several sets of classification regarding navigation in ice. As the experience grows and the knowledge on ice properties gets better, it is possible to optimize these classifications. This will strongly increase safety, and the number of accidents will decrease.

Calculation of ice-induced resistance have proven to be difficult, and a lot of research have been carried out on this subject. In the design phase, the best way to calculate this is by model tests. This is a good way to estimate the resistance, but tends to be both expensive and time demanding. Therefore, the calculation of ice-induced resistance is mainly based on analytical models.

In addition to dealing with increased resistance due to ice, the vessel must also be able to withstand ice-induced loads. These loads will occur throughout operations in ice, and will constantly vary in terms of force and form. It is therefore important to ensure that vessels are properly classified, so that the hulls are capable of dealing with the forces.

1.1 Objective

In this master thesis, the following topics will be presented:

- Presentation of ice covered areas.
- Review of different types of sea ice, and the mechanical and physical properties.
- An introduction to ship-ice interaction.
- A presentation of KV Svalbard.
- A review of rules and classifications when designing a vessel to operate in ice-infested waters.
- An introduction to finite element analysis. Both linear and non-linear theory will be presented.
- Presentation of three models for calculation of ice resistance, Lindqvist, Riska and Keinonen. These models will also be compared.
- A parameter study of the presented ice resistance models.
- Full scale resistance from KV Svalbard will be calculated from measurements. This will be compared with the results from the empirical models.
- A finite element analysis of a panel in the bow area of KV Svalbard. A parameter study will be conducted to see how different parameters affected the response.

1.2 Scope and Limitations

The main focus in this master thesis will be on KV Svalbard and the ice conditions this ship is exposed to. This Norwegian coast guard vessel is operating in the Barents Sea, which is a part of the Arctic Ocean. Thus, the main emphasis in the classification chapter will be rules regarding vessels operating in Arctic waters.

For the resistance, the scope is to see how the empirical ice resistance compared to the resistance from the measurements of KV Svalbard.

For the finite element analysis, the main objective is to determine how the different parameters involved influence the response for the chosen panel. Therefore, the focus will be on local forces. As the ship moves in ice, broken ice need to be displaced, and more interactions between the ship and broken ice will occur. In this thesis, only the first interaction will be investigated.

Chapter 2

Ice Covered Areas

2.1 Introduction

For ships in ice-infested waters, there are two main regions in mind; the Baltic and the Arctic. These are regions which are covered in ice periods of the year. In this master thesis the Arctic ice conditions will be in focus, but to clearly see the differences, some information on the Baltic conditions is also presented.

When designing a vessel, it is important to determined which regions the vessel will operate. From area to area there are big variations in ice thickness and strength. It is therefore essential to know the conditions where the vessel is going to operate to ensure the optimal ice-strengthening.

2.2 Baltic region

The Baltic area is the sea enclosed by Sweden, Finland and the Baltic countries. This region has limited exchange of water with the North Sea. As a consequence of this, the salinity in the Baltic is less than in other oceans. The salinity in the northern Baltic is as low as 4 ppt (Riska 1997). The Baltic is also relatively shallow, with an average depth of 56 m, and the deepest point at 460 m. Due to this, the thermal inertia of the Baltic is relatively small, and the formation of ice is closely dependent on the changes is air temperature. Most of the ice is therefore only seasonal, which prevents the ice in reaching the same thicknesses as in the Arctic.

2.3 Arctic region

There are many ways to define the Arctic areas, as shown in Figure 2.1 (AMAP 1997). These include:

- The area north of the Arctic Circle
- The area where the mean temperature in July is equal of less than 10^{o}C
- The area north of the tree line

How the ice strength varies from the two regions can be hard to determine. As opposed to the Baltic area, the Arctic area contains a lot of multi-year ice. This ice is a lot thicker and stronger than first-year ice. In multi-year ice the thickness can be in the range from 3 to 4 meters, while for first-year ice this in normally below 2 meters. In the Arctic, the salinity is also a lot higher than in the Baltic. Here, the salinity is approximately 35 ppt. Multi-year ice contains significantly less brine, leading to lower salinity in this ice than in other parts of Arctic waters. How the salinity affects the density and strength of the ice is described in Section 3.2.

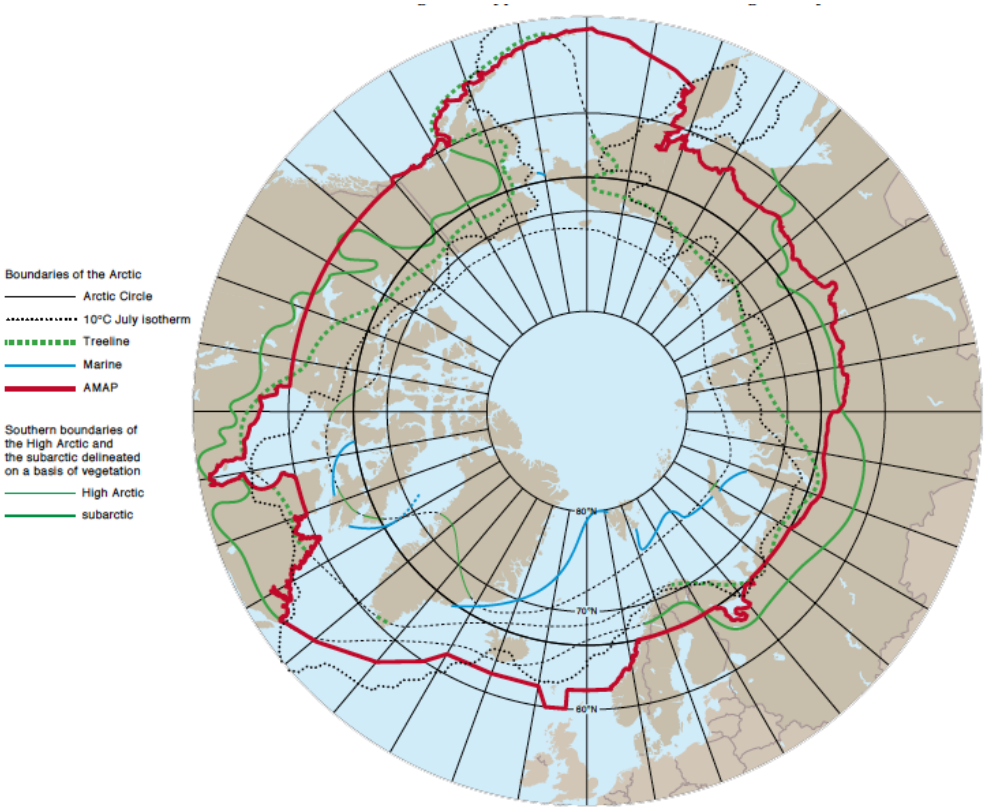

FIGURE 2.1: Different definitions of the Arctic area (AMAP 1997).

The Arctic region contains a significant part of the worlds oil and gas resources. A lot of these resources have jet to be explored, due to the high concentration of multi-year ice. As a consequence of global warming, the ice concentration is decreasing, which makes it possible to explore fields previously unavailable. As shown in Figure 2.2, the Arctic sea ice extent are significantly lower in the recent years compared to the mean value between 1981-2000 (Portal 2017). This decrease in expected to continuing in the years to come.

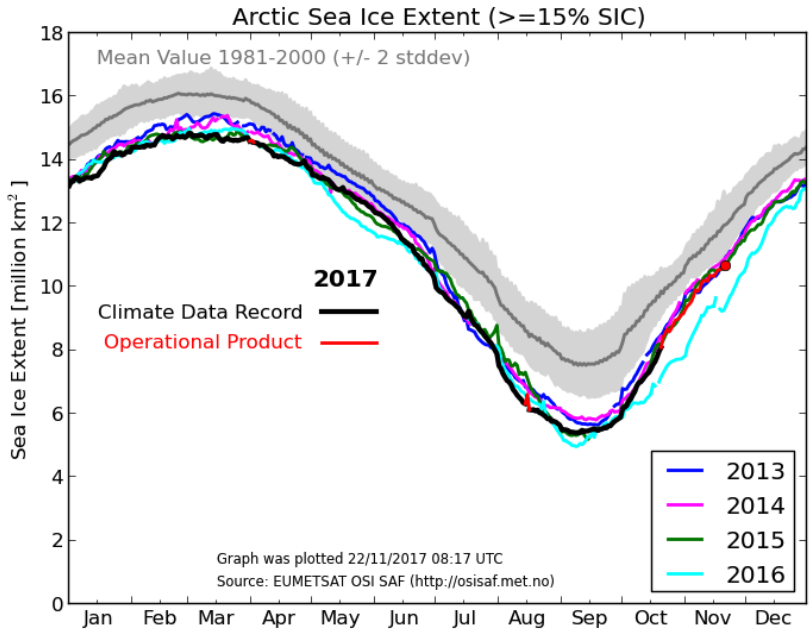

FIGURE 2.2: Arctic sea ice extent (Portal 2017)

Another opportunity opened by global warming is the possibility of using the Arctic as a route of transportation. As the sea ice melts, the Arctic Ocean is open for shipping for longer periods of the year. Earlier, operation in these areas have required escort from icebreaker throughout the year. This is expensive and have therefore in most cases not been an alternative. But as a consequence of this warming, in addition to the improved ice strengthening of vessels, ships can now operated unassisted periods of the year.

Two of these alternative routes, the Northwest Passage and the Northern Sea Route, are shown in Figure 2.3 (AMAP 2011). The Northern Sea Route is 40% shorter than the current routes between Europe and the Pacific. Being able to use these route will reduce the transportation costs in addition to a decrease in global emissions.

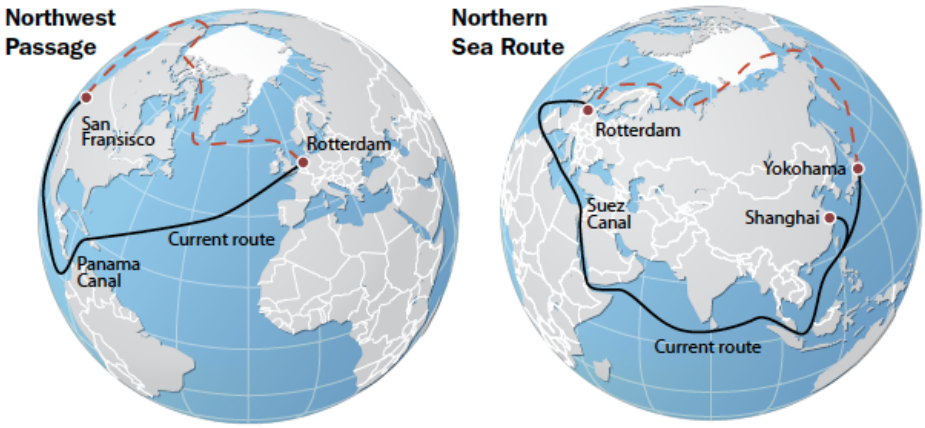

FIGURE 2.3: The Northwest Passage and the Northern Sea Route (AMAP 2011)

With all of these possibilities, the surrounding countries try to claim as big parts of the Arctic areas as possible. With huge oil and gas resources jet to be explored, there this a big opportunity for the surrounding countries to utilize on this. With an increase in traffic in these areas, there will also be an increase in activity at ports along the route. This could potentially be a big source of income for these ports.

Chapter 3

Sea ice

3.1 Types of sea ice

To properly describe sea ice, different names for features, forms and types are used. Here, the most common of these definitions are briefly mentioned and described. These definitions will be used in later parts of this thesis.

As the temperature in the water decreases, ice is formed. There are many types of sea ice, and in order to describe them they need to be organized. Sea ice can be organized by age (Fequet 2005), as shown in Table 3.1.

Type of sea ice	Description
NEW ICE	Recently formed ice, where the ice crystals are only weakly frozen together.
NILAS	Thin and elastic ice, which is easily bent under pressure. Can be up to 10 cm thick.
YOUNG ICE	Transition stage between nilas and first-year ice. The thickness is in the region from 10 to 30 cm.
FIRST-YEAR ICE	Ice with maximum one year/winter of growth. Thickness greater than 30 cm.
SECOND-YEAR ICE	Ice that have survived one summer. Thicker than first-year ice, and stands higher out of the water.
MULTI-YEAR ICE	Ice that have survived multiple summers. Smooth surface and almost free of salt.

TABLE 3.1: Types of sea ice organized by age

When organizing according to age, the ice is mainly divided into ice that have survived a melting and ice that have not been subjected to one. This is due to the differences in salinity and the mechanical wear and tear of the sea ice. Thus, there is a major difference from first-year to second-year ice.

Another way of organizing ice is based on the distance from shore. This is shown in Figure 3.3. Here, different zones are created due to the motion of the ice. Close to shore is the fast ice zone. In the fast ice zone the ice is mostly connected to the sea floor and the ice remains fast and unbroken. In steep coastlines without islands, this zone may be neglected. In the pack ice zone the ice is broken and mainly free floating. This is a term used for any area of the ice, other than fast ice (Riska 2011).

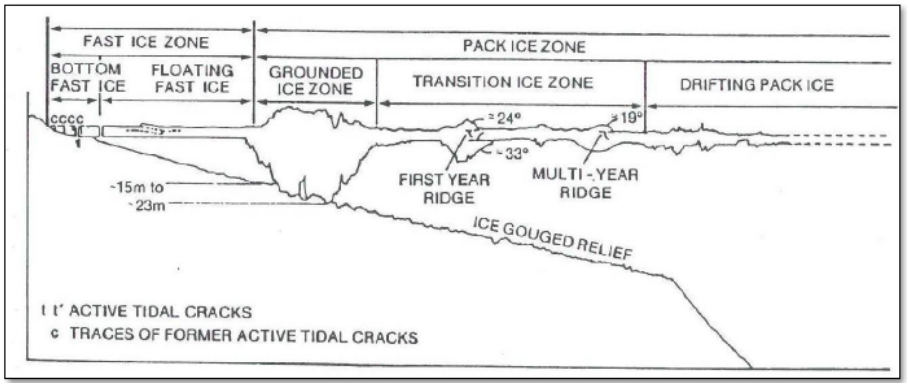

FIGURE 3.1: Organizing of ice based on distance to shore (Riska 2011)

To properly describe ice, it is also important to distinguish between different forms and features. The ice is changing constantly, and to understand its behavior, it needs to be organized. The most usual forms and features are presented in Table 3.2 (Fequet 2005):

Features of sea ice	**Description**
LEVEL ICE	Sea ice with no deformations.
DEFORMED ICE	General term for ice squeezed together.
PANCAKE ICE	Circular pieces of ice with diameter from 30 cm to 3 m, and a thickness up to 10 cm. Raised rims due to waves and pieces striking against each other.
FRAZIL ICE	Collection of ice crystals in the water.
SLUSH	Snow mixed with water and/or ice surface.
GREASE ICE	A later stage of freezing than frazil ice.
ICE CAKE	Flat piece of ice, with less than 20 m across.
ICE FLOE	Flat piece of ice, with more than 20 m across.
ICE BRECCIA	Pieces with different stages of development frozen together.
BATTURE FLOES	Large, thick, uneven and discoloured ice floes.
BRASH ICE	Fragmented ice.
GROUNDED ICE	Floating ice which is aground in shallow water.
ICE RIDGES	A wall of broken ice driven together by pressure.
HUMMOCKS	Broken ice pressured together and forced upwards. Always the last ice to melt.

TABLE 3.2: Forms of sea ice

Here, the two main categories when describing sea ice is whether it is deformed or undeformed. Undeformed ice, often called level ice has no mechanical deformation and consists only of one layer. Deformed ice are typically deformed by environmental factors, and can often be divided into rafted ice and ice ridges (Tuhkuri 2014). Rafted ice can be defined as one ice sheet ice overrides another. This process can happen multiple times which lead to several layers. Ice ridges can be defined as in Table 3.2; a wall of broken ice driven together by pressure.

In addition to the forms and features, the concentration of the sea ice will also be important. This value tells how much of the total sea water are that are covered with ice. The concentration, C, is given as:

$$C = \frac{A_{ice}}{A_{tot}} \tag{3.1}$$

Where,

- A_{ice} is the part of the area covered with ice
- A_{tot} is the total area

3.2 Physical and mechanical properties

To calculate the ice-induced resistance, and from that design the vessels optimally, the different properties of the sea ice need to be known. This is important both in terms of safety and economics. The properties of sea ice are depending on environmental factors. With these factors varying, designing vessels for ice-infested regions are therefore challenging. Most of the information in this section is found from Timco and Weeks 2010 and Riska 2017.

3.2.1 Growth and microstructure

Sea ice is a material which is composed of solid ice, brine and gas, depending on the temperature. As a consequence of varying environmental conditions, several different grain structures are possible, with granular, columnar and discontinuous columnar as the most common.

As the sea water freezes, the ice tries to reject the salts. However, the salts are not removed completely, and brine pockets are formed within the ice sheet. Sea water typically contains in the region of 32 to 35 ppt salt, while first-year sea ice has an average salinity of 4 to 6 ppt. During the summer months some of the ice sheets melt and brine pockets are released. Therefore, multi-year ice usually has a low salinity compared to first-year ice, and the properties of the multi-year ice are closer to those of freshwater ice than they are to first-year ice. Because of this multi-year sea ice is stronger than first-year sea ice.

Multi-year ice has a quite varying and chaotic grain structure, which is a result of both thermal growth and mechanical deformation. It is also frequently isotropic, in contrast to first-year sea ice that sometimes can be highly anisotropic.

3.2.2 Ice thickness

Ice thickness is one of the most important parameters in regards to engineering. The thickness will directly influence the resistance force from the ice and how the ice will fail. The thickness is also directly related to the speed ships can go in ice-covered regions.

For new ice, the thickness are strongly dependent on the following parameters:

- Air temperature
- Snow type
- Freezing time
- Wind speed

The dependency of these parameters are the reason why ice in the Arctic is always thicker than other region, mainly due to the low air temperature and the length of the

cold season (freezing time). To estimate the thickness of new ice, the Stefan equation can be used:

$$h_i = \sqrt{\frac{2k_i}{\rho_{ice}L} * (T_b - T_a)t} \tag{3.2}$$

Where;

- h_i = ice thickness
- k = thermal conductivity
- ρ_{ice} = ice density
- L = latent heat of fusion of ice
- T_b = temperature at bottom
- T_a = temperature at top
- t = freezing time

This equation can only be used for first-year ice, and tends to overpredict the thickness of the ice, since it do not take into account important parameters such as the effect of snow cover, wind speed and the ocean heat flux. It is therefore normal to multiply with an empirical factor to compensate for this simplification.

Older ice can be very thick. This thickness is a combination of thermal growth and consolidation of pressure-ridges. However, there have been a significant decrease in ice thickness in the Arctic region in recent years. For older ice there have been considerable debate regarding the thickness, and there are no simple formulas for calculation of this value.

In design, it is common to use an equivalent ice thickness, h_{eq}, which is higher than the ice thickness. In an area, the original ice thickness profile may look as shown in Figure 3.2. To take the ridges into account, the equation for equivalent ice thickness (Riska 2017) may be used:

$$h_{eq} = Ch_i + \mu k H_R^2 \tag{3.3}$$

Where;

- C = Ice concentration
- μ = Average ridge density (ridges per kilometer)
- k = 3.2
- H_R = Average ridge thickness

FIGURE 3.2: Ice thickness profile (Riska 2017)

3.2.3 Ice density, salinity and temperature

Another important ice parameter is the density. From the density one can find the weight of the ice. The weight will strongly influence the impact ice will have on a vessel. The density is also important with regards to the buoyancy force. This buoyancy is dependent on the difference in density between the ice and the water, and small variations can make a large impact on this force.

The salinity of ice is one of the most important parameters for the density. The ice salinity is expressed as the ratio between weight of salt and the mass of the ice, described as ppt (parts per thousand). The proposed average salinity of an first-year ice sheet can be estimated using the following equation:

$$S_i = 4.606 + \frac{91.603}{h_i} \tag{3.4}$$

Where,

- S_i is the average salinity [ppt]
- h_i is the ice thickness [cm]

The importance of salinity relative to the density is shown in Figure 3.3. From this figure one can also see that for higher salinity, the density is more dependent on the temperature than for lower ones. For higher salinity, there will be more brine in the ice, which is more sensitive to changes in the temperature. Temperature is an essential property for ice. The freezing point of seawater with a salinity of 35 ppt is -1.8° Celsius (NSIDC 2017).

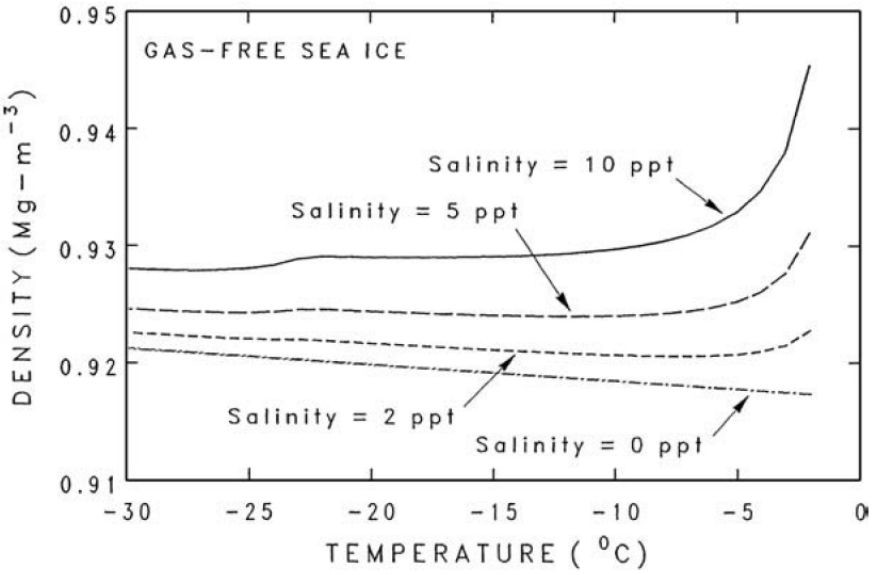

FIGURE 3.3: Density vs temperature for different salinities (Timco and Weeks 2010).

3.2.4 Ice porosity

In some cases it can be useful to know the amount of gas in the ice. For instance, this will be significant when brine drainage has occurred. The total porosity can be expressed as:

$$v_T = v_b + v_a \tag{3.5}$$

Where;

- v_T = total porosity
- v_b = relative brine volume
- v_a = relative air volume

The relative brine volume can be calculated as a function of salinity and temperature of the ice. The following equation is valid for ice temperatures in the range of -0.5°C to -22.9°C.

$$v_b = S_i\left(\frac{49.185}{|T|} + 0.532\right) \tag{3.6}$$

3.2.5 Tensile strength

When interactions between ice and ships occur, the tensile strength of the ice defines the maximum tensile strength the ice can handle before breaking. The most influential parameter for the tensile strength is the temperature. As the temperature increases, the tensile strength decreases. Measuring the tensile strength has proven to be both

difficult and time consuming. Hence, not many tests have been performed to find the true tensile strength of sea ice. However, it is found that this strength lays in the region of 0.2 to 2 MPa.

3.2.6 Flexural strength

Flexural strength (bending strength) is measured from how the ice can resist bending before failing. For a ship going in ice-covered waters, the ice will normally fail in bending. The ship slides on top of the ice to break by bending instead of by crushing. Because of this, flexural strength is essential, even though this strength is not a basic material property. A lot of measurements have been carried out to find the flexural strength of sea ice. When measuring this strength, there are two different methods used: The cantilever beam test and the simple beam test. Both tests are based on simple elastic beam theory. Information on these test can be found in Timco and Weeks 2010.

A large number of parameters will affect the flexural strength of the ice. The most important parameter is the brine volume. The flexural strength for first-year ice as a function of brine volume are shown in Equation 3.7. This assumption is based on that as the porosity of the ice increases, the flexural strength decreases. It is important to note that this relationship in only valid for growing ice. Warm and decaying ice has an open structure, leading to high porosity despite low salinity.

$$\sigma_b = 1.76e^{-5.88\sqrt{v_b}} \tag{3.7}$$

Where;

- σ_b = flexural strength of ice
- v_b = brine volume fraction

Data from a large number of investigations were collected and plotted as shown in Figure 3.4. Since the flexural strength is dependent on the salinity, the strength will be higher for fresh water ice than for sea water ice. From this it is possible to assume that the flexural strength is higher for old ice compared to first-year ice, due to the lower salinity. As shown, the flexural strength is approximately 1.75 MPa for fresh water ice, and decreases with larger brine volume.

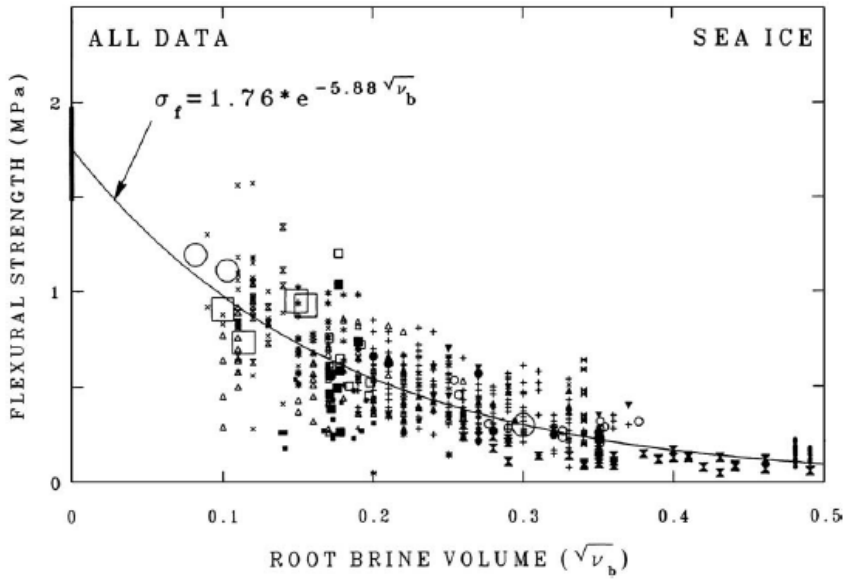

FIGURE 3.4: Flexural strength relative to brine volume (Timco and Weeks 2010)

By using Equation 3.7, the flexural strength can be plotted as a function of ice temperature and thickness. This plot is presented in Figure 3.5, and will be used to determine the flexural strength used in this master thesis.

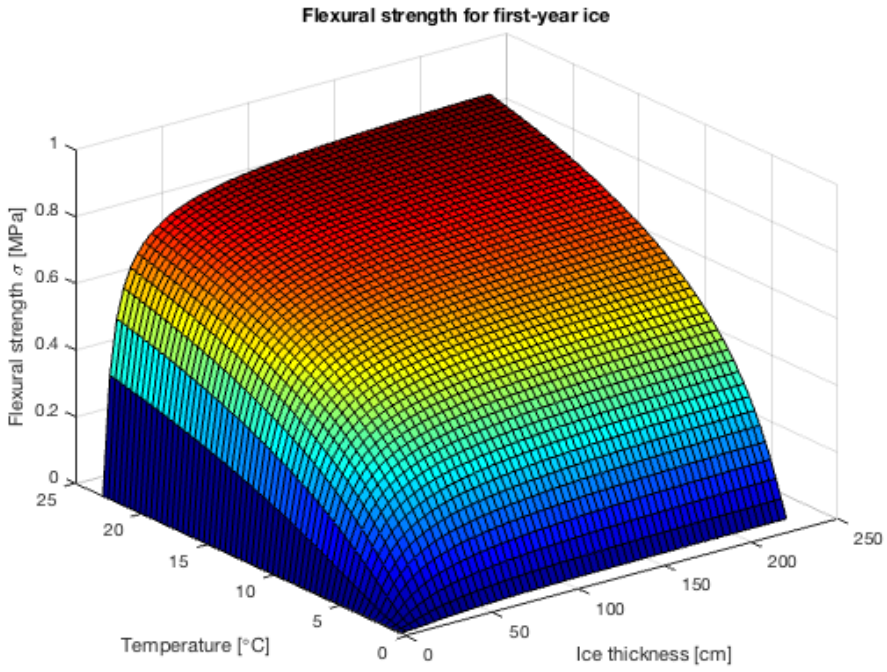

FIGURE 3.5: Flexural strength

3.2.7 Compressive strength

Another important parameter is the compressive strength. In collisions between ship and ice, the ice often fails due to compression. Failure can also occur during formation of large compression pressure ridges. Since sea ice often fails due to compression, there have been extensive studies on this property. It is found that a number of factors influence the measured compressive strength of sea ice. The most important parameters are:

- Temperature
- Salinity
- Density
- Ice type
- Crystal size
- Orientation

3.2.8 Young's modulus

The ratio between stress and strain for elastic behavior is known as the Elastic modulus (E). For sea ice, there is a lot of confusion related to this parameter. Langleben 1962 performed a series of test to determine the elastic modulus of ice. They found that the E-modulus behaves linearly as a function of brine volume:

$$E = 10 - 0.0351 * v_b \tag{3.8}$$

For a brine volume of 0 ppt the E-modulus is 10 GPa, while for a brine volume of 100 ppt it is 6.5 GPa. The relation between brine volume and elastic modulus is shown in Figure 3.6

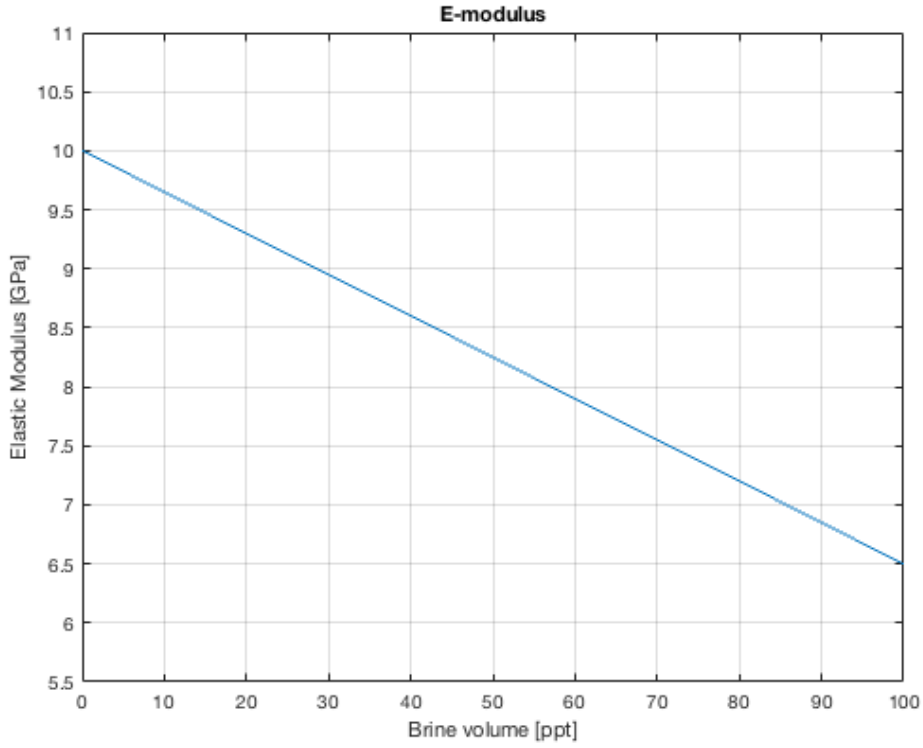

FIGURE 3.6: E-modulus relative to brine volume

3.2.9 Selected values in further calculations

Later in this thesis, the ice resistance will be calculated according to several empirical resistance formulations. The selected input parameters used are presented in Table 3.3. Some of these parameters will also be used when calculating an empirical ice pressure.

Plots for the flexural strength of ice and the elastic modulus are presented earlier in this chapter. For a temperature of -10°C and an ice thickness between 1 and 2 meters, the flexural strength will be approximately 650 KPa. By reading Figure 3.6, the E-modulus is found to be $9*10^9$. The other input parameters are chosen as presented in Riska 1997.

TABLE 3.3: Selected input parameters for further calculations

Dimension	Value
Temperature	-10°C
σ_b	650 KPa
μ	0.15
E	$9*10^9$ Pa
$\rho_{saltwater}$	1.025 t/kg^3
ρ_{ice}	0.900 t/kg^3
ν	0.3

Chapter 4

Ship-ice interaction

Information in this chapter is found from Riska 2017, Riska 2011 and Riska and Kämäräinen 2011.

For ships going in ice-infested waters, interactions with ice will occur. When designing vessels for interaction with ice, it is important to see the difference between global and local forces. Global forces is the total force one interaction will have on a ship, e.g. a collision with a single ice floe. These forces are important when determining the strength of larger structural elements. In this thesis, only the local pressure will be investigated. The local forces refer to the loads on single structural elements.

Ice can be broken in many ways and several breaking mechanisms have been suggested. The forces present are shown in Figure 4.1. However, the most effective method for breaking ice has been proven to be breaking by bending. This, combined with ice crushing as a consequence of local loads, are the two main parts of the term ice breaking.

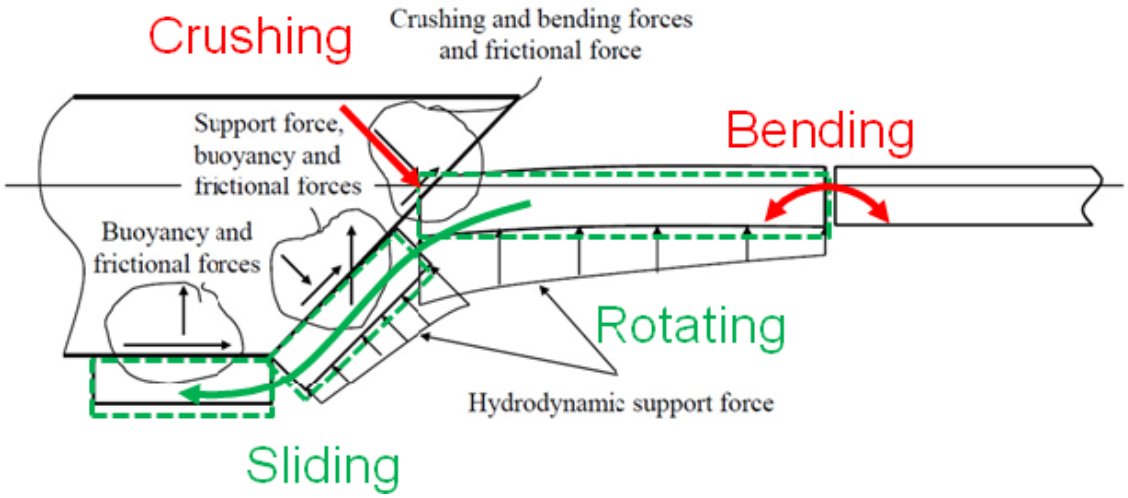

FIGURE 4.1: Forces present in interactions between ship and ice (Riska 2017)

When ice is broken, the broken ice needs to be displaced. This will lead to more interactions between the ship and the broken ice as the ship is moving. In this master thesis only the first interaction between ship and ice will be investigated, and the effects the broken ice will have on the hull will therefore not be accounted for.

4.1 Load Patch

In interactions between ship and ice, the load patch will vary. To simplify this, the load patch area can be idealized as shown in Figure 4.2b. Here, the total load patch area, A_c, are described by the load length, L, and the load height, h_c. This is shown in Equation 4.1.

$$A_c = L * h_c \tag{4.1}$$

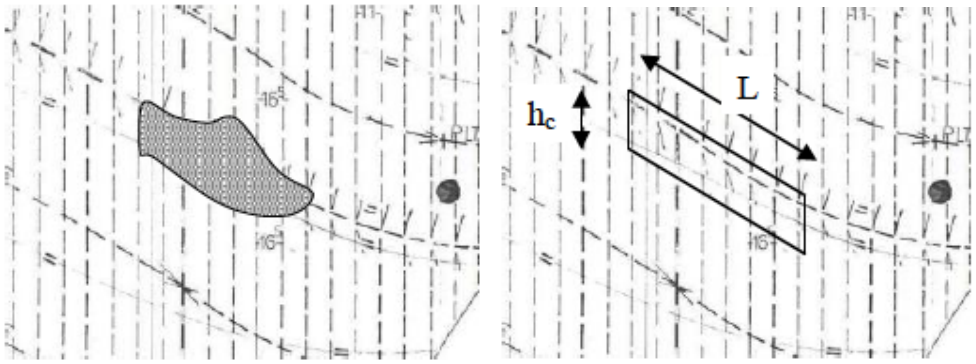

(A) Actual load patch (B) Idealized load patch

FIGURE 4.2: Load patches for local ice pressure (Riska 2017)

Over the years, the idea of the load height has developed. This development is presented in Figure 4.3. Before 1985, the ice load height was given by the ice thickness. In 1985, the ice load height was changed based on ice load measurements. These measurements showed that the load height was significantly lower than the ice thickness, and to take this into account, a ice class factor was introduced.

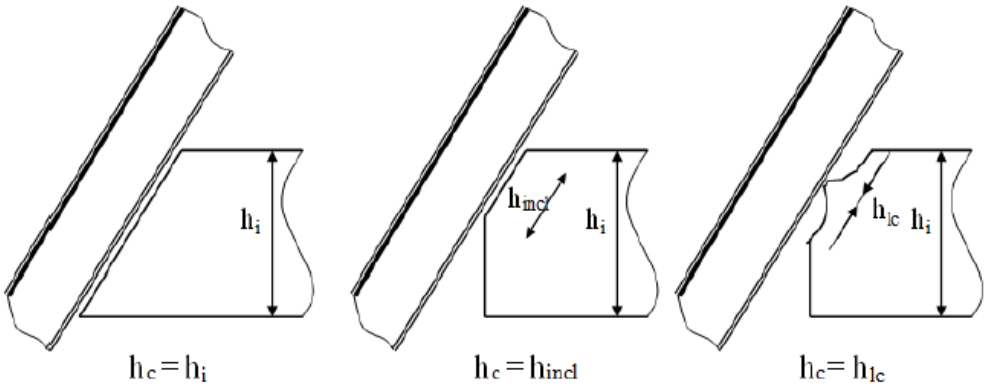

FIGURE 4.3: Load height (Riska 2017)

The load length is the length of the load that affect the response in the member. This length should in design be chosen to give maximum stress. For transverse framing, the design load length can be set equal to the frame spacing.

4.2 Ice pressure

The total force acting on the ship hull at one ice loading event can then be described as in Equation 4.2.

$$F = p_c * A_c \tag{4.2}$$

Where p_c is the ice pressure.

During interaction between ship and ice, post crushing, the forces that occur are presented in Figure 4.4. F_n represents the normal force and F_u represents the frictional force component.

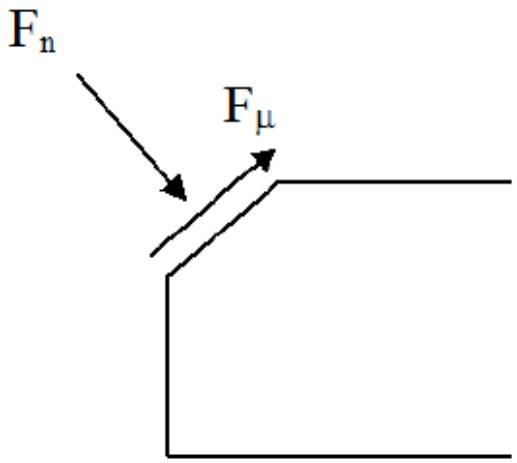

FIGURE 4.4: Forces acting during ship-ice interaction (Riska 2017)

The direction of the frictional force component is determined by the ship motion. By using a coefficient of friction, μ, the frictional force can be given as:

$$F_\mu = \mu * F_n \tag{4.3}$$

The normal force can then be divided into a vertical and a horizontal component. In a situation with bending of the ice, the vertical force component will be the only one interesting. The limit of this component will be given by the bending strength of the ice. The vertical force can be given as:

$$F_B = F_n(sin\beta_n - \mu cos\beta_n) \tag{4.4}$$

Where β_n is the frame angle, the angle between F_n and horizontal.

When considering a static case, the vertical force component can be estimated based on the static bearing capacity of ice. This gives a force as given in Equation 4.5.

$$F_B = C * \sigma_f * h_i^2 \tag{4.5}$$

Where;

- C is a constant dependent on the horizontal boundary geometry of the ice floe. In simplifications this can be set to 0.5 (typical values ranging from 0.25 to 1).
- σ_f is the flexural strength of ice
- h_i is the ice thickness

By combining Equation 4.2, 4.4 and 4.5, the pressure can by found as in Equation 4.6. This is done in some similarity as in the master thesis by Stephan 2017.

$$p_c = \frac{F_n}{A_c} = \frac{C * \sigma_f * h_i^2}{A_c * (sin\beta - \mu * cos\beta)} \tag{4.6}$$

Where σ_f can be found as shown in Section 3.2.6.

Chapter 5

KV Svalbard

KV Svalbard is a Norwegian coast guard vessel, with classification Icebreaker Polar 10. An icebreaker supports other vessels in harsh ice conditions, and can rescue vessels that get stuck in ice. In Chapter 8, there will be a presentation and comparison of three empirical models for calculation of ice resistance. In that chapter, KV Svalbard will be used as a reference ship. This vessel will also be used in a finite element analysis later in this master thesis.

FIGURE 5.1: Picture of KV Svalbard (ACCESS 2012)

5.1 Main parameters

KV Svalbard is the largest ship in the Norwegian coast guard, and is specialized for operations in Arctic waters. It is designed for ice breaking in 1 meter of solid ice, or 4 meters of broken ice. KV Svalbard mainly operate in areas close to Svalbard (Forsvaret 2014). The main parameters of this vessel, found from Thorsen 2012, are shown in Table 5.1.

TABLE 5.1: Main parameters for KV Svalbard (Thorsen 2012)

Dimension	Value
Displacement	6375 ton
Length of water line, L	89 m
Breadth, B	19.1 m
Draught, T	6.5 m
Stem angle, ϕ	33 deg
Water line entrance angle, α	59 deg
Length of parallel sides, L_{par}	36.32 m
Length of bow section, L_{bow}	27.24 m

5.2 Ice load monitoring system

The ice load monitoring system (ILM) project was created by DNV (now DNVGL), with the aim to increase knowledge about the actual ice conditions different vessels were exposed to, and how the ice-induced stresses would affect the hull. In the winters of 2007 and 2008, KV Svalbard was equipped with a prototype of this system, resulting in a lot of information on the experienced ice conditions. The information on this system was found from B. Leira et al. 2009. During the weeks of monitoring a lot of information were measured, including engine power, vessel speed, ice thickness and ice loads.

Fibre optic strain sensors were installed on girders and stiffeners in all parts of the hull. 66 optic sensors were mounted on nine frames of the vessel. The system is based on spot checks of critical frames, and as shown in Figure 5.2, these critical frames are mostly placed in the bow area. The support reactions are measured rather than the local strains in single plates, which allows the forces acting on a larger part of the hull to be estimated.

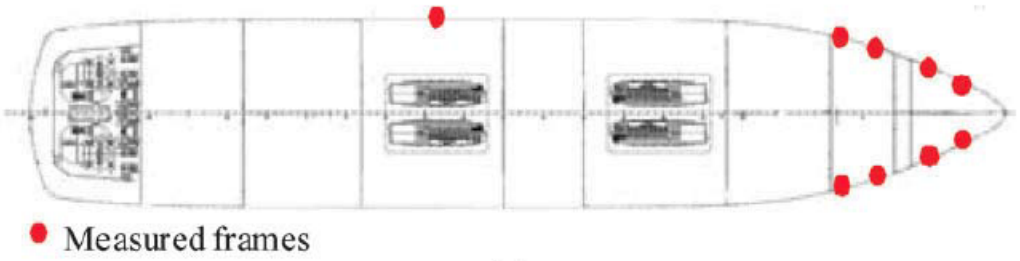

FIGURE 5.2: Measured frames at KV Svalbard (B. Leira et al. 2009)

To find the ice thickness, electromagnetic instrument were combined with a sonic distance-measurement system. The electromagnetic (EM) instrument measures the distance between the instrument and the water below the ice. Since sea ice has a negligible electrical conductivity compared to sea water, a magnetic field will be induced in the water by the instrument. The distance is then calculated from the strength of this magnetic field. The distance from the EM instrument to the top of the ice is measured using the

sonic distance-measurement system. In addition, the distance between the EM instrument and the sonic system need to be accounted for. From this, the ice thickness can be obtained from Equation 5.1.

$$h = d_{EM} - d_{sonic} - d_{dif} \tag{5.1}$$

Where;

- d_{EM} = Distance from EM instrument to the sea water [m]
- d_{sonic} = Distance from the sonic system to the top of the ice [m]
- d_{dif} = Distance between EM instrument to the sonic system [m]

While using this ice load monitoring system, the vessel got satellite images from the Norwegian Meteorological Institute to get information about the ice conditions. This information was used to plan optimal routes.

In the bridge they located a screen connected to the ILM system. Here, the stresses on the hull, as well as other measured parameters were displayed. Both the instant and the statistical values were presented.

5.3 H-V curve

Later in this thesis, the measured power from KV Svalbard will be used to find the resistance of the vessel in ice. To clearly see the operational area of KV Svalbard, the H-V curve will be calculated, using the method as presented in Riska 2011. The H-V curve shows the maximum vessel speed for a vessel at certain ice thicknesses. Parameters necessary for these calculations were found from Teien 2014 and are presented in Table 5.2.

TABLE 5.2: Parameters for H-V curve for KV Svalbard (Teien 2014)

Dimension	Value
Propeller diameter	3.3 m
Power	10 MW
Open water speed	18 knop
K	0.98

Chapter 6

Classifications of ships

6.1 Introduction

Most of the information in this chapter is found from "Ships for navigation in ice" by DNVGL 2016 and Riska 2017.

In 1971, the first modern ice class rules were published. These were based on analyzes of ice damage, and from that the strength level were obtained. These classifications were the first Finnish-Swedish ice class rules. Over the years there have been a continuous development in ice classifications, and as the knowledge and technology has improved, the rules now ensures safety for vessels and their workers.

All ships need to be classified according to rules from different classification societies in order to operate commercially. Operations in ice-infested waters exposes vessels to loads they would not experience in other regions. On this basis, specific classifications for navigation in ice are developed.

Classification societies tends to divided the classification for ice into two parts, one for operation in the Baltic region and one for the Arctic region. In addition, IACS have developed a set of polar rules for all ships constructed of steel and intended for operation in ice-infested polar waters. All classification societies, except the Russian Register, have adopted the IACS ice classes.

In the DNV GL classification, "Ships for navigation in ice", the rules are divided into three parts. The first part is classification for ships in the Baltic regions. This part was originally developed by the Finnish-Swedish class societies, and later implemented in DNV GL. The second part is made for ships travelling in the Arctic regions. The third and final part, Polar Class, is a common rule set ships travelling in ice-infested polar waters. The rules and classifications presented in this chapter are in general equivalent to the IACS Unified Requirements for Polar Ships.

6.2 Baltic region

The Finnish-Swedish ice class rules are originally used for vessels going in Baltic waters, but they are also used as industry standard for first-year ice (Riska 2017). All classifications societies, with the exception of IACS and Russian register have adopted these classifications as their first-year ice rules. The DNV GL ice classes are accepted as equivalent to the Finnish-Swedish ice classes as shown in Table 6.1.

DNV GL	**Finnish-Swedish**	**Ice condition**
ICE-1A*	1A Super	Difficult ice condition without assistance of icebreakers.
ICE-1A	1A	Difficult ice condition with assistance of icebreakers when necessary.
ICE-1B	1B	Moderate ice condition with assistance of icebreakers when necessary.
ICE-1C	1C	Light ice condition with assistance of icebreakers when necessary.

TABLE 6.1: DNV GL ice classes and the equivalent Finnish-Swedish ice classes and the description of these classes

The ice thickness corresponding to these classes are shown in Table 6.2.

DNV GL ice classes	**Ice thickness h_0**	**Ice thickness h**
ICE-1A*	1.0	0.35
ICE-1A	0.8	0.30
ICE-1B	0.6	0.25
ICE-1C	0.4	0.22

TABLE 6.2: DNV GL ice classes and the corresponding heights

Where,

- h_0 = Level of ice thickness not exceeded [m]
- h = The ice height actually under ice pressure [m]

6.3 Arctic region

For vessels operating in the Arctic regions, classification are divided into Polar, Ice and Icebreaker classes. How this is divided is presented in Table 6.3. The requirements in this section apply to icebreakers and other vessels intended to operate without assistance in Arctic regions.

Ice Conditions				
CLASS NOTATION	TYPE OF ICE ENCOUNTERED	NOMINAL ICE STRENGTH	NOMINAL ICE THICKNESS	LIMITING IMPACT CONDITIONS
ICE-05 ICE-10 ICE-15	Winter ice with pressure ridges	4.2 5.6 7.0	0.5 1.0 1.5	No ramming anticipated
POLAR10 POLAR20 POLAR30	Winter ice with pressure ridges and multi-year ice and floes and glacial ice inclusions	7.0 8.5 10.0	1.0 2.0 3.0	Occasional ramming
Icebreaker	As above	As above	As above	Repeated ramming

TABLE 6.3: Vessels in Arctic waters

6.3.1 Design Loads

The design ice load for ships in the Arctic region is based on finding a local pressure. This local pressure is then be applied over a relevant contact area.

Vertical design force

The vertical design force component due to head on ramming is given by Equation 6.1.

$$P_{ZR} = P_R * F_{EL} \quad [kN] \tag{6.1}$$

$$P_R = 28(\frac{C_R E_{IMP}}{tan\gamma})^{0.6}(\sigma_{ice} tan\alpha)^{0.4} \quad \text{in general} \tag{6.2}$$

$$\text{For spoon bows:} \quad tan\alpha = 1.2\frac{B^{0.1}}{\sqrt{cos\gamma}} \tag{6.3}$$

$$F_{EL} = \sqrt{\frac{E_{IMP}}{E_{IMP} + C_L P_R^2}} \tag{6.4}$$

$$E_{IMP} = E_{KE}\frac{tan^2\gamma}{tan^2\gamma + 2.5} \tag{6.5}$$

$$C_L = \frac{L^3}{3 * 10^{10} I_V} \tag{6.6}$$

$$E_{KE} = \frac{1}{2}\Delta V_{ram}^2 \quad (kNm) \tag{6.7}$$

Where;

- I_V = moment of inertia in m^4 about the neutral axis of the midship section
- C_R = 1 for class notation POLAR and 2 for class notation Icebreaker
- σ_{ice} as shown in Table 6.3
- α and γ as shown in Figure 6.2
- V_{RAM} = design speed when ramming may occur [m/s]

Total design force normal to the shell plating

The total design force normal to the shell plating in the bow area due to an oblique impact with an ice feature is given by Equation 6.8.

$$P_{OI} = \frac{P_{ZR}F_{SIDE}}{cos\gamma} \quad [kN] \tag{6.8}$$

$$F_{SIDE} = \frac{1.9}{tan^{0.4}\alpha}\left(\frac{\sigma_{ice}}{E_{KE}}\right)^{0.05} \tag{6.9}$$

Compression loads midships

All vessels shall withstand line loads acting simultaneously in the horizontal plane at the water level on both sides of the hull. These line loads are assumed to arise when a vessel in trapped between moving ice floes. The design line loads can be calculated from Equation 6.10:

$$q = \frac{165}{sin\beta_f}(h_{ice})^{1.5} \quad [kN/m] \tag{6.10}$$

$$\text{For vertical side shells} \quad (\beta_f < 10^o): \qquad q = 950(h_{ice})^{1.5} \quad [kN/m] \tag{6.11}$$

Where;

- h_{ice} = average ice thickness as shown in Table 6.3
- β_f = angle of outboard flare at the water level

Local ice pressure

The local ice pressure should be withstood by all vessels as defined by the different class notation and as applied on the different ice reinforced areas. The design pressure should be applied over a contact area corresponding to the type of load in question. The basic ice pressure is in general found from:

$$p_o = 1000F_A\sigma_{ice} \quad [kN/m^2] \tag{6.12}$$

Where F_A is the correction factor for ice reinforcement in different parts of the hull. This factor is in general 1.0 for the bow and stern area and 0.6 for the midship. For other parts of the ship or special cases of class notation, the correction factor can be found in DNVGL 2016.

The design pressure can be found from:

$$p = F_B p_o \quad [kN/m^2] \tag{6.13}$$

Where F_B is the correction factor for the size of the design contact area A_C:

$$\begin{aligned} F_B &= \frac{0.58}{A_C^{0.5}} \quad for \quad A_C \leq 1.0m^2 \\ F_B &= \frac{0.58}{A_C^{0.15}} \quad for \quad A_C > 1.0m^2 \end{aligned} \tag{6.14}$$

6.3.2 Local strength

The requirements for local strength apply to members directly exposed to local ice pressure. These members are plates, stiffeners and girders. For ships, the plating contributes to the largest part of structural weight. The thickness of the exposed plates should in general not be less than:

$$t = 23 k_a \frac{s^{0.75}}{h_o^{.25}} \sqrt{\frac{k_w p_o}{m_p \sigma_f}} + t_k \quad [mm] \tag{6.15}$$

$$k_a = 1.1 - \frac{s}{l}, \quad \text{maximum 1.0, minimum 0.85} \tag{6.16}$$

$$k_w = 1.3 - \frac{4.2}{(\frac{a}{s} - 1.8)^2}, \quad \text{maximum 1.0} \tag{6.17}$$

Where;

- k_a = aspect ratio factor
- k_w = influence factor
- p_o = ice pressure
- m_p = bending moment factor, found from Table F1 in DNVGL 2016
- σ_f = yield stress of material
- t_k = corrosion addition
- s = spacing between stiffeners
- l = effective span of stiffener
- h_0 = effective height of contact area, in general = $0.4h_{ice}$

The section modulus shall in general not be less than:

$$Z = \frac{41 h_o^{1-\alpha} l^{2-\alpha} p_o w_k}{\sigma sin\beta}, \quad (\text{cm})^3 \tag{6.18}$$

Where,

- h_o is the contact area or the stiffener spacing, which ever is smallest
- α is 0.5 for contact area less than 1 m^2
- w_k is the section modulus corrosion factor
- σ is 0.9* σ_{ice}
- β is the angle of web with shell plating

$$\beta = tan^{-1}(\frac{tan\gamma}{sin\phi}) \tag{6.19}$$

Where γ and ϕ can be found from Figure 6.1:

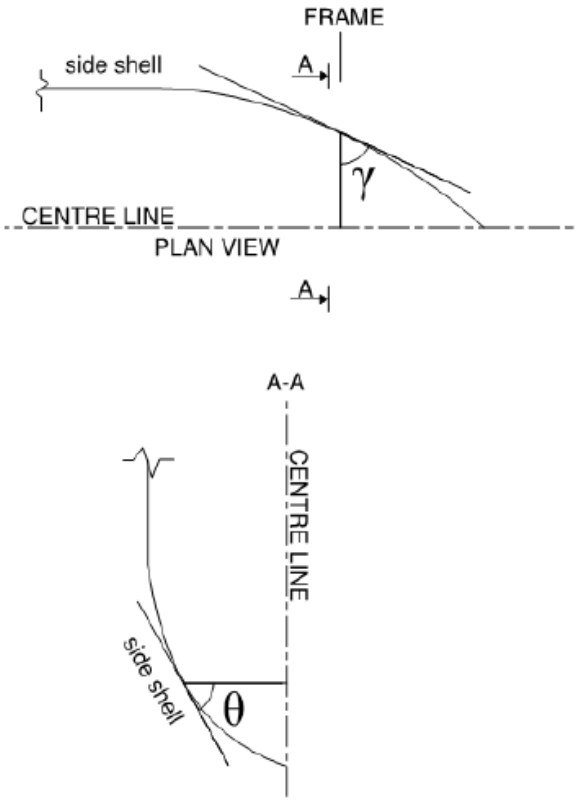

FIGURE 6.1: Angels needed to determine β from DNVGL 2016

6.4 Polar class

The polar classifications are organized by time spent in ice-infested waters. These classifications apply to ships constructed in steel. The organization of polar classes are shown in Table 6.4, where the different Polar Classes are presented. In addition, ships planned for icebreaking for the purpose of escort and ice management, with polar class PC1-PC6, may be given the notation "Icebreaker" additionally.

Polar Class	Description
PC-1	Year-round operation in all Polar waters.
PC-2	Year-round operation in moderate multi-year ice conditions.
PC-3	Year-round operation in second-year ice which may include multi-year ice inclusions.
PC-4	Year-round operation in thick first-year ice which may include old ice inclusions.
PC-5	Year-round operation in medium first-year ice which may include old ice inclusions.
PC-6	Summer/autumn operation in medium first-year ice which may include old ice inclusions.
PC-7	Summer/autumn operation in thin first-year ice which may include old ice inclusions.

TABLE 6.4: Types of sea ice organized by age

Whenever the hull and machinery are made to satisfy different classes, then the ship shall be assigned the lower of these in the classification certificate. If the hull or machinery complies with requirement of higher polar classes, this is to be registered in the certificate or an appendix thereto.

6.4.1 Design Ice Loads

For all Polar ships, determining requirements to resist ice loads are based on a glancing impact on the bow. The design load is given by an average pressure (P_{avg}) uniformly distributed over an area of height (b) and width (w). These values are dependent on the bow shape. To find the parameters it is required to calculate the following characteristics for sub-regions of the bow area:

- Shape coefficient (fa_i)
- Total glancing impact force (F_i)
- Line load (Q_i)
- Pressure (P_i)

To determine the ice load parameters in other parts of the hull, the fixed load patch aspect ratio, AR = 3.6, is necessary. These parameters are independent of the hull shape.

The parameters defining glancing impact load are presented in Table 6.5.

Polar Class	*Crushing Failure Class Factor (CF_F)*	*Flexural Failure Class Factor (CF_F)*	*Load Patch Dimensions Class Factor (CF_D)*	*Displacement Class Factor (CF_{DIS})*	*Longitudinal Strength Class Factor ($CF_{L)}$*
PC-1	17.69	68.60	2.01	250	7.46
PC-2	9.89	46.80	1.75	210	5.46
PC-3	6.06	21.17	1.53	180	4.17
PC-4	4.50	13.48	1.42	130	3.15
PC-5	3.10	9.00	1.31	70	2.50
PC-6	2.40	5.49	1.17	40	2.37
PC-7	1.80	4.06	1.11	22	1.81

TABLE 6.5: Parameters for glancing load

The parameters associated with the glancing impact load are functions of the hull angles. These angles are found in Figure 6.2.

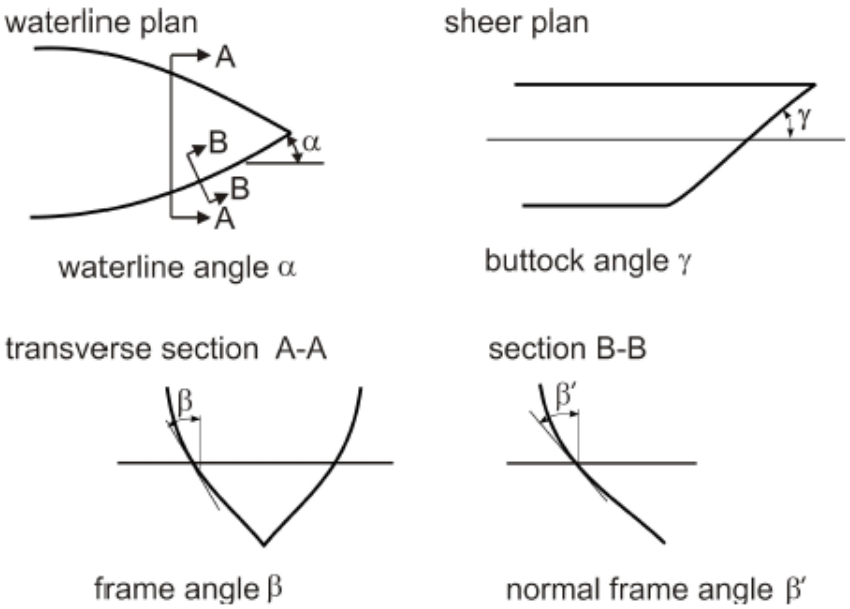

FIGURE 6.2: Hull angles (DNVGL 2016)

Where;

- β' = normal frame angle at upper ice waterline
- α = upper ice waterline
- γ = buttock angle at upper ice waterline
- tan(β) = tan(α)/tan(γ)
- tan(β') = tan(β)*cos(α)

The bow area load characteristics are dependent on a shape coefficient fa_i. This coefficient can be found as shown in the following equations:

$$fa_i = min(fa_{i,1}; fa_{i,1}; fa_{i,1}) \tag{6.20}$$

$$fa_{i,1} = (0.097 - 0.68(\frac{x}{L_{wl}} - 0.15)^2 * \frac{\alpha_i}{\sqrt{\beta'_i}} \tag{6.21}$$

$$fa_{i,2} = \frac{1.2 * CF_F}{sin() * CF_C * \Delta_{tk}^{0.64}} \tag{6.22}$$

$$fa_{i,3} = 0.60 \tag{6.23}$$

Where;

- i = sub-region considered
- L_{wl} = ship length measured at the upper ice waterline
- x = distance from the forward perpendicular to station under consideration
- α = waterline angle
- β' = normal frame angle
- Δ_{tk} = ship displacement
- CF_C and CF_F from Table 6.5

From this the total bow force can be found as shown in Equation 6.24.

$$F_i = fa_i * CF_C * \Delta_{tk}^{0.64}[MN] \tag{6.24}$$

The force in other hull parts can be found as shown in Equation 6.25.

$$F_{NonBow} = 0.36 * CF_C * DF[MN] \tag{6.25}$$

Where the ship displacement factor, DF, can be determined from the following equations.

$$DF = \Delta_{tk}^{0.64} \qquad if \quad \Delta_t k \leq CD_{DIS} \tag{6.26}$$

$$DF = CF_{DIS}^{0.64} + 0.10(\Delta_t k - CF_{DIS}) \qquad if \quad \Delta_{tk} > DF_{DIS} \tag{6.27}$$

After finding the force, the load patch aspect ratio, AR, can be found. For the bow this can be determined from:

$$AR_i = 7.46 * sin(\beta_i') \geq 1.3 \tag{6.28}$$

The line load for the bow can be found from Equation 6.29. The line load for the other hull parts can be found from Equation 6.30.

$$Q_i = \frac{F_i^{0.61} * CF_D}{AR_i^{0.35}} \quad [MN/m] \tag{6.29}$$

$$Q_{NonBow} = 0.639 * FNonBow^{0.61} * CF_D \quad [MN/m] \tag{6.30}$$

The pressure can be found as shown in Equation 6.31.

$$P_i = F_i^{0.22} * CF_D^2 * AR_i^{0.3} \quad [MPa] \tag{6.31}$$

When all these values are determined, the design load parameters can be calculated. The width can be found by:

$$w_{Bow} = \frac{F_{Bow}}{Q_{Bow}} \tag{6.32}$$

$$w_{NonBbow} = \frac{F_{NonBow}}{Q_{NonBow}} \tag{6.33}$$

The height can be found from:

$$b_{Bow} = \frac{Q_{Bow}}{P_{Bow}} \tag{6.34}$$

$$b_{NonBow} = \frac{w_{Bow}}{3.6} \tag{6.35}$$

And the average pressure from:

$$P_{avg} = \frac{F}{b * w} \quad [MPa] \tag{6.36}$$

Where;

- F = F_{Bow} or F_{NonBow}, dependent on the hull area under consideration
- b = b_{Bow} or b_{NonBow}, dependent on the hull area under consideration
- w = w_{Bow} or w_{NonBow}, dependent on the hull area under consideration

6.4.2 Local strength

To be able to resist the ice load, a minimum shell plate thickness is needed. For transversely framed plating, this thickness can be found from:

$$t_{net} = 500s\sqrt{\frac{AF * PPF_p * P_{avg0}}{\sigma_F}}\frac{1}{1+\frac{s}{2b}} \quad [mm] \tag{6.37}$$

Where;

- s = frame spacing
- AF = Hull area factor (Values found in DNVGL 2016)
- PPF_p = Peak pressure factor (Values found in DNVGL 2016)
- P_{avg} = Average patch pressure
- σ_F = Minimum upper yield stress of material
- b = Height of design load patch

6.5 Comparison

In this chapter, different rules have been presented. This includes the DNV GL Arctic classes and the IASC Polar classes. One of the main differences between these classifications are the organization. DNV GL divide their ice classes into geographical areas, the Baltic region and the Arctic region. IACS, on the other hand, divide their ice classifications independent of geographical area. Their focus is entirely on what ice resistance the vessels will be exposed to and for which periods.

In the master thesis from Holm 2012, a numerical comparison between the Polar and Arctic classifications was performed. He found that for higher classes, the Polar regulations are more conservative than the Arctic, while for lower classes, it is the other way around. Another major difference he found was the dependency of displacement. From this it was possible to find that for high displacement, the Polar classes were the most conservative, while for low displacement, the Arctic classes were the most conservative.

Chapter 7

Finite Element Analysis

The Finite Element Method, FEM, is the most versatile and is the dominating approach for structural analysis, especially of complex marine structures. The method can be applied to a wide variety of problems in engineering mechanics (Moan 2003).

In the event of ship-ice interaction, large displacements and deformations can come as a consequence. In the case of these large deformations, linear elastic behavior may no longer be valid. Here, a non-linear model could be used. In this chapter the differences between linear and non-linear analysis will be presented.

7.1 Linear Finite Element Analysis

Informations in this section is found mainly from Bell 2013.

In cases with linear elastic behavior of the material and small deformations, linear finite element method can be used. In linear analysis equilibrium of forces are fulfilled, meaning that the sum of forces are equal to zero. These forces induce stresses, which again is related to the strains (Hooke's law).

An elastic body subjected to loading will deform. After loading, the change in position consists of both a rigid body movement and a deformation (change of length). The rigid body movement is defined by displacements u, v and w in x-, y- and z-direction, respectively. Here, the focus is deformations of the body. Hence, the relative change of length of the body, defined as the normal strains in x-, y-, and z-direction, is as shown in Equation 7.1.

$$\begin{aligned} \varepsilon_x &= \frac{\partial u}{\partial x} \\ \varepsilon_y &= \frac{\partial v}{\partial y} \\ \varepsilon_z &= \frac{\partial w}{\partial z} \end{aligned} \tag{7.1}$$

The angular deformations of the body can be described by the angle γ, which defines the shear strains. For small displacements this can be found as in Equation 7.2.

$$\begin{aligned}\gamma_{xy} &= \gamma_x + \gamma_y = \frac{\partial u}{\partial y} + \frac{\partial v}{\partial x} \\ \gamma_{yz} &= \gamma_y + \gamma_z = \frac{\partial v}{\partial z} + \frac{\partial w}{\partial y} \\ \gamma_{zx} &= \gamma_z + \gamma_x = \frac{\partial u}{\partial z} + \frac{\partial w}{\partial x}\end{aligned} \tag{7.2}$$

The strain, ε, can be expressed in terms of the stress, σ. This is shown in Equation 7.3.

$$\varepsilon = \frac{\sigma}{E} \tag{7.3}$$

This is known as Hooke's law. In linear theory, the Young's modulus, E, is assumed to be constant, leading to a linear relation between stress and strain as shown in Figure 7.1.

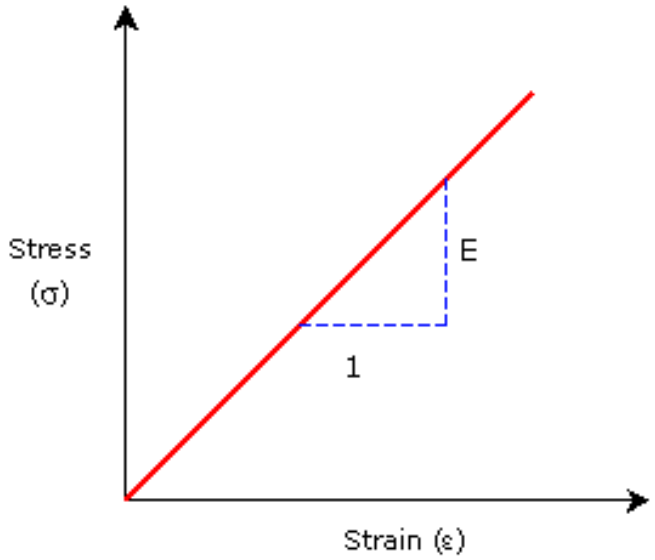

FIGURE 7.1: Linear relation between stress and strain (Solidworks 2013)

For a linear elastic, isotropic material, the normal components can be expressed as:

$$\begin{aligned}\varepsilon_x &= \frac{1}{E}(\sigma_x - \nu\sigma_y - \nu\sigma_y) \\ \varepsilon_y &= \frac{1}{E}(\sigma_y - \nu\sigma_x - \nu\sigma_z) \\ \varepsilon_z &= \frac{1}{E}(\sigma_z - \nu\sigma_x - \nu\sigma_y)\end{aligned} \tag{7.4}$$

Where ν is the Poisson ratio. Similarly, the shear components:

$$\begin{aligned}\gamma_{xy} &= \frac{2(1+\nu)}{E}\tau_{xy} = \frac{1}{G}\tau_{xy} \\ \gamma_{yz} &= \frac{2(1+\nu)}{E}\tau_{yz} = \frac{1}{G}\tau_{yz} \\ \gamma_{zx} &= \frac{2(1+\nu)}{E}\tau_{zx} = \frac{1}{G}\tau_{zx}\end{aligned} \tag{7.5}$$

Where G is the shear modulus.

In general, the system of equation to be solved can be written as:

$$\mathbf{M}\ddot{\mathbf{r}} + \mathbf{C}\dot{\mathbf{r}} + \mathbf{K}\mathbf{r} = \mathbf{R} \tag{7.6}$$

Where;

- **M** is the mass matrix
- **C** is the damping matix
- **K** is the stiffness matrix
- **R** is the external forces
- $\ddot{\mathbf{r}}$, $\dot{\mathbf{r}}$ and **r** are the vectors of acceleration, velocity and displacement, respectively

By neglecting inertia forces and damping force, the equation of motion can be reduced to:

$$\mathbf{K}\mathbf{r} = \mathbf{R} \tag{7.7}$$

Which by inverting gives the solution for the displacement vector **r**:

$$\mathbf{r} = \mathbf{K}^{-1}\mathbf{R} \tag{7.8}$$

Doing linear analysis, a lot of assumptions need to be done. Linear material behavior can be a quite good assumption for some material, such as steel, but not good for at all for others, such as reinforced concrete. For non-linear material behavior and large deformations, non-linear analysis should be used.

7.2 Non-linear Finite Element Analysis

Information in this section is found from Moan 2003 and Sævik 2017.

In the case of calculating the ultimate strength of structures that buckle, the assumptions of linear material behavior and small displacement needs adjustments. Compared to linear analysis, non-linear analysis are more time consuming. The different types of non-linearities are usually divided into three parts:

- Geometrical non-linear behavior
- Material non-linear behavior
- Non-linear boundaries

Here, the first two are important when approaching the maximum capacity of a structure.

7.2.1 Geometrical non-linear behavior

Geometrical non-linearities are usually associated with large displacements. This is not necessarily the case, as these problems often include small displacements.

When solving problems involving geometrical non-linearities, the continuous non-linear displacements are replaced with a series of linear increments. The geometry may change during deformation, and the stiffness, $\mathbf{K}$, will now be dependent upon the displacement, r, as presented in Equation 7.9

$$\mathbf{K}(\mathbf{r})\mathbf{r} = \mathbf{R} \tag{7.9}$$

For certain loads, this equation can be solved analytically using iterative methods. To express the equilibrium condition, Equation 7.9 can be written on a differential form, as shown in Equation 7.10.

$$d\mathbf{R} = \frac{d}{d\mathbf{r}}(\mathbf{K}(\mathbf{r})\mathbf{r})d\mathbf{r} = \mathbf{K}_I d\mathbf{r} \tag{7.10}$$

Where $\mathbf{K}_I$ is the incremental stiffness, consisting of two parts, $\mathbf{K}_\mathrm{o}$ and $\mathbf{K}_\mathrm{G}$. $\mathbf{K}_\mathrm{o}$ is the linear initial stiffness, while $\mathbf{K}_\mathrm{G}$ is the incremental stiffness due to changes in the geometry, often called the geometric stiffness. Equation 7.10 can be solved using incremental methods.

7.2.2 Non-linear material behavior

In linear analysis, the relation between stress and strain is assumed to be linear. When the stress exceed a certain level, this linearity no longer applies, and a non-linear elasto-plastic condition prevails. This condition is shown in Figure 7.2.

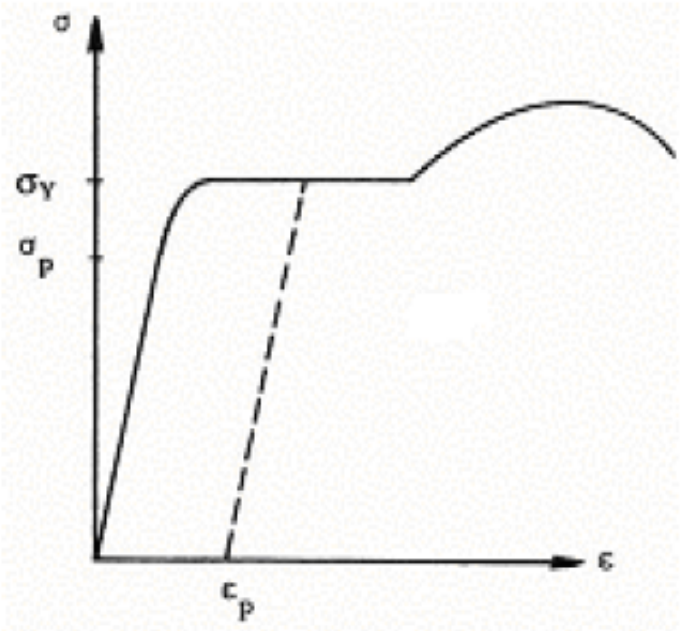

FIGURE 7.2: Non-linear relation between stress and strain (Moan 2003)

Where σ_p is the proportional limit for stress-strain and σ_y is the yield stress level. As the stress above σ decreases, unloading takes place along the dashed line, and when the stress is back as zero, the residual plastic strain, ε_p, remains.

7.2.3 Non-linear boundaries

The third non-linearity is connected to the boundary conditions. These non-linearities can occur when large displacement leads to surfaces coming into or out of contact. Stresses and displacements of contacting bodies are normally not linearly dependent on loads. Doubling of the loads to not necessarily double the displacements. This type of non-linearity may happen even for linear material behavior. A typical contract problem is shown in Figure 7.3.

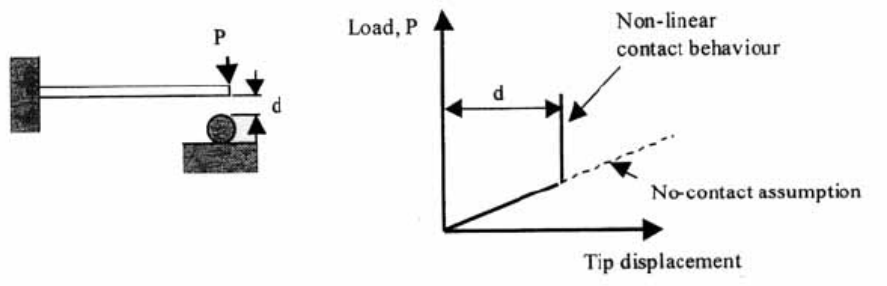

FIGURE 7.3: Typical non-linear behavior due to boundaries (Moan 2003)

7.2.4 Solution techniques

Multiple techniques exist for solving these non-linear problems. Here, the incremental method is presented. This method are also called *Euler-Cauchy method*.

Incremental methods provides a solution by stepwise applying the external loading. For each step, $\Delta \mathbf{r}$ is determined, and the total displacement is then found by adding each displacement increment. Based on this displacement the incremental stiffness matrix can be calculated. For load increment "m+1" the solution can be found from:

$$\begin{aligned} \Delta \mathbf{R_{m+1}} &= \mathbf{R_{m+1}} - \mathbf{R_m} \\ \Delta \mathbf{r_{m+1}} &= \mathbf{K_I(r_m)^{-1}} \Delta \mathbf{R_{m+1}} \\ \Delta \mathbf{r_{m+1}} &= \mathbf{r_m} + \Delta \mathbf{r_{m+1}} \end{aligned} \tag{7.11}$$

An improvement to the Euler-Cauchy method, as presented in Moan 2003, can be achieved by an equilibrium correction. In step "m", the total load and calculated displacement are $\mathbf{R_m}$ and $\mathbf{r_m}$, respectively. The unbalanced between internal forces and total forces can be expressed by the residual force vector:

$$\mathbf{R_r} = \mathbf{R_{int}}(\mathbf{r_m}) - \mathbf{R_m} \tag{7.12}$$

This residual force can be accounted for in the next step, "m+1", as shown in Equation 7.13. This will reduce external loads and global equilibrium will be restored.

$$\Delta \mathbf{r_{m+1}} = \mathbf{K_I(r_m)^{-1}} \Delta \mathbf{R_{m+1}} - \mathbf{K_I(r_m)^{-1}} \mathbf{R_r} \tag{7.13}$$

Chapter 8

Models for calculation of ice-induced resistance

8.1 Introduction

To calculate the ice-induced resistance on hulls, analytical models can be used. In this chapter, three of these models will be presented, the Riska model, the Lindqvist model and the Keinonen model. While the Riska and Lindqvist models are based on trials from Baltic waters, the Keinonen model is based on trials from other areas as well.

The ice resistance of ships has been studied for a long time, with the main focus on ships in level ice. When calculating this resistance, the most important parameter are ice thickness and vessel speed. In addition, ice strength, friction and ice density are also of importance.

All models uses the same definitions of the hull angles, as shown in Figure 8.1. The stem angle, ϕ, is the angle between bow and water line. The water line entrance angle, α, is the angle between the water line and the longitudinal axis of the ship.

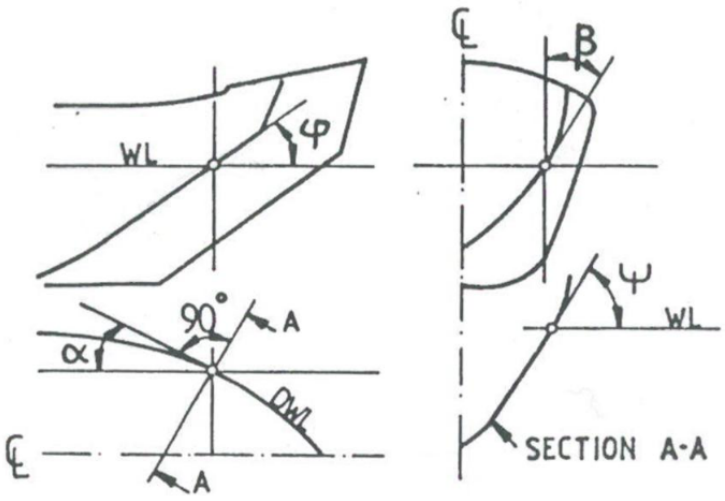

FIGURE 8.1: Ship hull angles (Riska 2011)

In addition to presenting the models, a comparison will be made. In this comparison the characteristics from KV Svalbard will be used.

8.2 Lindqvist

The information in this section is mainly found from Lindqvist 1989 and Erceg and Ehlers 2017.

The model developed by Gustav Lindqvist in 1989 is a simple way of calculating the level ice resistance. This model is a tool for evaluating the resistance, and a good way to show how the resistance is affected by the different main dimensions and hull angles. The parameters included in this method are:

- Main parameters
- Hull form
- Ice thickness
- Friction
- Ice strength

The Lindqvist model can not be a replacement for model testing, but can be used as a tool to find out which hull forms that need further testing. Not all resistance components are accounted for in this model, but the chosen ones are accepted as the dominating. The resistance in this model is divided into three parts; crushing, breaking by bending and submersion. In addition, the vessel speed is strongly decisive for the resistance.

8.2.1 Crushing

The crushing force is the main force at the stem. This force seems to never grow big enough to break the ice in the bending mode. Due to the wedge-shaped geometry at the stem the bending failure force is greater at the stem then elsewhere on the vessel.

The crushing force at the stem is hard to measure, and estimations are therefore necessary. The average vertical force acting on the ice is estimated as shown in Equation 8.1.

$$F_v = 0.5 * \sigma_b * h_{ice}^2 \tag{8.1}$$

Where,

- σ_b = bending strength of ice
- h_{ice} = ice thickness

By assuming that the friction force acts along the vertical, the resistance force in crushing can be found as shown in Equation 8.2.

$$R_c = F_v * \frac{tan\phi + \mu * \frac{cos\phi}{cos\psi}}{1 - \mu * \frac{sin\phi}{cos\psi}} \tag{8.2}$$

Where,

- μ = friction coefficient
- ϕ = stem angle
- α = water line entrance angle
- ψ = angle between the normal of the surface and a vertical vector = arctan($\frac{tan\phi}{sin\alpha}$)

8.2.2 Breaking by bending

Some distance after the stem, when the contact area gets larger, bending failure will occur. As the ship comes in contact with a sharp edge, the ice will be crushed until the force is big enough, and failure in shear occurs. The plane of failure is close to the contact area, and the crushing continues until the area reaches a certain size causing a bending failure. This case is shown in Figure 8.2. The resistance force from breaking by bending can be found as presented in Equation 8.3.

$$R_b = \frac{27}{64} * \sigma_b * B * \frac{H_{ice}^{1.5}}{\sqrt{\frac{E}{12*(1-\nu^2)*g*\rho_{sw}}}} * (tan\psi + \mu * \frac{cos\phi}{sin\alpha * cos\psi}) * (1 + \frac{1}{cos\psi}) \quad (8.3)$$

Where,

- B = breadth
- E = Young's modulus
- ν = Poisson coefficient
- ρ_{sw} = density of salt water

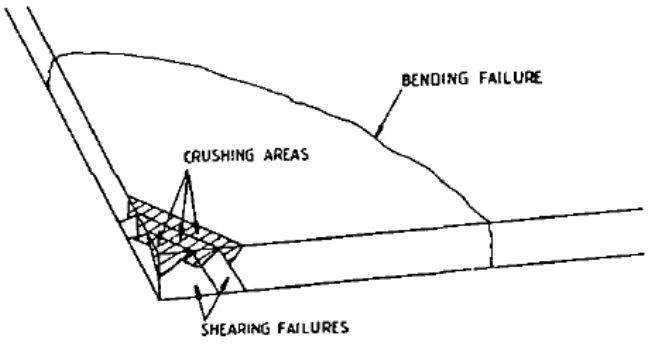

FIGURE 8.2: Bending by breaking (Lindqvist 1989)

8.2.3 Submersion

Calculation of the resistance due to submersion is uncomplicated. The resistance comes directly through the normal force and indirectly through the friction. To find the friction component, it is assumed that 70% of the hull below the water line is covered by ice. This assumption has been obtained from a series of model tests and full-scale observations.

The resistance from the normal force is not calculated separately for all surfaces, but instead found from potential energy. The resistance from submersion can be found from Equation 8.4.

$$R_s = \delta_\rho g H_{ice} B \left(T \frac{B+T}{B+2T} + \mu(0.7L - \frac{T}{tan\phi} - \frac{B}{4tan\alpha} + T * cos\phi * cos\psi * \sqrt{\frac{1}{sin^2\phi} + \frac{1}{tan^2\alpha}}) \right) \tag{8.4}$$

Where,

- δ = the difference in density between ice and water
- g = gravitational constant

8.2.4 Vessel speed

It is assumed that the resistance increases linearly with the speed. To make this a dimensionless term, the vessel speed is divided by the square root of ice thickness times the gravitational constant for the breaking resistance. Similarly, the speed is divided by the square root of the ship length times the gravitational constant, g. By using this, the total ice resistance can be calculated from Equation 8.5.

$$R_{Lindqvist} = (R_c + R_b)(1 + 1.4\frac{v}{\sqrt{gh_{ice}}}) + R_s(1 + 9.4\frac{v}{\sqrt{gL}}) \tag{8.5}$$

The model by Lindqvist presents an easy method for calculation of the ice resistance, and can be a useful tool in the design process.

8.2.5 Verification

In order test the reliability of the model, Lindqvist compared the results against full-scale resistance measurements for seven ships operating in Baltic ice conditions. From this comparison it was concluded that the model was reliable for larger ships, while the the speed-dependent part was less accurate for smaller vessels. When checking for different bow shapes, the model was found to be fairly accurate. Since the model was validated according to full-scale results from the Baltic, the biggest uncertainty is connected to changes in ice properties. The reliability to this model in other ice conditions is therefore questionable.

8.3 Riska

The information in this section is found mainly from Riska 1997, Riska 2011 and Erceg and Ehlers 2017.

The model developed by Riska was made originally for ships travelling in ice channels in the Baltic, with the purpose of estimating the power needed by ships to proceed in level ice. These requirements were to be included in the Finnish-Swedish ice class rules. This model was a result of a five year program, supported by the Finish and Swedish Maritime Administration. The Riska model was based on three previous formulations:

- Ionov (1988)
- Lindqvist (1989)
- Kämäräinen (1993)

Some assumptions were made to simplify this model. Even though both the strength and density of ice will vary, these are both set to be constant. This is also the case for the friction coefficient between ice and ship. As a consequence of this simplification, the ice thickness is the only ice-related variable to affect the resistance. Another simplification in this model is that it only includes the stem angle, while the other hull angles are not accounted for.

To use the Riska model, the total resistance need to be divided into two parts, ice resistance and open water resistance, as shown in Equation 8.6. The open water resistance can be found from model tests. This resistance is usually very small relative to the ice resistance in ranges of speed in which icebreaking usually takes place.

$$R_{total} = R_{ice} + R_{openwater} \tag{8.6}$$

The ice resistance consists of two parts, one dependent on speed and one independent. The speed-dependent part acts linear to ship speed. The ice resistance can be found as shown in Equation 8.7.

$$R_{ice} = C_1 + C_2 * V \tag{8.7}$$

C1 and C2 are constants and can be determined from Equation 8.8 and 8.9

$$C_1 = f_1 \frac{1}{2\frac{T}{B} + 1} BL_{par}h_i + (1 + 0.021\phi)(f_2 Bh_i^2 + f_3 L_{bow}h_i^2 + f_4 BL_{bow}h_i) \tag{8.8}$$

$$C_2 = (1 + 0.063\phi)(g_1 h_1^{1.5} + g_2 Bh_i) + g_3 h_i (1 + 1.2\frac{T}{B})\frac{B^2}{\sqrt{L}} \tag{8.9}$$

Where:

- T = draught [m]
- B = breadth [m]
- L = length [m]
- L_{par} = length of parallel sides section [m]
- L_{bow} = length of bow [m]
- h = ice thickness [m]
- V = vessel speed [m/s]
- ϕ = stem angle [deg]

The values for the constants:

- f_1 = 0.23 kN/m^3
- f_2 = 4.58 kN/m^3
- f_3 = 1.47 kN/m^3
- f_4 = 0.29 kN/m^3
- g_1 = 18.9 kN/(m/s*$m^{1.5}$)
- g_2 = 0.67 kN/(m/s*m^2)
- g_3 = 1.55 kN/(m/s*$m^{2.5}$)

8.4 Keinonen

Information in this section is found from Erceg and Ehlers 2017.

From one of the most thorough studies on ship performance in ice ever, Keinonen el al. developed a resistance formulation based on full-scale trials and operator interviews. A total of 18 icebreakers were involved, covering all interesting aspects, including:

- Ship sizes
- Bow shapes
- Engine powers
- Design features
- Environmental conditions
- Hull conditions
- Operational profiles

To calculate the total resistance of icebreaking ships, Keinonen divided the resistance into three components, as shown in Equation 8.10.

$$R(v)_{total} = R(v)_{ow} + R(1m/s)_{ice} + R(> 1m/s)_{ice} \tag{8.10}$$

Where,

- $R(v)_{ow}$ is the open water resistance
- $R(1m/s)_{ice}$ is the level ice resistance at the speed of 1 m/s
- $R(>1m/s)_{ice}$ is the level ice resistance at speeds above 1 m/s. Can be considered the speed-dependent component.

To correct for different conditions, correction factors were introduced. For the hull conditions, C_h, this were found to be 1.0 for inerta coating, 1.33 for four-month old bare steel, and 1.9 for one-year old bare steel. For the water salinity factor, C_s, this were found to be 0.8 for freshwater ice, 0.9 for brackish ice, and 1.0 for saline ice.

In addition, the bow form will strongly influence the resistance. The Keinonen formulation is therefore divided into two parts, one for rounded hull forms and one for chined hull forms. For level ice resistance at 1m/s, Equation 8.11 represents ships with fully formed bows and Equation 8.12 represents ships with sharp chined shoulders.

$$\begin{aligned} R(1m/s)_{ice} = 0.015 * h_e^{1.5} * C_s * B^{0.7} * L^{0.2} * T^{0.1} * (1 - 0.0083(t + 30)) * C_h * \\ (0.63 + 0.00074 * \sigma_f) * (1 + 0.0018(90 - \psi)^{1.6}) * (1 + 0.003(\beta - 5)^{1.5}) \end{aligned} \tag{8.11}$$

$$R(1m/s)_{ice} = 0.08 + 0.017 * h_e^{1.25} * C_s * B^{0.7} * L^{0.2} * T^{0.1} * (1 - 0.0083(t + 30)) * C_h * (0.63 + 0.00074 * \sigma_f) * (1 + 0.0018(90 - \psi)^{1.4}) * (1 + 0.004(\beta - 5)^{1.5}) \quad (8.12)$$

The accuracy of these formulations were found to be fairly accurate in the ranges presented in Table 8.1.

TABLE 8.1: Range of accuracy

Parameter	Min value	Max value
Ice thickness	0.5m	1.7m
Flexural strength of ice	150 kPa	700 kPa
Average flare angle	40°	80°
Average buttock angle	12°	40°

For the speed-dependent part of the formulation, this is based on the same procedure as in the development of the speed-independent component. Ice thickness was found to have a linear influence on the speed-dependent component.

$$R(> 1m/s)_{ice} = 0.009 * (\frac{v_{increased}}{\sqrt{gL}}) * B^{1.5} * L^{0.5} * h_e * (1 - 0.0083(t + 30)) * C_h * (1 + 0.0018(90 - \psi)^{1.6}) * (1 + 0.004(\beta - 5)^{1.5}) \quad (8.13)$$

$$R(> 1m/s)_{ice} = 0.009 * (\frac{v_{increased}}{\sqrt{gL}}) * B^{1.5} * L^{0.5} * h_e * (1 - 0.0083(t + 30)) * C_h * (1 + 0.0018(90 - \psi)^{1.4}) * (1 + 0.003(\beta - 5)^{1.5}) \quad (8.14)$$

Here, h_e is the equivalent ice thickness. This will be taken as h_{ice} since the snow thickness is not known.

8.5 Comparing the models

When calculating the resistance according to Lindqvist, the resistance is divided into three parts; crushing, breaking by bending and submersion. For the Riska and the Keinonen model, this is not the case. Here the ice resistance is divided into two parts; one speed dependent and one independent. For instance, if you are interested in the crushing force, this is only possible to get from the Lindqvist model.

The Riska model is also quite limited when it comes to different bow shapes. Here, the stem angle is the only parameter available, and it is therefore not possible to estimate resistance for different bow shapes.

As shown in Table 9.1, the Lindqvist model has more parameters involved, especially parameters that are ice-related. In the Riska model a lot of these parameters are incorporated through coefficients, and are therefore not possible to change. The Riska model is developed from full-scale tests in the Baltic, and this in therefore the area where it is most applicable. This can lead to problem when using the model in areas with different ice conditions.

As the Riska model, the Lindqvist formulation is also developed for use in Baltic waters, and the reliability in other areas are questionable. Here the Keinonen model has a clear advantage. Since this model is developed from results from other areas as well, it can be assumed that this will be the more trustworthy in waters with other values for such as ice flexural strength and salinity.

8.5.1 Plots

To compare the three presented models, the parameters from KV Svalbard were used. The two main parameters used in this comparison are ice thickness and vessel speed. By plotting these values against the resulting ice resistance, it is possible to see how changing these parameters will affect the resistance.

The input parameters for KV Svalbard are the same for every model. This is not the case for the chosen values for the ice parameters. Since these values are implemented through constants in the Riska formulation, they can not be modified. Later in this thesis, the full scale resistance of KV Svalbard will be used in a comparison with the empirical formulations. The values presented in Table 3.3 will therefore be used to achieve optimal results.

The plot for the Lindqvist model is presented in Figure 8.3. As shown, the resistance calculated for a vessel speed of 4 m/s and an ice thickness of 2 meter is approximately 4.5 MN.

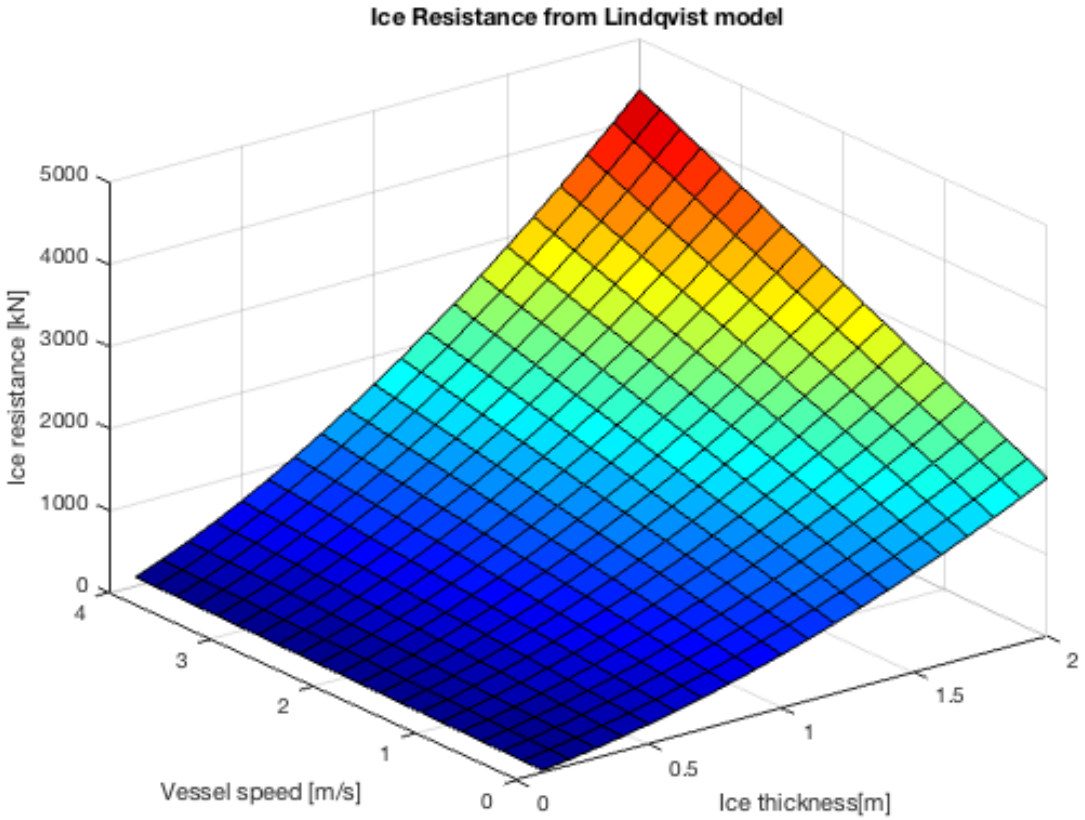

FIGURE 8.3: Plot of resistance from Lindqvist model

From this plot of the Riska model one can see that maximum ice resistance at an ice thickness of 2 meter and a vessel speed of 4 m/s is approximately 3.25 MN. This is approximately 28% lower than for the Lindqvist model. This plot is presented in Figure 8.4.

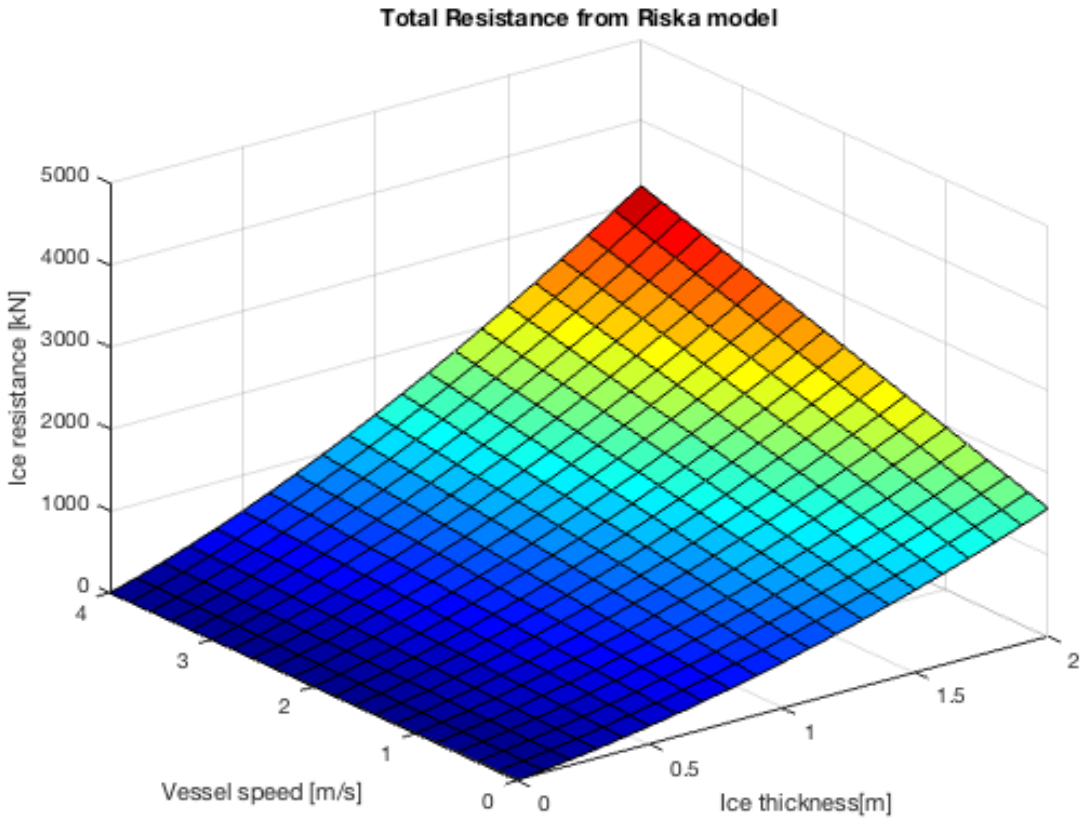

FIGURE 8.4: Plot of resistance from Riska model

The plot for the Keinonen model shows that the resistance for a vessel speed of 4 m/s and an ice thickness og 2 meter is approximately 3.9 MN. This is approximately 13% lower than for the Lindqvist model.

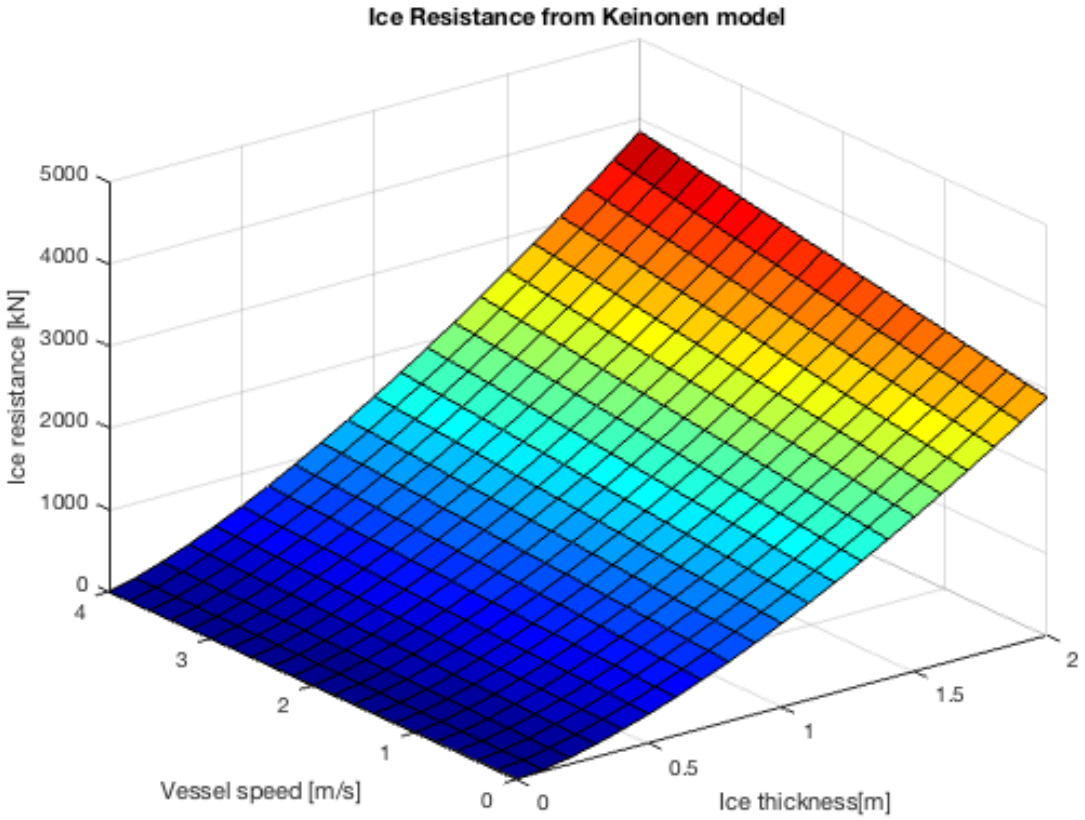

FIGURE 8.5: Plot of resistance from Keinonen model

In Figure 8.6 the resistance calculated from the three models are compared for an ice thickness of 0.2 meter and a varying vessel speed.

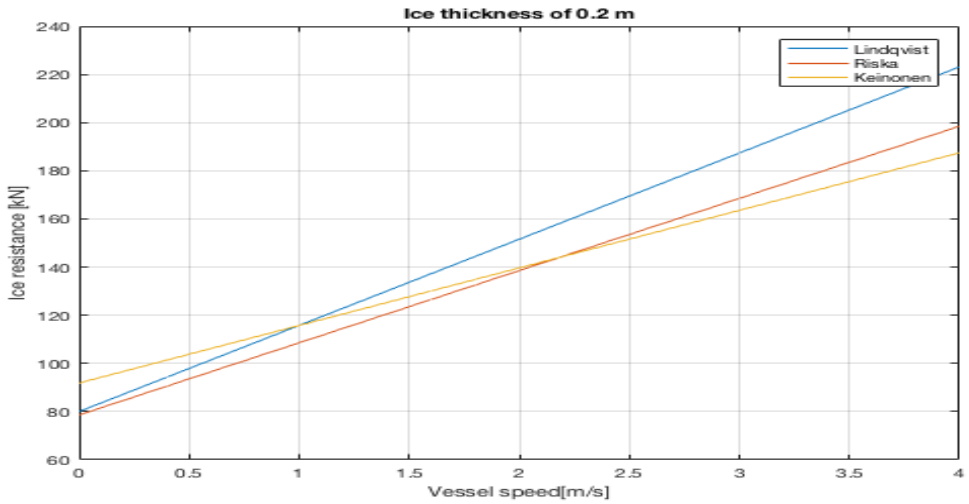

FIGURE 8.6: Riska vs Lindqvist vs Keinonen for ice thickness of 0.2 meter

From the figure above one can see that the difference between the graphs is quite small, with a 17% difference from the highest to the lowest resistance at max vessel speed. One can also see that the lines are relatively parallel to each other. In Figure 8.7 a similar comparison is presented, here with an ice thickness of 1.6 meter.

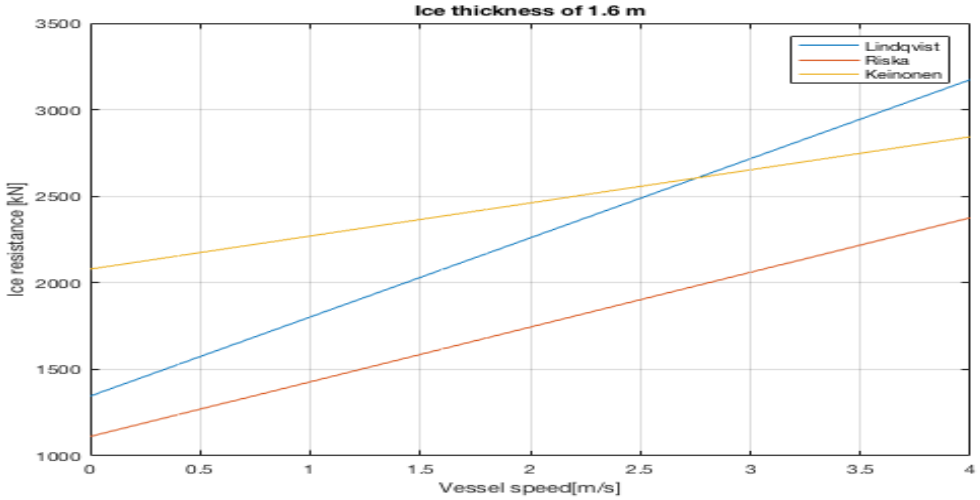

FIGURE 8.7: Riska vs Lindqvist vs Keinonen for ice thickness of 1.6 meter

In Figure 8.7, the difference between highest and lowest resistance at maximum vessel speed is bigger. Here, this difference is 25%. One can also see that the different lines no longer are that parallel, with especially the graph for Keinonen different from the others. For all cases with a constant ice thickness, the models increase linearly with speed.

In Figure 8.8 the two models are compared for a varying ice thickness and and a vessel speed of 0.4 m/s. For low speeds, the predicted resistance from Keinonen is a lot higher than the other, with a 41% difference at maximum ice thickness compared to the Riska formulation.

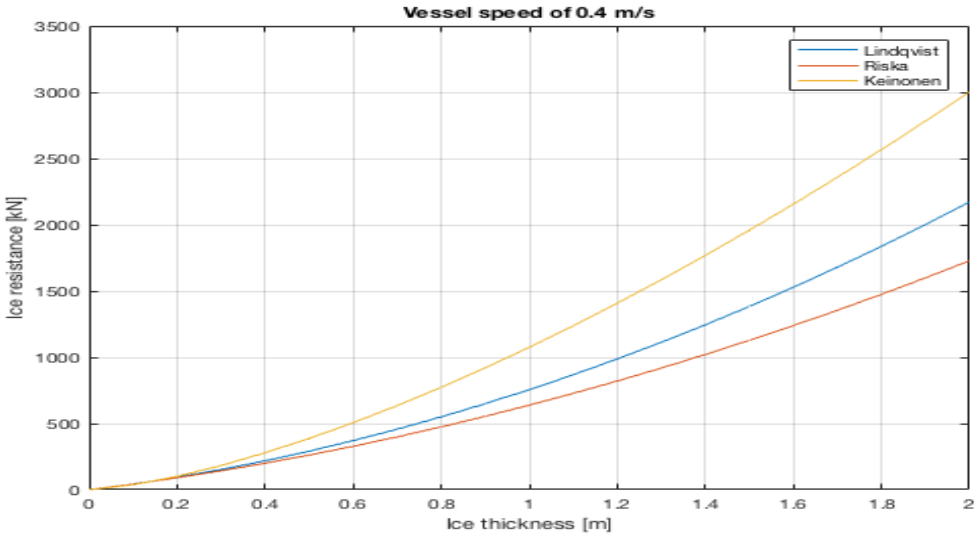

FIGURE 8.8: Riska vs Lindqvist vs Keinonen for vessel speed 0.4 m/s

Figure 8.9 shows a varying ice thickness and a vessel speed of 3 m/s. Here, one can see that the Keinonen and Lindqvist predicts nearly the same resistance, while Riska gives approximately 25% less for maximum ice thickness. All of these models have an exponential relation to the ice thickness.

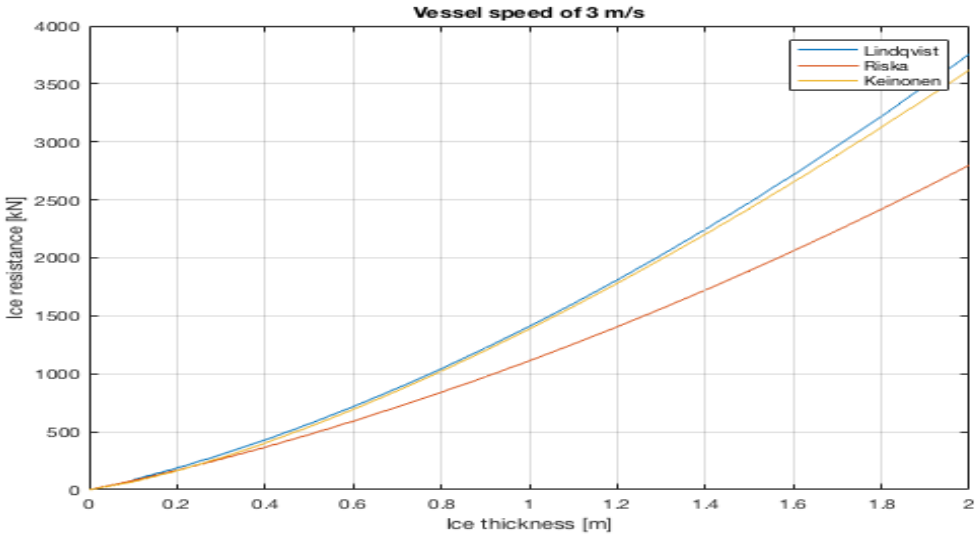

FIGURE 8.9: Riska vs Lindqvist vs Keinonen for vessel speed 3 m/s

From the previous plots, one can see that the resistance estimated from Riska is lower than the resistance from the two other models. Since Riska uses other input values, this difference is natural. In Figure 8.10 and Figure 8.11, the models are compare with the same input values. This gives a better understanding of how the models compare to each other. The values used in Riska 1997 are presented in Table 8.2.

TABLE 8.2: Parameters from Riska

Dimension	Value
σ_b	500 KPa
μ	0.15
E	$2*10^{11}$ Pa
$\rho_{saltwater}$	1.025 t/kg^3
ρ_{ice}	0.900 t/kg^3
ν	0.3

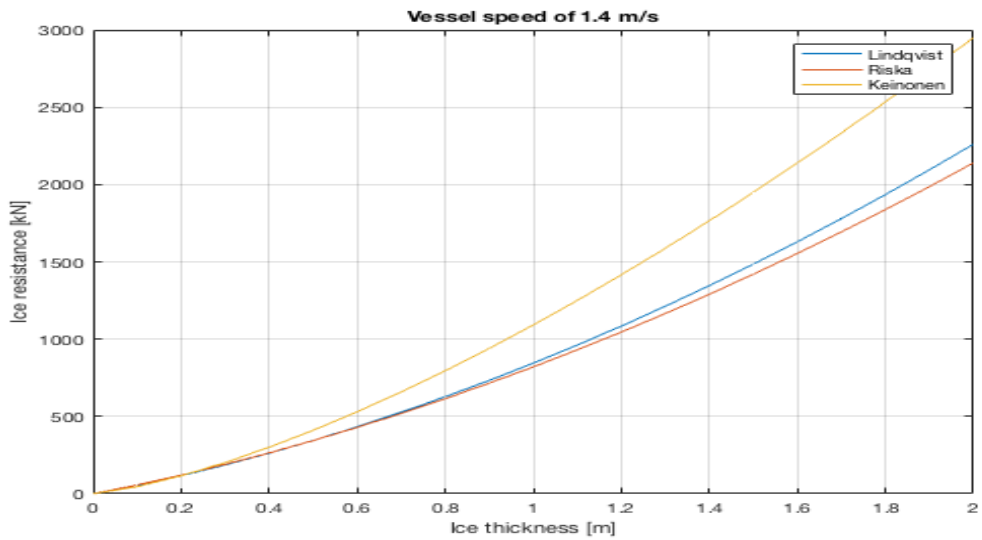

FIGURE 8.10: Riska vs Lindqvist vs Keinonen for vessel speed 1.4 m/s - New parameters

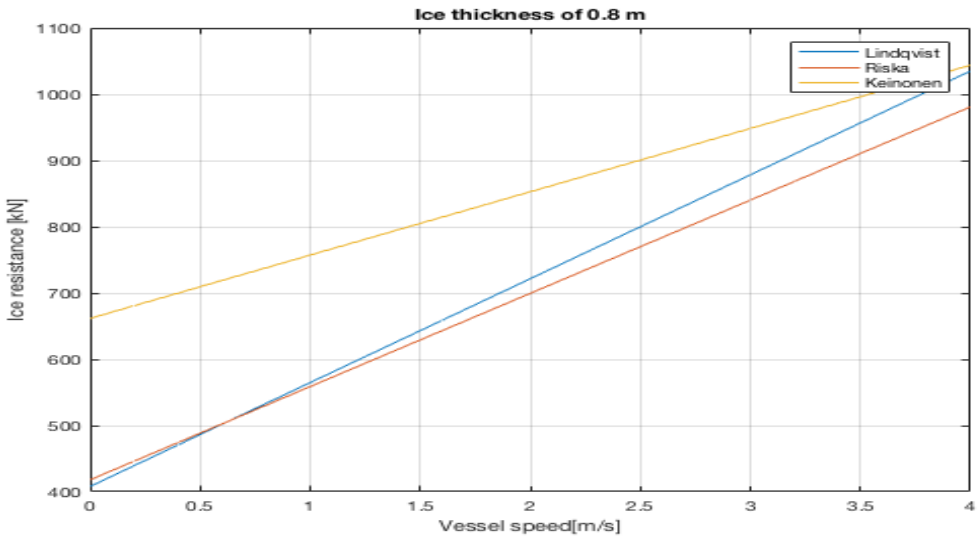

FIGURE 8.11: Riska vs Lindqvist vs Keinonen for ice thickness 0.8 m - New parameters

Here, one can see that the difference between the models at maximum resistance is lower. For low vessel speed, the calculated resistance from Keinonen seems to be over predicted compared to the resistance from the two other empirical resistance formulations. For high speeds, this difference is significantly lower. Plots for other combinations of vessel speed and ice thickness can be found in Appendix A.

Keinonen is the only one of these that are based on trials outside the Baltic waters. Since the Arctic will be in focus in this thesis, it is reasonable to assume that this model is the more precise. Nevertheless, this can not be verified without the true ice resistance for the vessel. The resistance found from KV Svalbard will be presented later in this thesis.

Chapter 9

Parameter study - Empirical models

Knowing the exact values for the different parameters can in many cases be difficult, and the values are usually chosen with some uncertainty. In this section, the presented resistance formulations will be investigated with regards to the available parameters. Since there are uncertainties connected to several of the parameters, there may be errors connected to the selected values.

To check the sensitivity in the different formulations, the results are presented with changing values for the different parameters. This sensitivity is presented as the ratio between the calculated resistance with and without modified parameter values. In the three presented models there are some variation in changeable parameters. In Erceg and Ehlers 2017 the involved parameters were presented as shown in Table 9.1.

Parameter	**Symbol**	**Lindqvist**	**Riska**	**Keinonen**
Ship speed	v	x	x	x
Ship length	L	x	x	x
Ship breadth	B	x	x	x
Ship draft	T	x	x	x
Bow length	L_{bow}		x	
Parallel mid-body length	L_{par}		x	
Waterline angle	α	x		
Buttock angle	β			x
Bow flare angle	ψ	x		x
Stem angle	ϕ	x	x	
Ice thickness	h	x	x	x
Flexural strength	σ	x		x
Youngs modulus	E	x		
Temperature				x
Poisson's coefficient	ν	x		
Density of ice	ρ_{ice}	x		
Density of water	ρ_{sw}	x		x
Hull-ice friction	μ	x		x
Snow thickness	h_s			x
Ice surface temperature	t			x
Hull condition factor	C_h			x
Factor of salinity of water	C_s			x

TABLE 9.1: Comparison of involved parameters

In this investigation, a MATLAB script developed by Skår 2011 was used. Some modifications have been made, with the additional resistance formulation, Keinonen, and different limits for changing the parameters. In this thesis the change of parameteres are set to 30%. In most cases a change this big will not be possible without affecting other variables. Nevertheless, this will clearly illustrate the importance of each parameter. In the thesis, only results for an ice thickness of 1.25 m and a vessel speed of 2.5 m/s will be presented, with results from other combinations of vessel speed and ice thickness presented in Appendix B.

9.1 Length of bow

The length of bow, L_{bow}, is one of the parameters used in the Riska model. As shown in Figure 9.1, the resistance will decrease when decreasing the length og bow. In reality, this variable can not be changed without modifying other parameters, since this change will strongly affect the total length and displacement of the vessel.

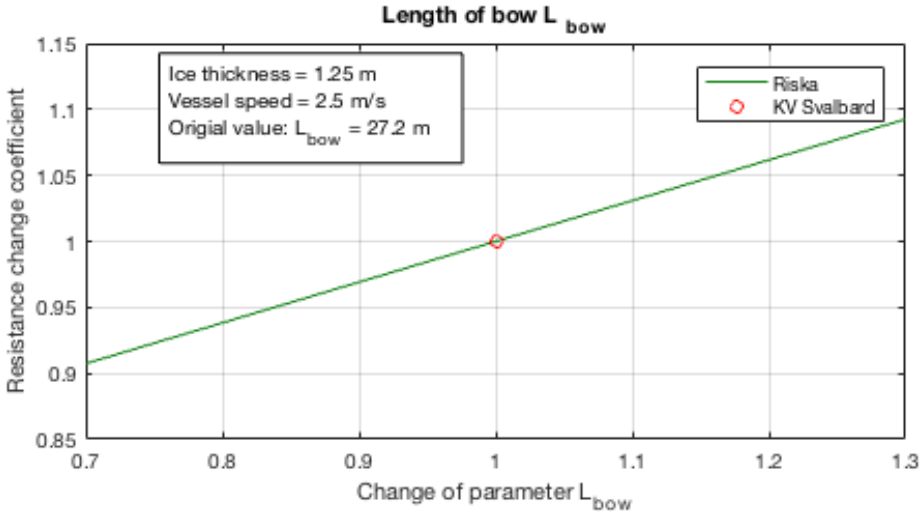

FIGURE 9.1: Sensitivity when changing the length of bow

9.2 Length of parallel mid-body

As with the length og bow, the length of parallel mid-body is a parameter used in the Riska formulation. Neither this parameter can be changed without causing major changes to the vessel. Figure 9.2 shows the sensitivity when changing this value.

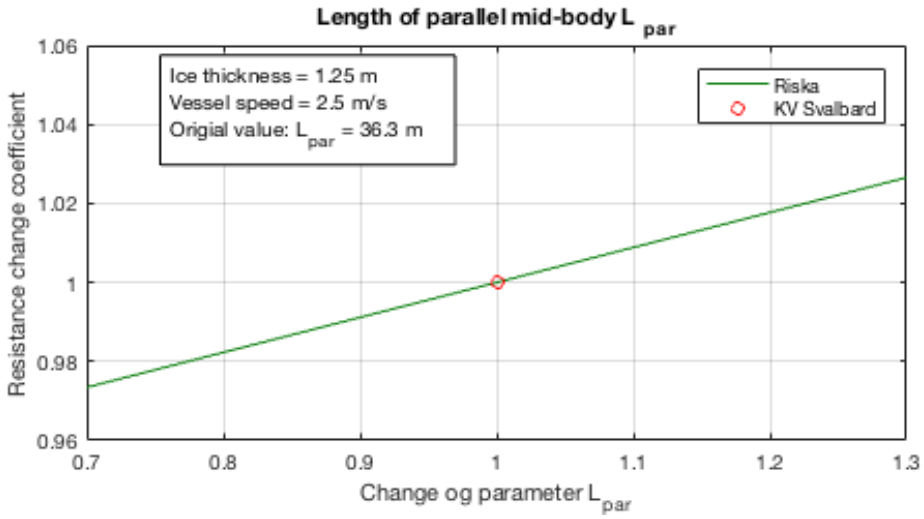

FIGURE 9.2: Sensitivity when changing the length of parallel mid-body

9.3 Water line entrance angle

The water line entrance angle, α, is used in the Lindqvist model. As shown in Figure 9.3, the changes in resistance is quite small for an increased angle. For an 30% increase in water line entrance angle, the resistance decreases less than 1%. For a decrease in the alpha angle, this will have a bigger impact on the resistance. Here it is shown that decreasing the angle will affect the resistance, and this will get bigger for larger variations of this parameter.

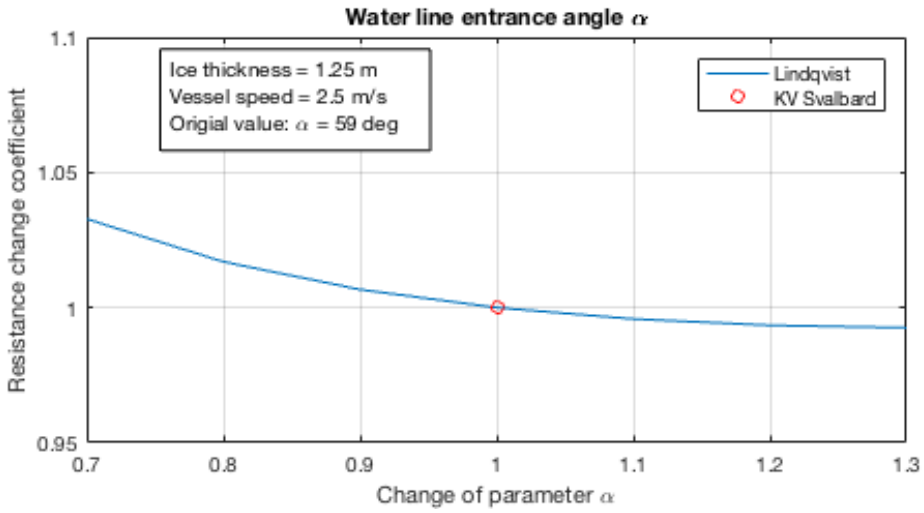

FIGURE 9.3: Sensitivity when changing the water line entrance angle

9.4 Buttock angle

The buttock angle, β, is only included in the Keinonen model. For a 30% increase in the buttock angle, the resistance increases 16%. For a 30% decrease, the resistance decreases 13%. From the plots in Appendix B, one can see that this relation is the same for other combinations of vessel speed and ice thickness.

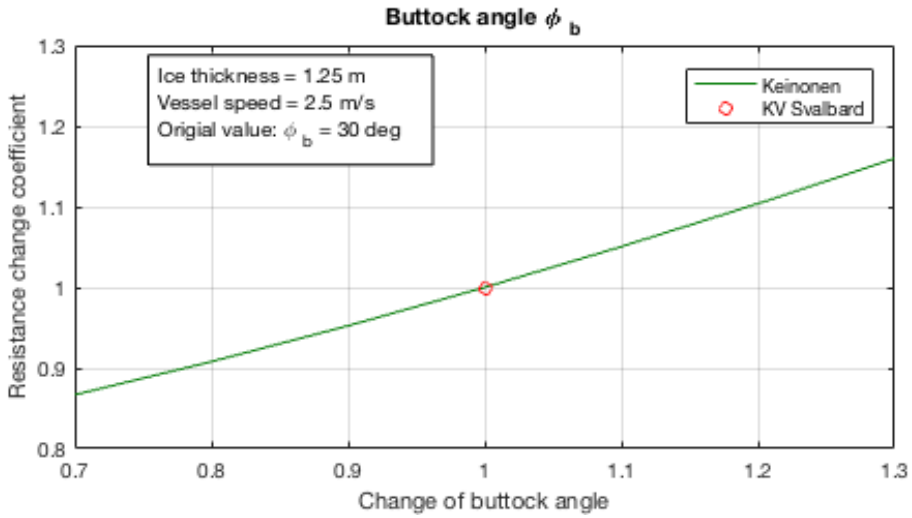

FIGURE 9.4: Sensitivity when changing the buttock angle

9.5 Stem angle

The stem angle ϕ is important in both the Riska and the Lindqvist model. As shown in Figure 9.5, the stem angle affects the Riska formulations linearly, while it is affecting the Lindqvist formulation more exponentially. One can also see that changes in this parameter will have a bigger influence on the Lindqvist than on the Riska. The same behavior is also found for different combinations of vessel speed and ice thickness as presented in Appendix B.

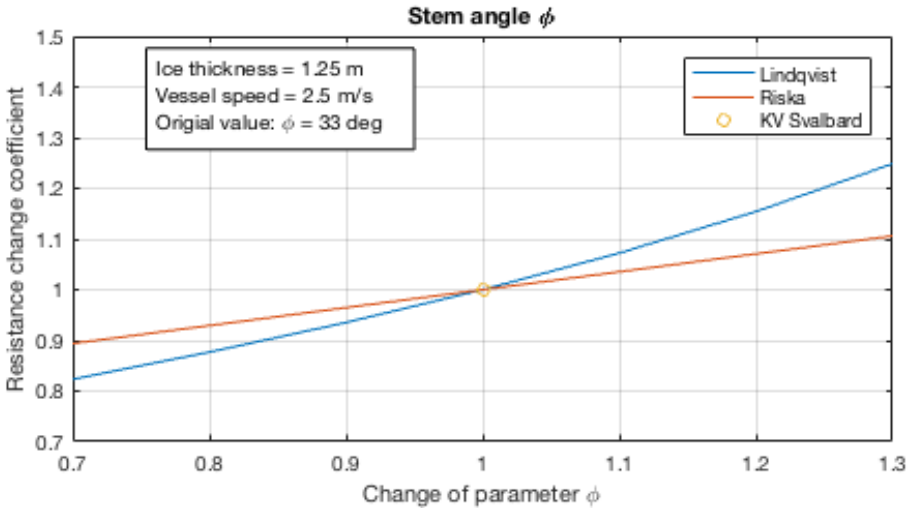

FIGURE 9.5: Sensitivity when changing the stem angle

9.6 Flexural strength

For the flexural strength, σ, this is a parameter in the Keinonen and the Lindqvist model. For the Riska model, this parameter in implemented through constants. As shown in Figure 9.6, both models behave linearly to the flexural, but that the change of this value will have a bigger impact on the Lindqvist than the Keinonen formulation. From Appendix B, one can see that this is also the case for different speeds and ice thicknesses.

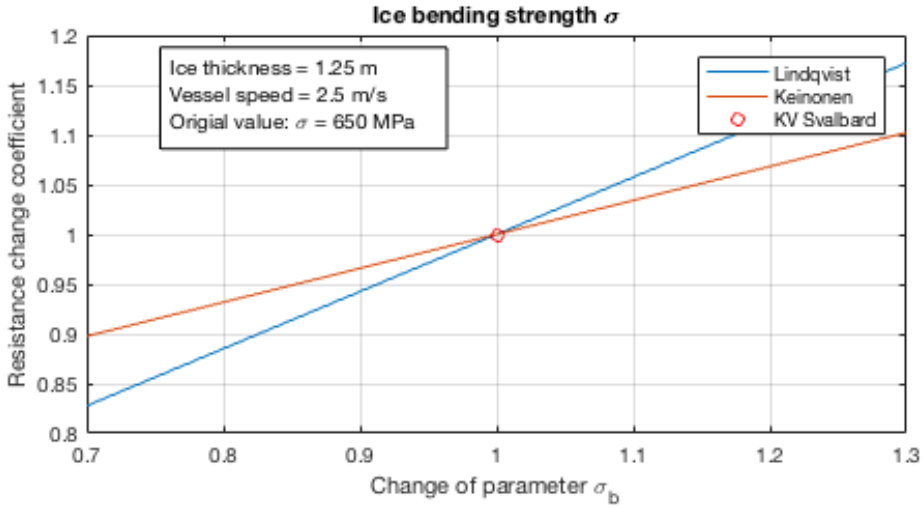

FIGURE 9.6: Sensitivity when changing the flexural strength

9.7 Hull-ice friction coefficient

Hull-ice friction coefficient, μ, is a parameter in Lindqvist and behaves linearly. As for the flexural strength, this parameter is included in Riska through constants. From Figure 9.7, one can see that for a 30% increase/decrease in the hull-ice friction coefficient the resistances increases/decreases approximately 13%. Additional plot from Appendix B show the same trend.

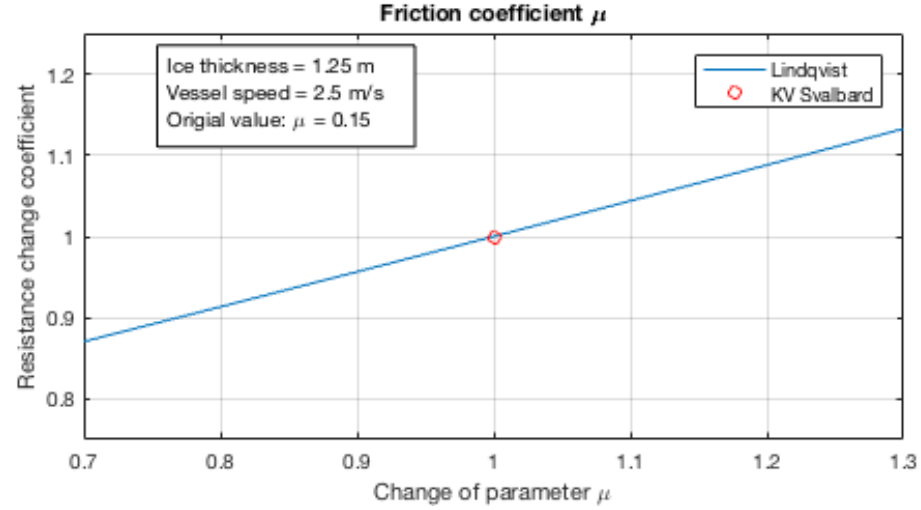

FIGURE 9.7: Sensitivity when changing the friction coefficient

9.8 Temperature

Changes in temperature are only accounted for in the Keinonen model. In reality, changing this value will lead to changes in other parameters, as shown in Figure 3.5. Here one can see that the flexural strength of sea ice is strongly connected to the temperature.

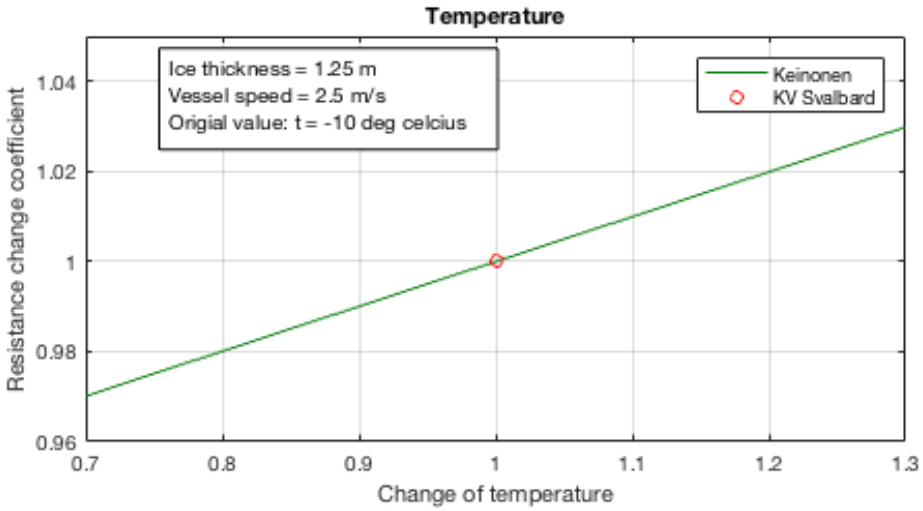

FIGURE 9.8: Sensitivity when changing the temperature

9.9 Parameter study conclusion

As mentioned, result for other combinations of vessel speed and ice thickness are presented in Appendix B. A summary of the result are presented in Table 9.2. Here, the different changes in resistance for modified parameters are shown.

The sensitivity of the Riska model is hard to determine for several of the parameters. In this formulation, multiple parameters are included through constants and can therefore not be modified. Nevertheless, it is reasonable to assume that the sensitivity will be in the same order of magnitude as the the Lindqvist formulation.

TABLE 9.2: A summary of resistance changes when modifying parameters

		Resistance - h [m] - v [m/s]														
		h=0.5, v=5			h=0.75, v=4			h=1, v=3.25			h=1.25, v=2.5			h=1.5, v=1.5		
Parameter	**Change**	Lin	Ris	Kei	Lin	Ris	Kei	Lin	Ris	Kei	Lin	Ris	Kei	Lin	Ris	Kei
LENGTH OF	0.7	-	0.93	-	-	0.92	-	-	0.92	-	-	0.91	-	-	0.89	-
BOW L_{BOW}	1.3	-	1.07	-	-	1.08	-	-	1.08	-	-	1.09	-	-	1.11	-
LENGTH PARALLEL	0.7	-	0.978	-	-	0.977	-	-	0.976	-	-	0.973	-	-	0.97	-
MID-BODY L_{PAR}	1.3	-	1.022	-	-	1.023	-	-	1.024	-	-	1.027	-	-	1.03	-
WATER LINE	0.7	1.03	-	-	1.03	-	-	1.03	-	-	1.03	-	-	1.03	-	-
ENTRANCE ANGLE α	1.3	1	-	-	0.99	-	-	0.99	-	-	0.99	-	-	0.99	-	-
BUTTOCK	0.7	-	-	0.87	-	-	0.87	-	-	0.87	-	-	0.87	-	-	0.87
ANGLE β	1.3	-	-	1.14	-	-	1.14	-	-	1.14	-	-	1.14	-	-	1.14
STEM	0.7	0.87	0.9	-	0.85	0.9	-	0.83	0.9	-	0.82	0.9	-	0.87	0.9	-
ANGLE ϕ	1.3	1.2	1.1	-	1.22	1.1	-	1.23	1.1	-	1.25	1.1	-	1.2	1.1	-
FLEXURAL	0.7	0.87	-	0.93	0.85	-	0.92	0.84	-	0.91	0.83	-	0.9	0.82	-	0.89
STRENGTH σ	1.3	1.13	-	1.07	1.15	-	1.08	1.16	-	1.09	1.17	-	1.1	1.18	-	1.11
HULL-ICE	0.7	0.86	-	-	0.864	-	-	0.868	-	-	0.872	-	-	0.88	-	-
FRICTION μ	1.3	1.14	-	-	1.136	-	-	1.132	-	-	1.128	-	-	1.12	-	-
TEMPERATURE	0.7	-	-	0.97	-	-	0.97	-	-	0.97	-	-	0.97	-	-	0.97
°C	1.3	-	-	1.03	-	-	1.03	-	-	1.03	-	-	1.03	-	-	1.03

As shown in the table above, there is a large variation in the influence each parameter has on the resistance. One can also see that for some of the parameters there are big variations for different vessel speeds and ice thicknesses, while others are quite independent of these.

A parameter that experience relatively big variations for different combinations of speed and thickness is the flexural strength. For h=0.5 and v=5, the resistance changes 13% for a 30% change in flexural strength using the Lindqvist model. For a higher ice thickness and a lower vessel speed (h=1.5 and v=1.5) the flexural strength has a bigger influence. Here the resistance changes 18% for a 30% change i flexural strength.

Chapter 10

Estimation of resistance from measurements

From the results of the ice load monitoring system project, the ship resistance could be estimated. Following the procedure presented by Suyuthi, B. J. Leira, and Riska 2011, the resistance from KV Svalbard were found by utilizing Newton's second law and conservation of energy. This procedure is described below. The estimated resistance will be used to evaluate the results from the analytical resistance models presented in Chapter 8.

10.1 The work-kinetic energy theorem

The work-kinetic energy theorem states that the net work done by the forces, W_{net}, is equal to the changes in kinetic energy resulting from application of external forces. This can be expressed as:

$$W_{net} = \Delta K = K_f - K_i \tag{10.1}$$

Where,

- Δ K = change of kinetic energy
- K_f = final kinetic energy
- K_i = initial kinetic energy

The formulation shown in Equation 10.1 is based on Newton's second law:

$$F_{net} = \sum F = ma \tag{10.2}$$

$$W_{net} = \int_{S_i}^{S_f} ma \ \ dS \tag{10.3}$$

$$\Delta K = K_f - K_i = \frac{1}{2}mv_f^2 - \frac{1}{2}mv_i^2 \tag{10.4}$$

Where,

- m = mass of the ship
- v_f = final velocity
- v_i = initial velocity

To maintain a constant speed, it is obvious that to overcome the resistance force, $F_{resistance}$, a certain thrust force, F_{thrust}, is needed. This is shown in Figure 10.1

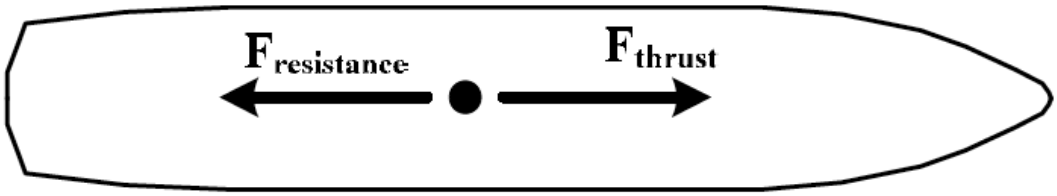

FIGURE 10.1: For a specific speed, total resistance experienced by the ship is balanced by thrust force (Suyuthi, B. J. Leira, and Riska 2011)

According to the work-kinetic energy theorem, the net work, W_{net}, is the sum of all works done by individual forces. In this case, work are done by propeller thrust and resistance. Hence:

$$W_{net} = W_{thrust} - W_{resistance} \tag{10.5}$$

10.2 Propeller thrust

To properly measure the propeller thrust, advanced measuring instruments are needed. However, power delivered to the shaft is available and can be used to estimate the thrust. This is a big simplification, and will give a higher resistance than expected, since the propeller efficiency is set to be one, but in reality will be lower. In further calculations, the propeller efficiency will be set to 0.9.

$$W_{thrust} = \int_{t_i}^{t_f} P \ dt \tag{10.6}$$

Where,

- t_f = final time
- t_i = initial time
- P = power delivered

10.3 Resistance

By using the presented equations, the total work done by resistance is equal to the sum of work done by thrust and change of kinetic energy.

$$W_{resistance} = \int_{t_i}^{t_F} P \ dt - \frac{1}{2} m(v_f^2 - v_i^2) \tag{10.7}$$

From this, the resistance force, $F_{resistance}$, is given by:

$$F_{resistance} = \frac{dW_{resistance}}{ds} \tag{10.8}$$

Chapter 11

Data selection

As mentioned in Section 5.2, the ILM project was created by DNV GL, and during the winters of 2007 and 2008 KV Svalbard was equipped with a prototype of this system. These measurements gave a lot of raw data, and to be able to use them some filtering was needed. To ensure good results, only periods with stable ice conditions were used.

To filter the results, Torstein Skaar developed a MATLAB script for automatic selection of data in his master thesis. To measure how a variable changes over a time span, the coefficient of variation was used. This coefficient is given as in Equation 11.1.

$$CV = \frac{\sigma}{|\mu|} \tag{11.1}$$

Where;

- σ is the standard deviation
- μ is the mean value

The variable of interest are vessel speed, ice thickness, engine power and vessel heading. In the MATLAB script different threshold values for the different variables are defined. The variables and maximum values for coefficient of variation used in this thesis are presented in Table 11.1. Due to the high variations in measured ice thickness, this value is allowed a higher coefficient of variation than the other variables.

TABLE 11.1: Variables of interest and max values for CV

Parameter	Max CV
Vessel speed	0.1
Ice thickness	0.5
Engine power	0.2
Vessel heading	0.4

To ensure that only relevant values were selected for further calculations, some values needed to be removed. Level ice in this geographical area is expected to be up to approximately 2 meters. Some of the measured data gives values a lot higher than this, which is likely caused by errors in measurement or interactions with ice ridges. These data are not relevant for this thesis, and data with an ice thickness above 2 meters are therefore removed.

11.1 H-V curve for KV Svalbard

To find areas of interest, the H-V curve for KV Svalbard is calculated. Using parameters as presented in Table 5.2, and calculating ice resistance according to Riska, the net thrust of KV Svalbard and ice resistance for different ice thicknesses are presented in Figure 11.1. Points of interactions between resistance and net thrust marks points on the H-V curve. This curve is presented in Figure 11.2.

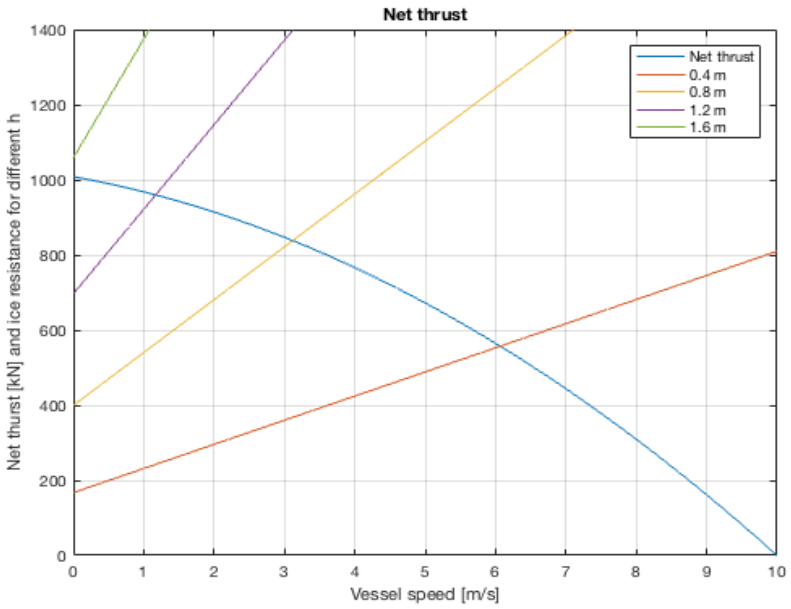

FIGURE 11.1: Net thurst of KV Svalbard and resistance for different ice thicknesses

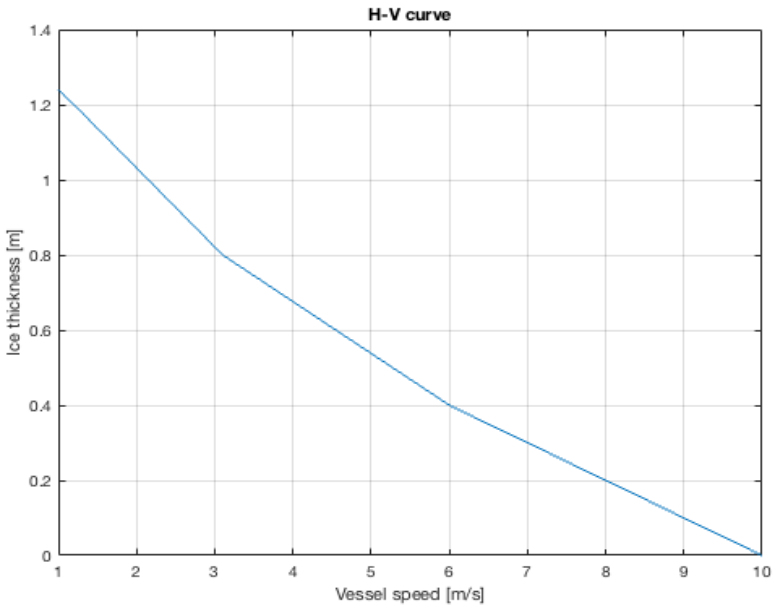

FIGURE 11.2: H-V curve for KV Svalbard

Chapter 12

Open water resistance

Information in this chapter is mainly found from Skår 2011.

To be able to compare the measured resistance from KV Svalbard with the resistance calculated from the empirical formulas, the open water resistance is needed. Both Riska and Keinonen divides their resistance formulas into ice resistance and open water resistance. Therefore, the open water needs to be added. Lindqvist do not mention the open water resistance, but it is assumed that this is also required for this model.

The open water resistance is found by reading the total resistance from KV Svalbard when the ice thickness is zero. By using the same routine in MATLAB as is Chapter 11, the open water resistance was found as a function of vessel speed. For low speeds, this resistance is approximately proportional to the vessel speed squared.

To find the resistance as a function of vessel speed, a least square regression was performed. This regression was controlled by using half of the data points for the regression and the remaining half to test it. The plot of regression is presented in Figure 12.1.

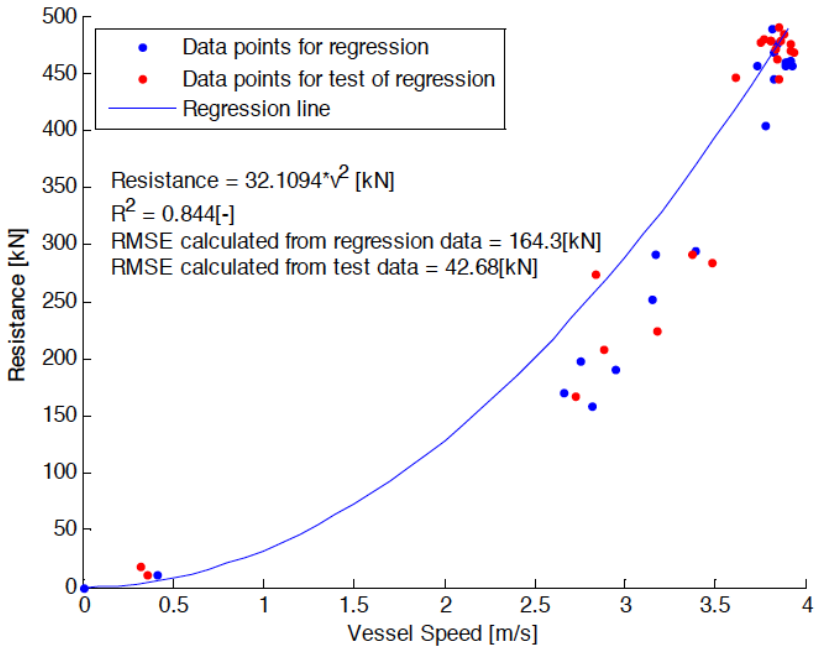

FIGURE 12.1: Open water resistance as a function of speed (Skår 2011)

Here, the blue points are used in the regression and the red points are used to test it. As shown, the curve follow the data points quite well. This is verified by the relatively high coefficient of determination, R^2 = 0.844. It is found that the open water resistance in kN is equal to 32.1094*v^2.

There are some sources of uncertainty connected to this method of calculating the open water resistance. It is assumed nos loss in energy from the propellers to net thrust. It is also assumed that the resistance will not be influenced by the likes of wind and waves.

From Figure 12.1 it is shown that all data points used in the calculations have roughly the same speed. It is therefore hard to determine the quality of the regression at lower speeds.

Chapter 13

Resistance KV Svalbard

13.1 Introduction

Using the information in Chapter 10, 11 and 12, the resistance for KV Svalbard has been calculated. The results will in this chapter be presented and compared with the resistance calculated from the three empirical ice resistance formulations. The calculated open water resistance will be added together with the ice resistance from Lindqvist, Riska and Keinonen to get more realistic results. The open water resistance is given by Equation 13.1, as presented in Figure 12.1. Here, v is the vessel speed.

$$R_{ow} = 32.1094 * v^2 \tag{13.1}$$

To see how the measured resistances compares with the empirical resistance, the ratios between them will be calculated.

$$\text{Lindqvist ratio} = \frac{R_{measured}}{R_{Lindqvist}} \tag{13.2}$$

$$\text{Riska ratio} = \frac{R_{measured}}{R_{Riska}} \tag{13.3}$$

$$\text{Keinonen ratio} = \frac{R_{measured}}{R_{Keinonen}} \tag{13.4}$$

Where,

- $R_{Measured}$ is the estimated resistance found from measurements
- $R_{Lindqvist}$ is the resistance calculated from the Lindqvist formulation
- R_{Riska} is the resistance calculated from the Riska formulation
- $R_{Keinonen}$ is the resistance calculated from the Keinonen formulation

13.2 Ratios

Using the automated routine from Skaar, the resistance was calculated from the measured data. The following figures shows how the ratios vary for different combinations of vessel speed and ice thickness. The presented figures show the resistance for a varying vessel speed. Additional figures showing the ratios for varying ice thicknesses and vessel speeds are presented in Appendix C.

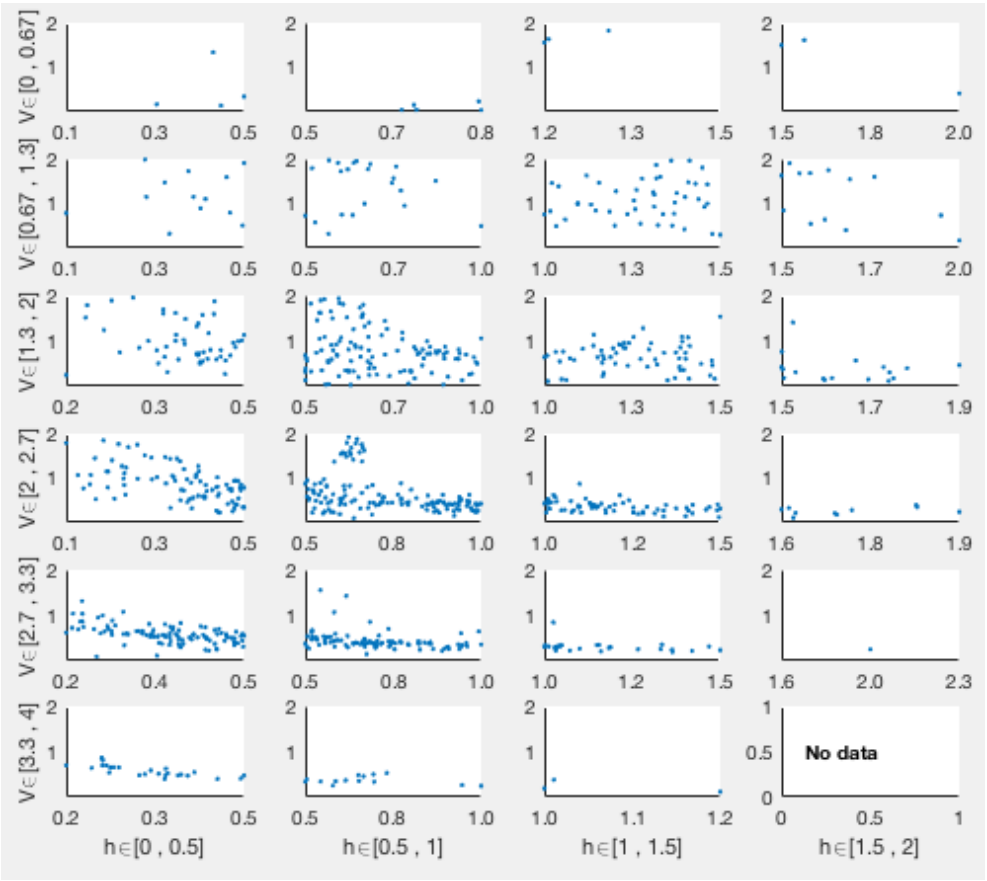

FIGURE 13.1: Ratios between measured and Lindqvist for varying thickness

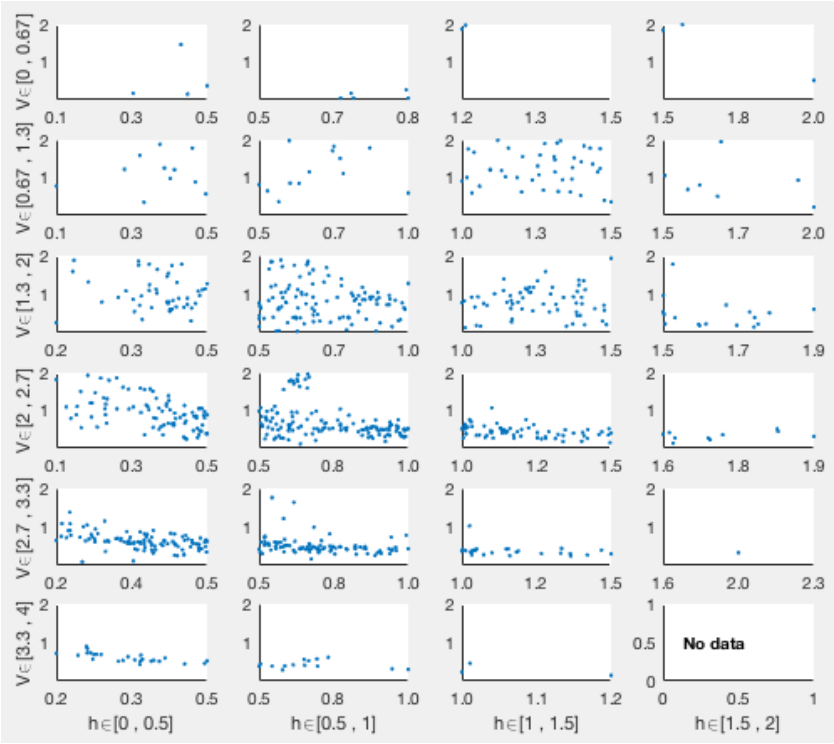

FIGURE 13.2: Ratios between measured and Riska for varying ice thickness

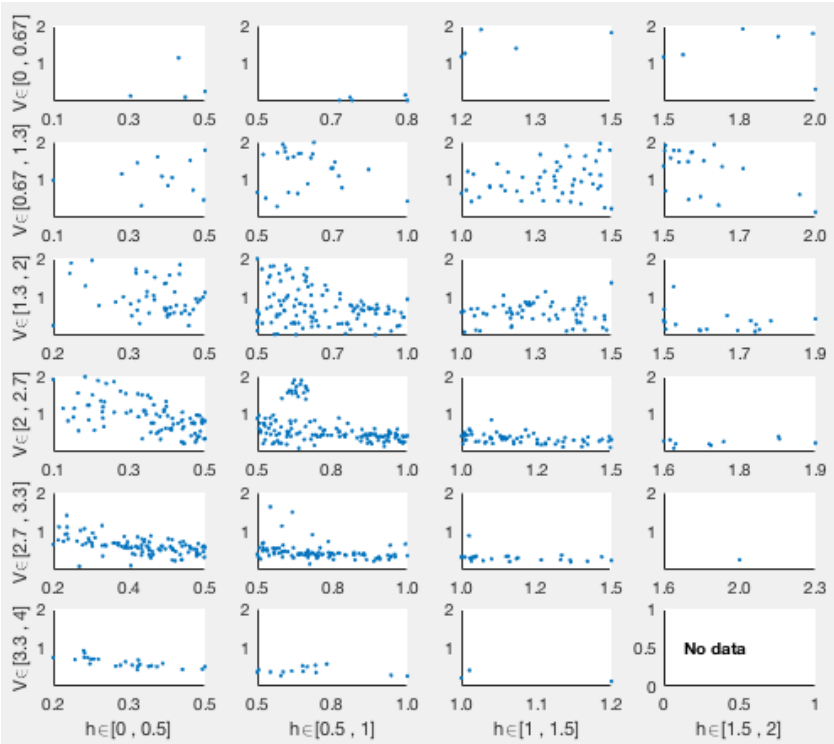

FIGURE 13.3: Ratios between measured and Keinonen for varying ice thickness

13.3 Higher quality data

The data used in this thesis are not of high quality. Finding areas with stable conditions are difficult, with big variations in ice thickness and temperature. The low quality of data have also been verified by a big scatter in the estimated ratios.

In the work for his PhD thesis, Abdillah Suyuthi worked with the same data as used in this master thesis (Thorsen 2012). He investigated a number of 30 second intervals, with relatively stable conditions. The following figures show ratios for varying vessel speed and ice thickness. Additional plot can be found in Appendix

13.3.1 Lindqvist ratios

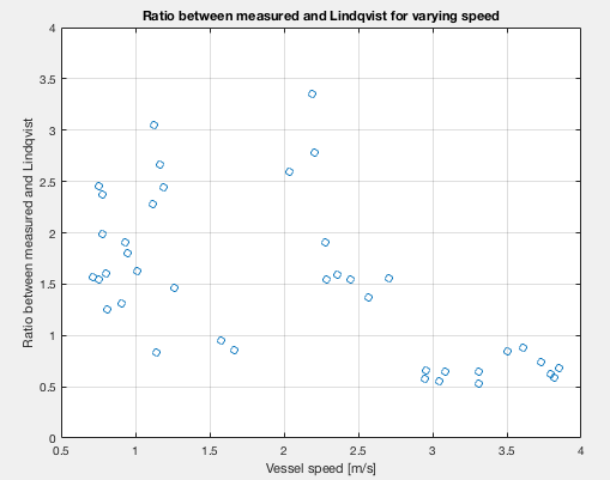

FIGURE 13.4: Varying vessel speed

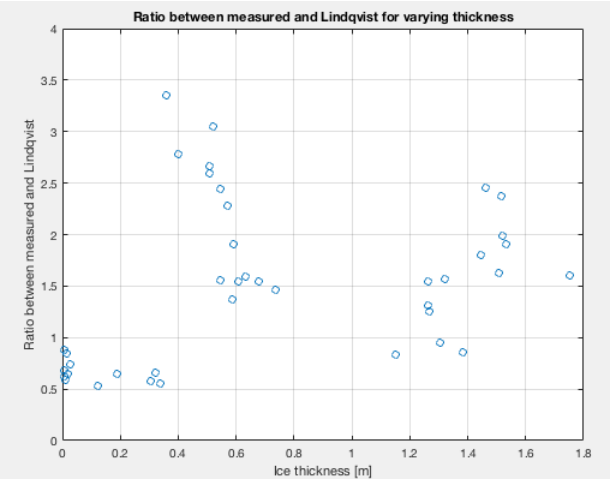

FIGURE 13.5: Varying ice thickness

13.3.2 Riska ratios

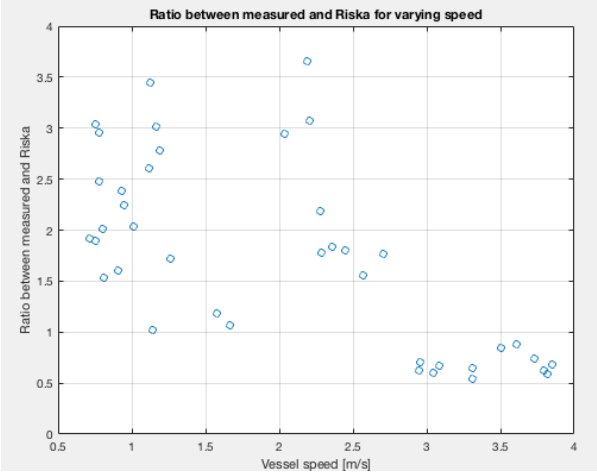

FIGURE 13.6: Varying vessel speed

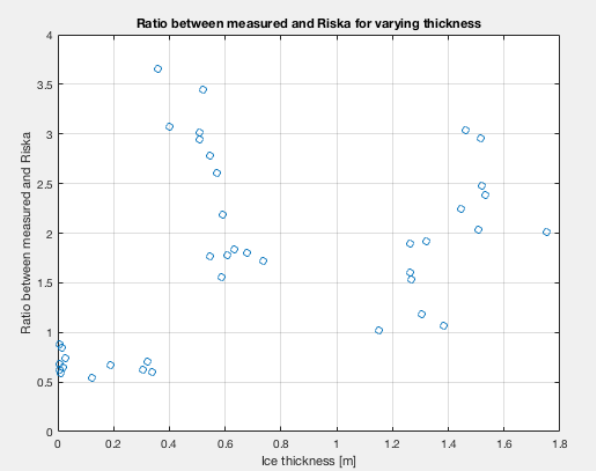

FIGURE 13.7: Varying ice thickness

13.3.3 Keinonen ratios

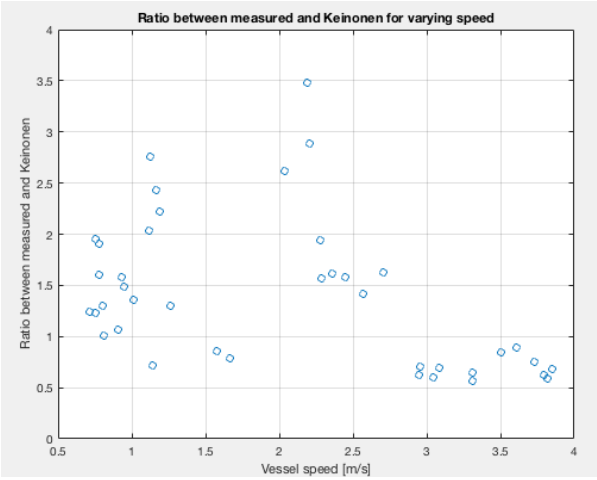

FIGURE 13.8: Varying vessel speed

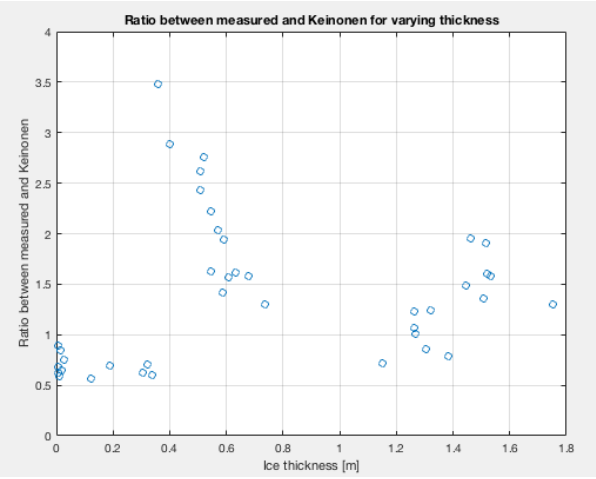

FIGURE 13.9: Varying ice thickness

13.4 Propeller efficiency

Without access to the propeller curves, the propeller efficiency is hard to determine. For the previous results, this efficiency is assumed to be 0.9. To see how the results are affected by different efficiencies, the the ratios between measured resistance and resistance from the empirical formulations are found for multiple propeller efficiencies. The different ratios are presented in Table 13.1.

TABLE 13.1: Mean ratio for different propeller efficiencies

Propeller efficiency	Lindqvist	Riska	Keinonen
100%	1.1724	1.3328	1.1489
90%	1.0546	1.1989	1.0334
80%	0.9368	1.0651	0.9180
70%	0.8190	0.9312	0.8025

As shown in the table above, the ratios decrease for lowered propeller efficiencies. This is as expected, as a lower efficiency leads to a decreased power consumption, which again leads to a lower resistance. To see how the the different ratios differ from the mean values, the different standard deviations are presented in Table 13.2

TABLE 13.2: Standard deviations for different mean ratios

Propeller efficiency	Lindqvist	Riska	Keinonen
100%	2.663	2.696	3.483
90%	2.397	2.462	3.135
80%	2.131	2.157	2.787
70%	1.864	1.887	2.439

Using the data from Suyuthi, ratios for different propeller efficiencies are presented in Table 13.3.

TABLE 13.3: Mean ratio for different propeller efficiencies using higher quality data

Propeller efficiency	Lindqvist	Riska	Keinonen
100%	1.672	1.936	1.540
90%	1.505	1.743	1.395
80%	1.337	1.549	1.239
70%	1.170	1.335	1.084

The standard deviations for different mean ratios using data from Suyuthi are presented in Table 13.4.

TABLE 13.4: Standard deviation for different mean ratios using higher quality data

Propeller efficiency	Lindqvist	Riska	Keinonen
100%	0.866	1.024	0.812
90%	0.780	0.922	0.731
80%	0.694	0.820	0.650
70%	0.607	0.718	0.569

13.5 Discussion

The figures in Chapter 13.2 shows the different ratios between empirical and measured resistance for different combinations of ice thickness and vessel speed. For all the figures, one can see that there is a high variation in the ratios for low vessel speed. For higher vessel speed, this variations is significantly lower. This trend can also be seen from the figures presented in Appendix C.

Using the higher quality data from Suyuthi, the different ratios were presented as with the data from Skaar. Here, the number of data points were significantly decreased. From the figures one can see the same trends as for the lower quality data. For lower vessels speeds, there are big variations in the ratios, while for higher speed this variation is lower. Using this data also gives stable conditions for low ice thicknesses.

Propeller efficiencies using data from both Skaar and Suyuthi are presented. Interestingly, the data from Skaar gives the best ratios, with the lowest variation from the empirical formulations. However, one can see that the standard deviations using the data from Skaar are significantly higher compared to the standard deviations from Suyuthi.

Chapter 14

Plate model and ice pressures

Vessel going in ice-infested waters will be exposed to ice loads. In chapter 15 the objective is to see how these ice loads affect local sections of a hull. This chapter describes the plate model and how this is created and analyzed using Abaqus. This includes material properties, boundary conditions and ice pressures.

The finite element analysis will be conducted using non-linear theory, as presented in Chapter 7. The model will be investigated using ice pressures as presented in Chapter 4.2 and according to the DNVGL regulations.

14.1 Hull section

In this analysis, KV Svalbard is used as a reference. Since an actual model of this vessel have not been available for this thesis, a model is created. Some assumptions have been made, and some of the chosen dimensions used is necessarily 100 percent accurate compared to KV Svalbard. The contact area and ice pressure remains constant throughout the analysis. In reality this will not be the case, with both pressure and contact area varying as the ship moves forward.

When determining the different dimensions needed in this analysis, this was done according to ice classifications from DNV GL. KV Svalbard has ice classification Icebreaker Polar 10, and these regulations will therefore be used when determining parameters such as stiffener plate thickness, section modulus, ice contact height and ice pressure.

The hull section chosen for this analysis is located in the bow area of the vessel. It is assumed that the section is at the water line of the ship, which means that the ice pressure will hit the middle part of the plate.

The boundary conditions for this plate were chosen to be fixed along the edges of the plate and in the clamping of the stiffeners. This is assumed to be reasonable, since the plate is fixed by longitudinal webs in the top and bottom and transverse girders at the sides.

14.1.1 Plate

The plate selected for this analysis has a height of 2.4 m. This corresponds with a stiffener spacing of 0.4 m. The breadth was chosen arbitrary and sat to be 2.4 m.

When choosing the plate thickness for this section, this was done as presented in Chapter 6.3.2. Here, the plate thickness can be found as:

$$t = 23k_a \frac{s^{0.75}}{h_o^{25}} \sqrt{\frac{k_w p_o}{m_p \sigma_f}} + t_k \quad [mm] \tag{14.1}$$

$$k_a = 1.1 - \frac{s}{l}, \quad \text{maximum 1.0, minimum 0.85} \tag{14.2}$$

$$k_w = 1.3 - \frac{4.2}{(\frac{a}{s} - 1.8)^2}, \quad \text{maximum 1.0} \tag{14.3}$$

By inserting values, k_a and k_w can be found to be 0.93 and 0.76, respectively. By reading Table F1 in DNVGL 2016, m_p is found to be 2.68. Inserting values into Equation 14.1, this gives a plate thickness of 28 mm. All dimensions chosen for this plate can be found from Table 14.1.

TABLE 14.1: Plate field dimensions

Parameter	Value
Stiffener spacing	0.4 m
Plate height	2.4 m
Plate breadth	2.4 m
Plate thickness	28 mm

For the model to be a good approximation of KV Svalbard, the plate is slightly curved. The values for this curvature were assumptions, and not based on data obtained from KV Svalbard. Hence, there are some uncertainty connected to this curvature.

14.1.2 Stiffeners

As with the plate thickness, the stiffener dimensions were chosen according to rules from DNVGL as presented in Chapter 6.3.2. By using Equation 6.18, the minimum section modulus for a stiffener can be found. Choosing values for both γ and ϕ to be 60 degrees, the β can be found to be approximately 63 degrees. This gives a minimum section modulus of 120.2 cm^3. Using this, the stiffener dimensions can be chosen as presented in Table 14.2.

TABLE 14.2: Stiffener dimensions

Parameter	Value
Flange thickness	18 mm
Flange width	120 mm
Web height	150 mm
Web thickness	18 mm

The chosen stiffener dimension gives a section modulus of 121 cm^3 , which is slightly higher than the required minimum given by DNVGL.

14.1.3 Material properties

In this model, the material properties chosen will be the same for the plate and the stiffeners. The values used are presented in Table 14.3.

TABLE 14.3: Material properties

Parameter	Value
Yield strength	490 MPa
Ultimate strength	674 MPa
Steel density	7.85
Elastic modulus	$2.07 * 10^{11}$ Pa

To estimate the plastic behavior of steel, the material was assumed to behave non-linear. Table 14.4 presents how this plastic behavior is applied in this master thesis (CAE 2013).

TABLE 14.4: Stress/strain from CAE 2013

Stress σ MPa	Plastic strain ϵ_p
490	0.0
513	0.002
526	0.0038
539	0.0065
554	0.011
568	0.0163
583	0.0219
610	0.0358
633	0.0509
652	0.0682
674	0.0901

14.1.4 Model

Using the dimensions for plate and stiffeners, a model has been created. The model is presented in Figure 14.1. Here both the plate, stiffeners and load patch area are clearly visible. The plate is colored green, the stiffeners are red and the load patch is colored yellow.

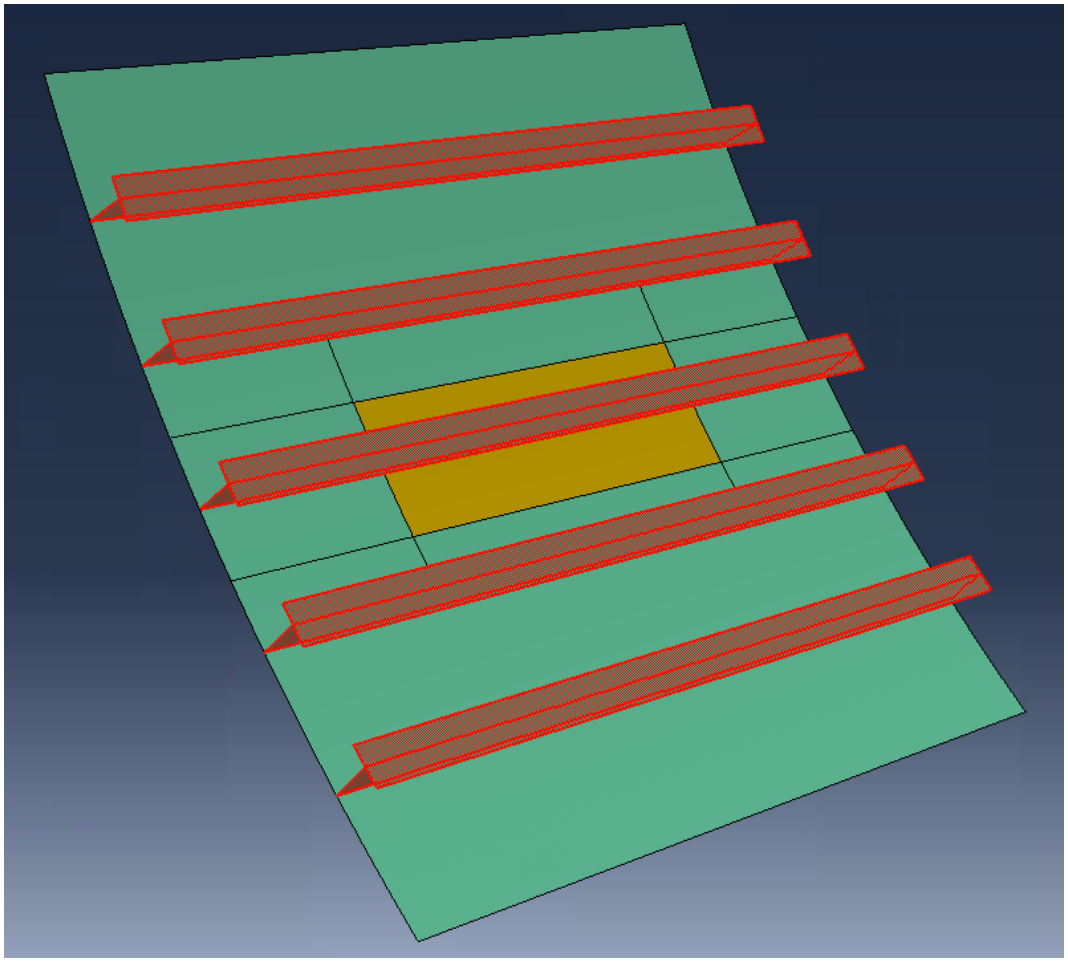

FIGURE 14.1: Plate model used in analysis

14.2 Ice pressures

As mentioned, two different ice pressures will be used in this analysis. The first ice pressure will be according to the ice classifications from DNV GL for KV Svalbard, while the second ice pressure will be based on empirical calculations.

14.2.1 Ice pressure according to DNVGL

KV Svalbard has classification Icebreaker Polar 10, which corresponds to nominal ice strength of 7 MPa and a nominal ice thickness of 1 m, as presented in Table 6.3. By using the procedure shown in Chapter 6.3.1, the design ice pressure can be calculated as:

$$p = F_B * 1000 * F_A * \sigma_{ice} \tag{14.4}$$

Where,

- F_B as shown in Equation 14.5 for contact area smaller than 1 m^2
- F_A = 1.0 for bow area
- σ_{ice} = 7 MPa

$$F_B = \frac{0.58}{\sqrt{A_c}} \tag{14.5}$$

In general, the contact area is set to $0.4h_{ice}$. This leads to a height of 0.4 m. The breadth of the pressure field was chosen to be 1.2 m, giving a contact area, A_c of 0.48 m. From this the design ice pressure is found to be 5.86 MPa.

14.2.2 Ice pressure from empirical calculations

As presented in Chapter 4.2, the ice pressure can be found as:

$$p_c = \frac{F_n}{A_c} = \frac{C * \sigma_f * h_i^2}{A_c * (sin\beta - \mu * cos\beta)} \tag{14.6}$$

Here, C is set to be 0.5, as presented in Chapter 4.2. The flexural strength of ice and the friction coefficient is chosen as shown in Table 3.3. The ice thickness and contact area is set to be the same as in Section 14.2.1.

TABLE 14.5: Values used to find ice pressure from empirical calculations

Parameter	Value
C	0.5
σ_f	650 KPa
h	1 m
A_c	0.48 m^2
β	63 degrees
μ	0.15

Inserting values from Table 14.5 into Equation 14.6, the empirical ice pressure is found to be 0.823 MPa.

14.2.3 Selected values

The two different ice pressures that are used in the analyzes are presented in Table 14.6. It is a big difference between the two ice pressures, with the pressure from DNV GL being roughly seven times higher than the one from empirical calculations. For a load patch area of 0.48 m^2, this corresponds to total forces of 2.813 and 0.395 MN for the DNV GL and empirical ice pressure, respectively.

TABLE 14.6: Values used to find ice pressure from empirical calculations

Ice pressure	Value
DNV GL ice pressure	5.86 MPa
Empirical ice pressure	0.823 MPa

When running a non-linear analysis, the total load is divided into smaller increments. The size of each increment are decided by the chosen value for the first increment and the total number of increments. In this case, the first increment is the model without ice pressure. The applied pressure will increase for every increment, until the sum of increments reaches 1 and the full pressure is applied to the model.

Chapter 15

Ice Pressure Analysis

Using Abaqus, the chosen plate section has been analyzed using the two ice pressures presented in Section 14.2. The pressures were assumed to be static and were applied in the centre of the plate, hitting the middle stiffener. Throughout the analyzes, the mesh size for the model was set to 20 mm. The objective of these analyzes is to see how the panel is affected by the two different ice pressures. In this master thesis the focus will be on Von Mises stresses and displacement.

Figure 15.1 and Figure 15.2 shows displacement and Von Mises stresses, respectively, for the plate section with ice pressure according to DNV GL regulations. For the empiric calculations, the displacements are shown in Figure 15.3 and the Von Mises stresses are shown in Figure 15.4. For additional plots of stresses in x- and z-direction, see Appendix D.

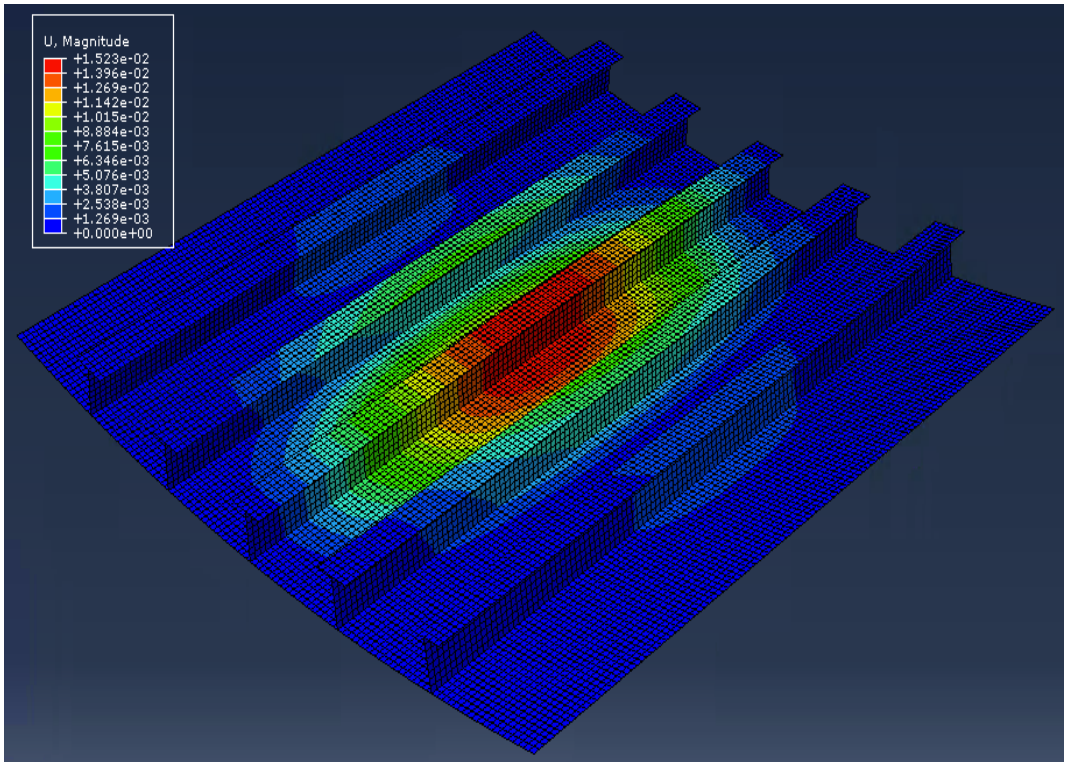

FIGURE 15.1: Displacement with ice pressure according to DNVGL

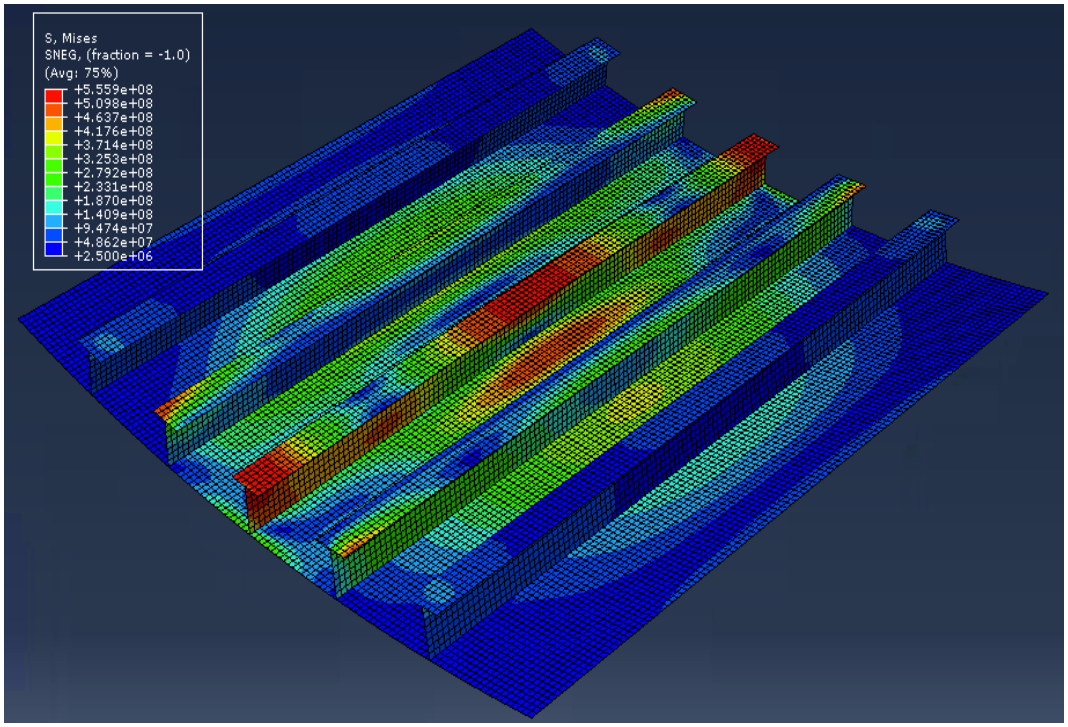

FIGURE 15.2: Von Mises stresses with ice pressure according to DNVGL

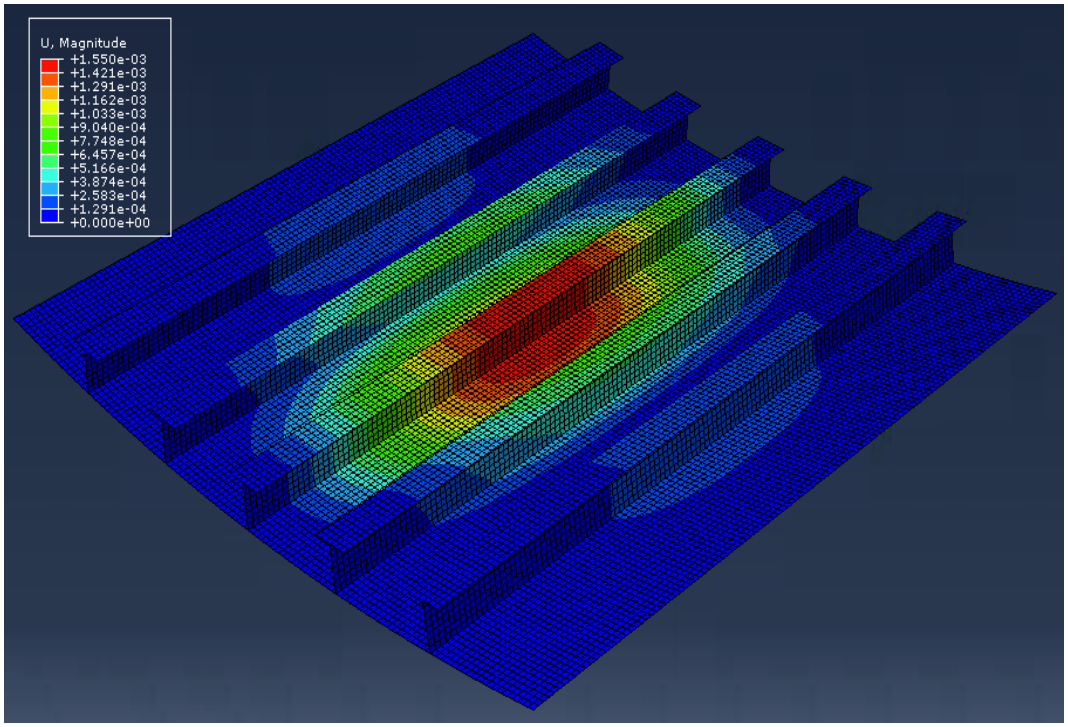

FIGURE 15.3: Displacement with ice pressure according to empiric calculations

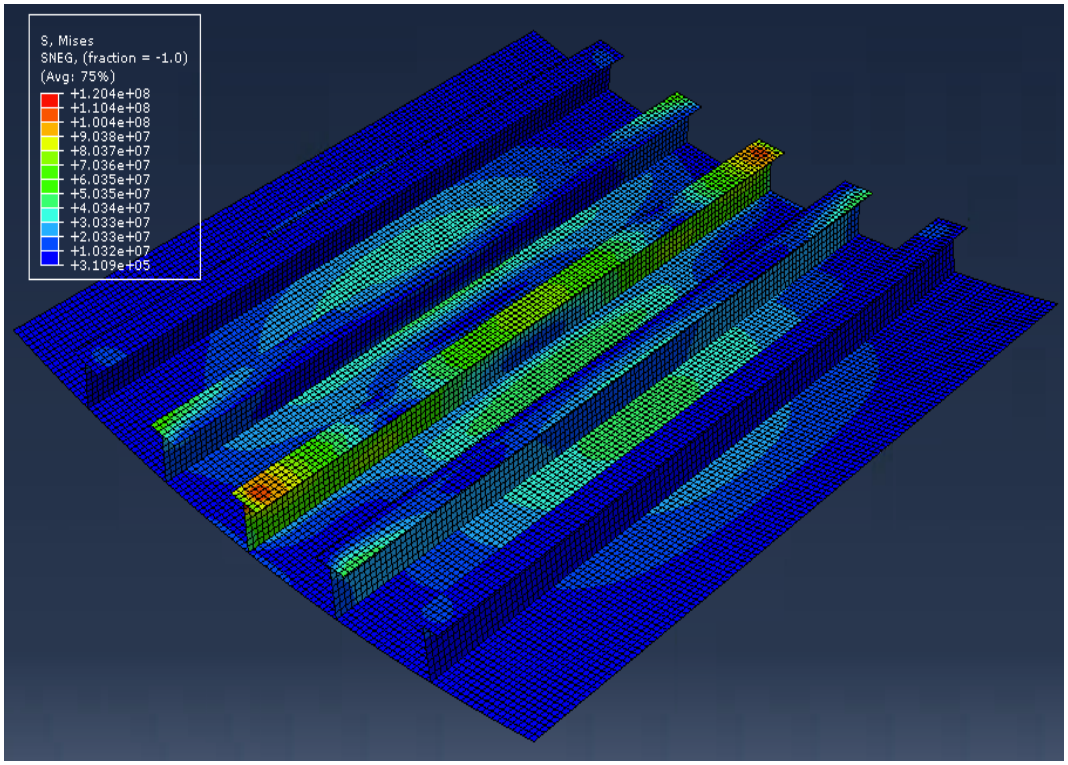

FIGURE 15.4: Von Mises stresses with ice pressure according to empiric calculations

From Figure 15.1, the maximum displacement was found to be 16.70 mm, located at the center of the plate section. From Figure 15.2, the maximum Von Mises stresses were found to be 552.2 MPa, located in the clamping of the middle stiffener. For the empirically calculated pressure, the largest displacement was found to be approximately 1.55 mm, while the highest Von Mises stresses were found to be 120.4 MPa.

As shown, stresses when using the DNV GL ice pressure are above the yield strength of steel, leading to plastic behavior of the material. This is not the case when using the empirical ice pressure, where stresses are below the yield strength. In both cases, the highest stresses are found in the clamping of the middle stiffener. This is natural, since if considering the middle stiffener as a fixed beam with a line load, the highest bending moment will be in the bearings.

15.1 Parameter study

To see how the outcome of the analyzes are affected by the different parameters, a parameter study will be conducted. Here, the following parameters will be evaluated: Load patch, stiffener dimensions, stiffener spacing and load angles.

15.1.1 Load patch

For the original load patch, the contact area was set to be 0.48 m^2. Since the contact height was chosen according to DNV GL regulations, this value will remain unchanged. For the contact length, this value was chosen arbitrary to be 1.2 m. To see how displacements and stresses change for different contact lengths, the analysis is repeated with two new contact areas. In the first case, the contact length is set to 0.8 m, and in second case it is set to 1.6 m.

For a contact length of 0.8 m, the displacement and stresses are shown in Figure 15.5 and Figure 15.6, respectively. For a contact length of 1.6 m, the displacement is shown in Figure 15.7 and the stresses in Figure 15.8.

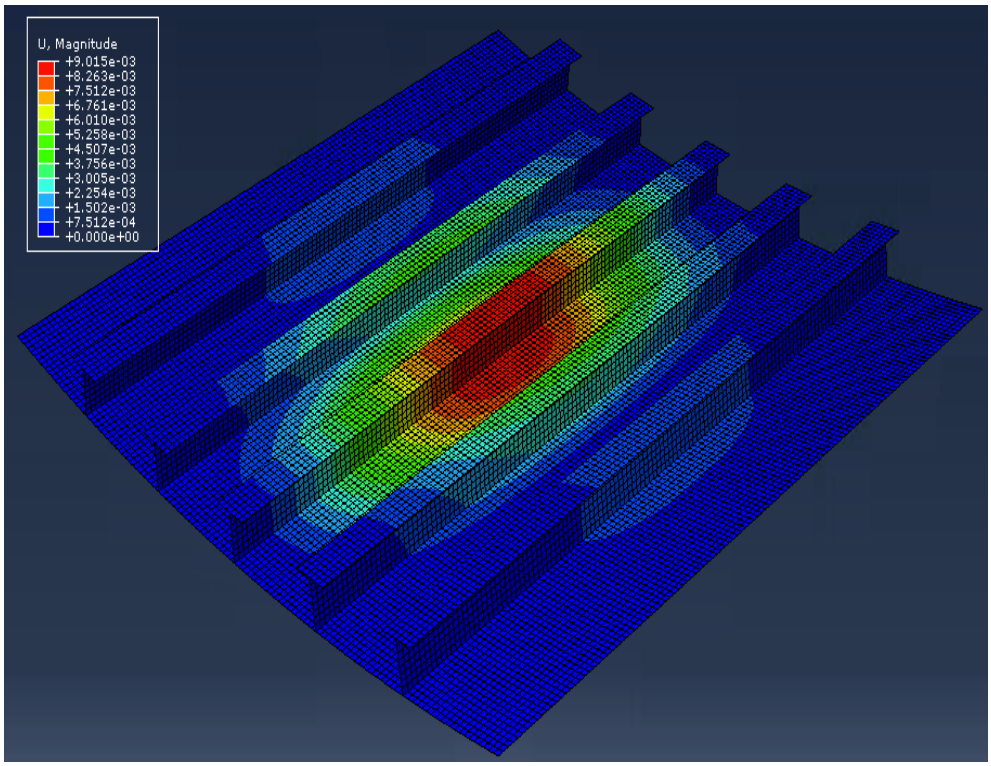

FIGURE 15.5: Displacement for a contact area of 0.32 m^2

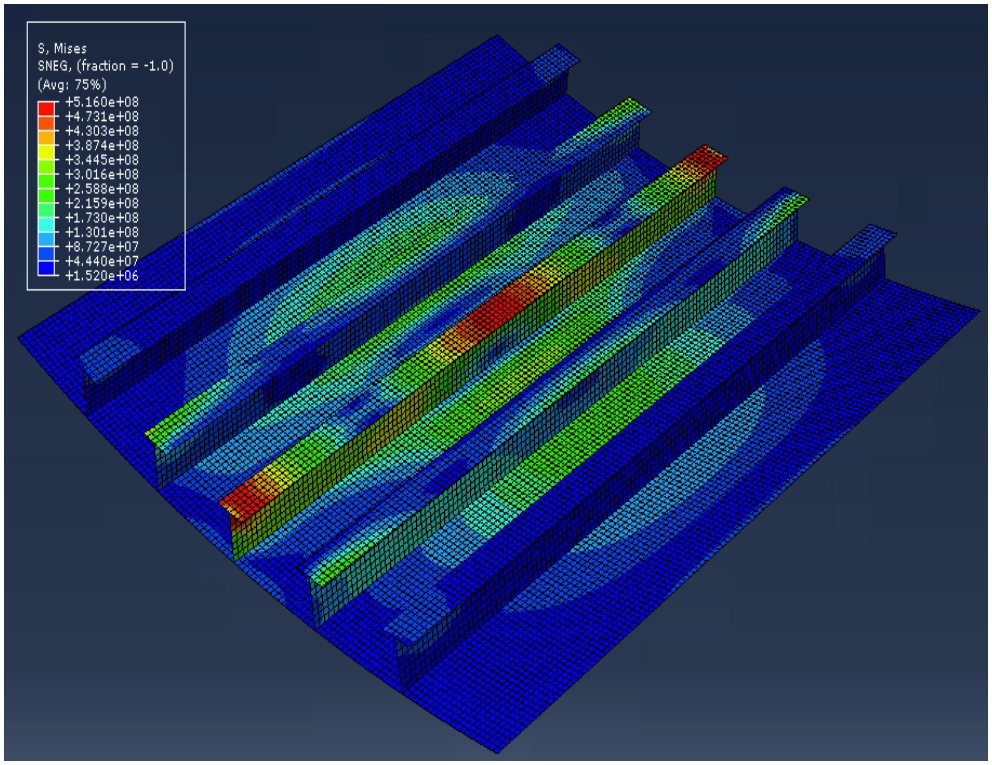

FIGURE 15.6: Stresses for a contact area of 0.32 m^2

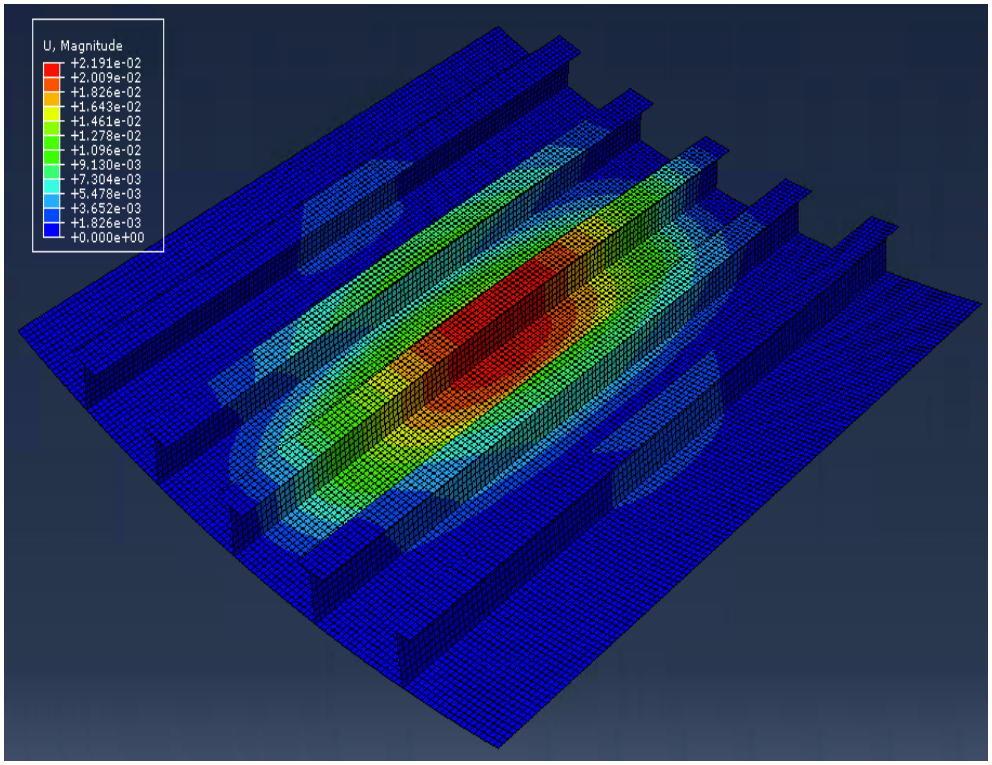

FIGURE 15.7: Displacement for a contact area of 0.64 m^2

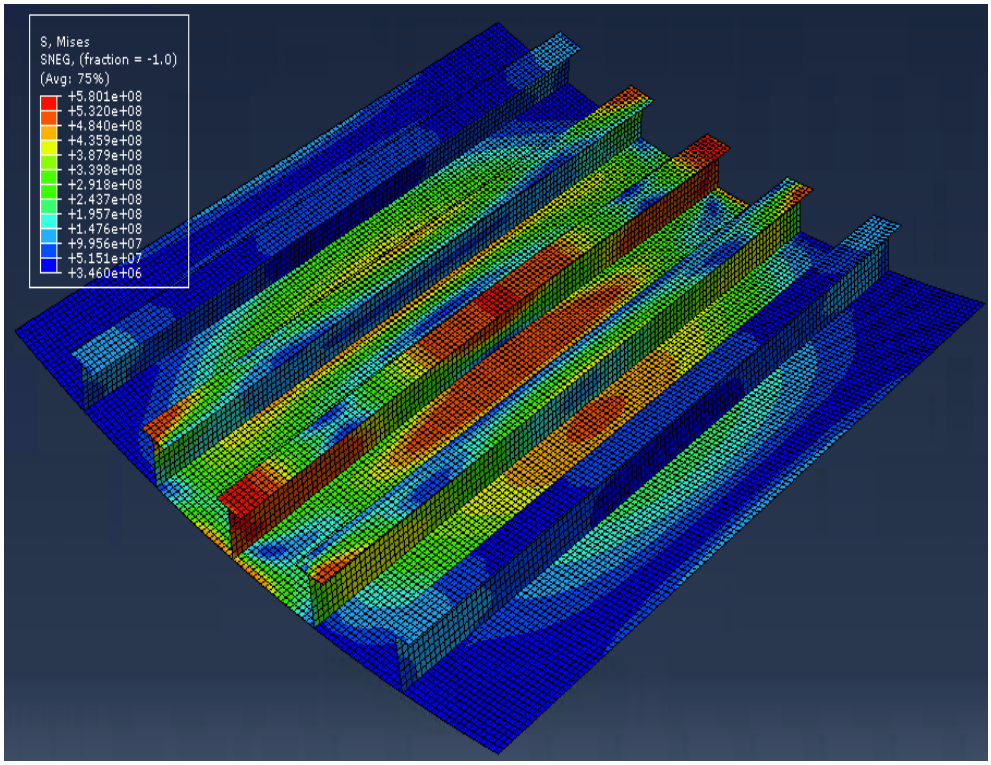

FIGURE 15.8: Stresses for a contact area of 0.64 m^2

Figures in this subsection shows displacements and Von Mises stresses when using the DNV GL ice pressure. Similar figures using the empiric ice pressure are shown in Appendix D.2. From Figure 15.5, the max displacement for a contact area of 0.32 m^2 was found to be 9.02 mm. Figure 15.6 shows that the max Von Mises stresses are found to be 516.0 MPa, located in the middle and in the clamping of the centre stiffener.

Figure 15.7 presents the maximum displacement for a contact area of 0.64 m^2. This value was found to be 21.92 mm. Finally, Figure 15.8 shows the maximum Von Mises stresses to be 580.1 MPa. Here, one can see that the stresses in the plate are significantly increased as compared to when the load patch area was 0.32 m^2.

15.1.2 Stiffener dimensions

The selected values for stiffener dimensions are presented in Table 14.2. To see how the response will change when modifying the stiffeners, a new analysis is performed without flanges on the stiffeners. To account for the lowered section modulus, the web height and thickness is modified as shown in Table 15.1.

TABLE 15.1: Stiffener parameters when removing the flange

Parameter	Value
Web height	200 mm
Web thickness	18 mm
Z	120.0 cm^3

The following figures shown the max displacements and Von Mises stresses when using the ice pressure from DNV GL. Figures when using the empirically calculated pressure are presented in Appendix D.3. Figure 15.9 show the maximum displacements and Figure 15.10 show the maximum Von Mises stresses.

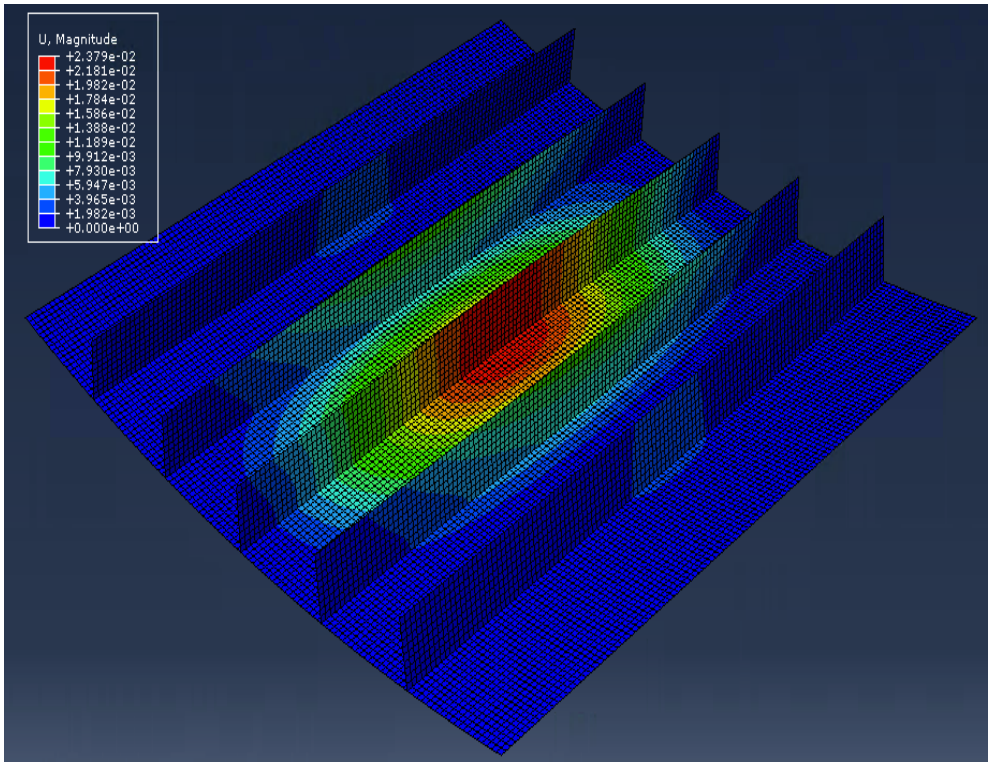

FIGURE 15.9: Displacements without flanges

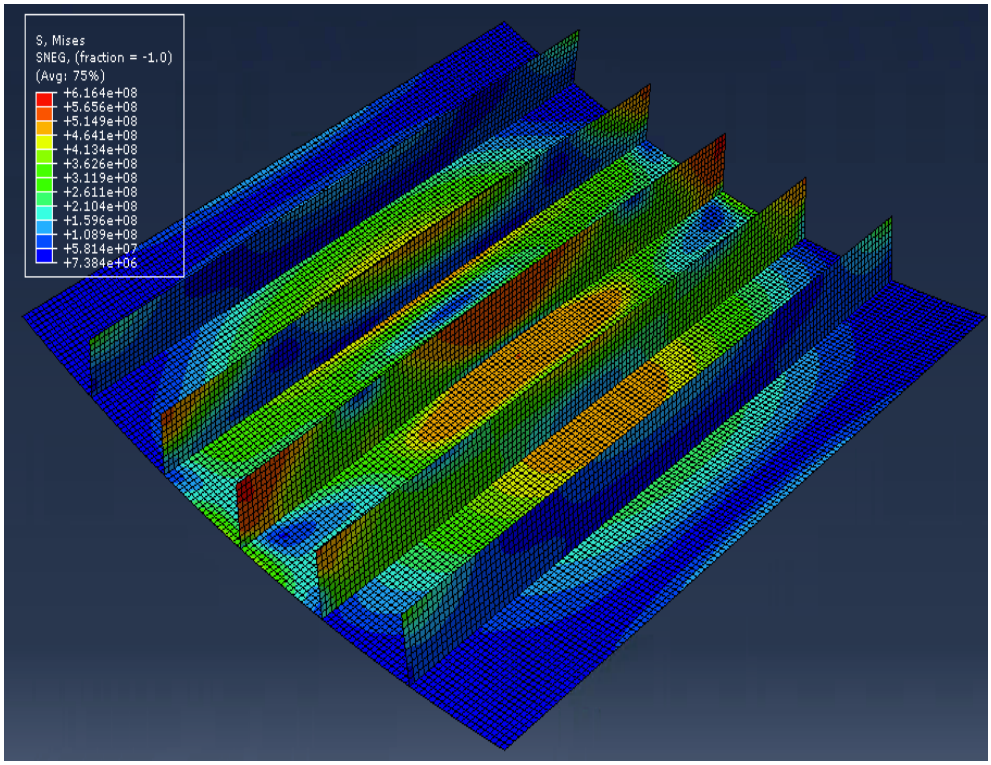

FIGURE 15.10: Stresses without flanges

From Figure 15.9, the max displacements are found to be 23.79 mm. Figure 15.10 gives maximum Von Mises stresses of 616.4 MPa.

15.1.3 Stiffener spacing

In the original analysis, the stiffener spacing was set to 0.4 m. To see how changing this parameter would influence the plate response, analyzes have been performed with stiffener spacing of 0.2 m and 0.6 m. For a stiffener spacing of 0.2 m, the required section modulus decreases. Using Equation 6.18, the new minimum section modulus is found to be 85.0 cm^3. On this basis, the new stiffener dimensions are as presented in Table 15.2.

TABLE 15.2: Stiffener parameters for a stiffener spacing of 0.2 m

Parameter	Value
Web height	140 mm
Flange width	100 mm
Thickness	15 mm
Z	85.2 cm^3

For a stiffener spacing of 0.6 m, the same stiffener dimensions as presented in Table 14.2 are used. The following figures show the plate response when using the ice pressure recommended from DNV GL. Response using the empiric ice pressure is presented in Appendix D.4. Figure 15.11 and 15.12 show displacement and stresses for a stiffener spacing of 0.2 m, while Figure 15.13 and 15.14 show displacement and stresses for a stiffener spacing of 0.6 m.

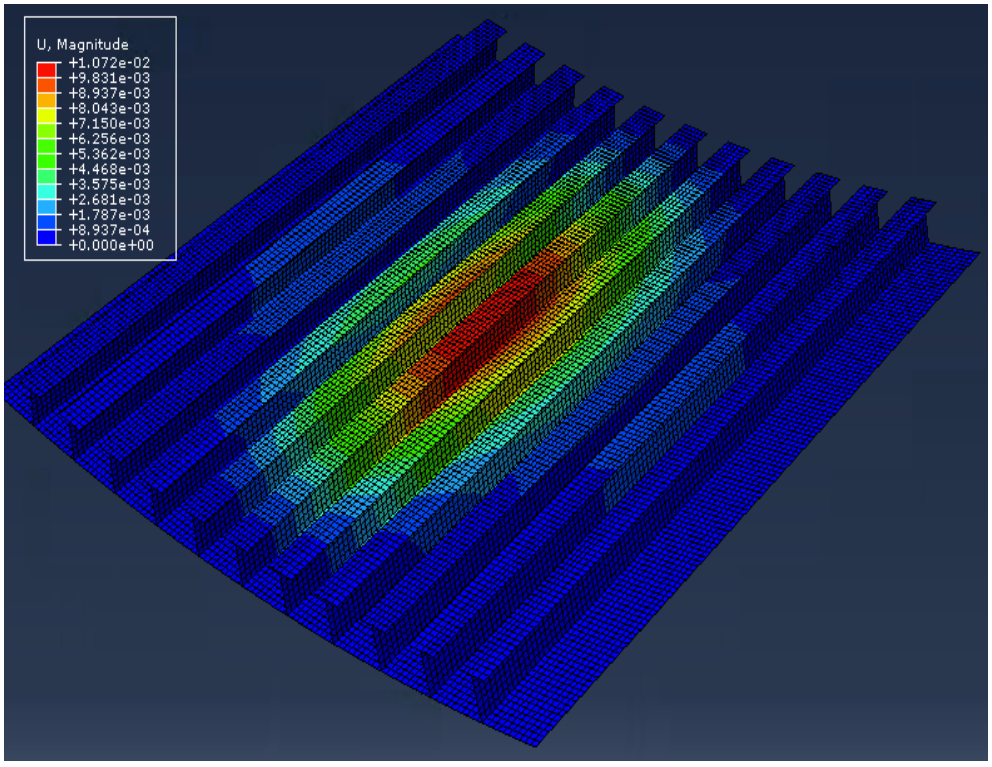

FIGURE 15.11: Displacement for a stiffener spacing of 0.2 m

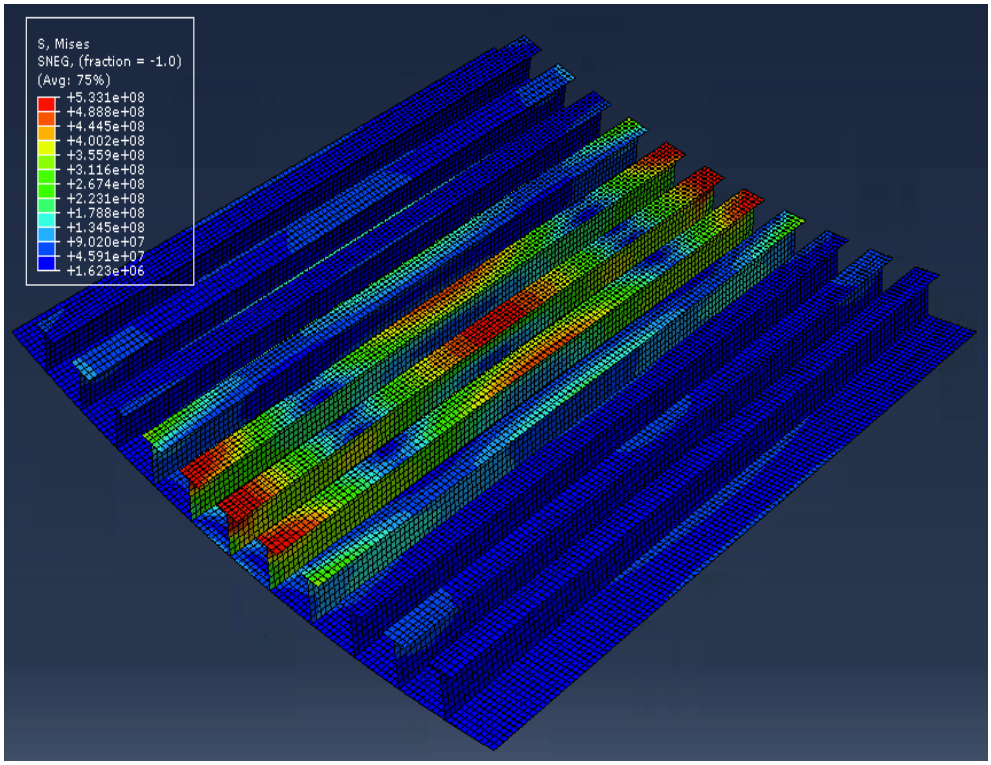

FIGURE 15.12: Stresses for a stiffener spacing of 0.2 m

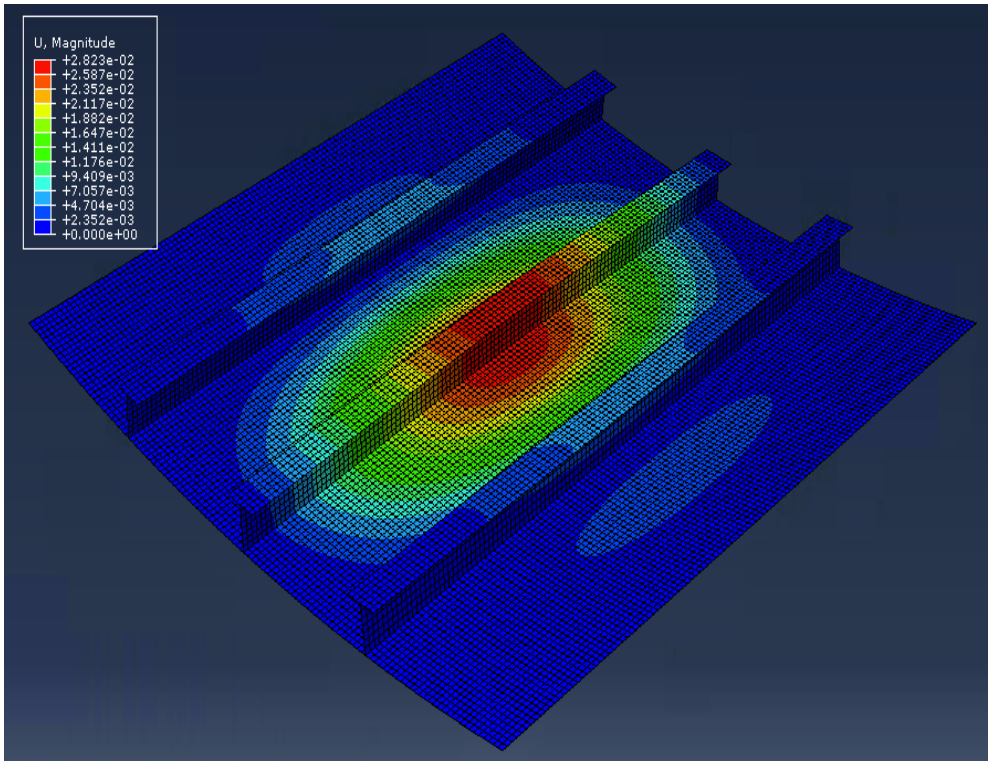

FIGURE 15.13: Displacement for a stiffener spacing of 0.6 m

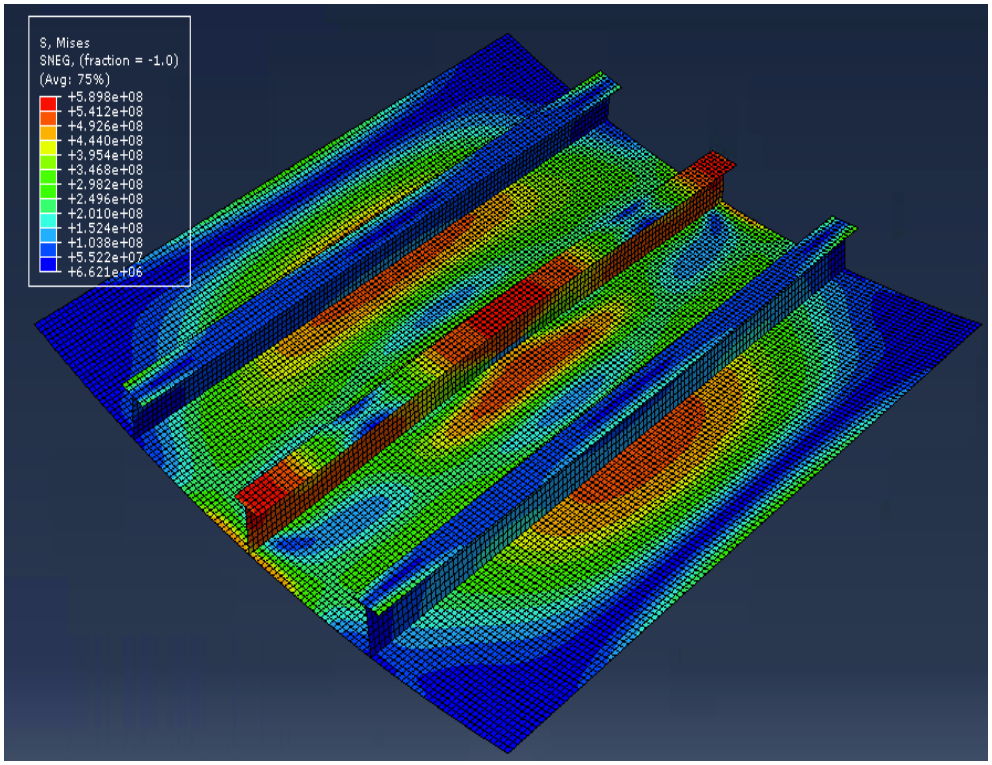

FIGURE 15.14: Stresses for a stiffener spacing of 0.6 m

From Figure 15.11, the max displacement is found to be 10.72 mm for s equal to 0.2 m. Figure 15.12 gives max Von Mises stresses of 533.1 MPa. For a stiffener spacing of 0.6 m, Figure 15.13 and 15.14 gives max displacement and Von Mises stresses of 28.23 mm and 589.8 MPa, respectively.

15.1.4 Load angles

For the load angles, these were set to be 60 degrees for both γ and ϕ, which gave a beta angle of 63 degrees. To compare, the analysis is also performed with γ and ϕ chosen to 45 degrees and to be 75 degrees. In the rules from DNV GL, the design ice pressure is independent on the load angles, and will therefore not be included in this investigation. Hence, only analyzes using the empirical ice pressure will be presented in this section.

For γ and ϕ set to 45 degrees, beta was calculated to be 54.7 degrees. For γ and ϕ equal 75 degrees, beta became 75.5. When calculating the empiric ice pressure, β is an important parameter, and changing this values will also change the empiric pressure. The new ice pressures are presented in Table 15.3.

TABLE 15.3: New ice pressures and minimum section modulus

β	**Empiric ice pressure**	$\mathbf{Z_{min}}$
54.7	927.6 KPa	131.2 cm^3
75.5	727.6 KPa	110.6 cm^3

Changing β will also influence the minimum section modulus for the stiffeners. The new minimums are shown in Table 15.3. New dimensions for the stiffeners are presented in Table 15.4.

TABLE 15.4: New stiffener dimensions

$\mathbf{Z_{min}}$	**Web height**	**Flange width**	**Thickness**	**Z**
131.2 cm^3	150 mm	150 mm	19 mm	133.1 cm^3
110.6 cm^3	140 mm	110 mm	19 mm	112.4 cm^3

Figure 15.15 and Figure 15.16 shows the new maximum displacement and Von Mises stresses for load angles of 45 degrees. For load angles of 75 degrees, the max displacement and Von Mises stresses are presented in Figure 15.17 and Figure 15.18, respectively.

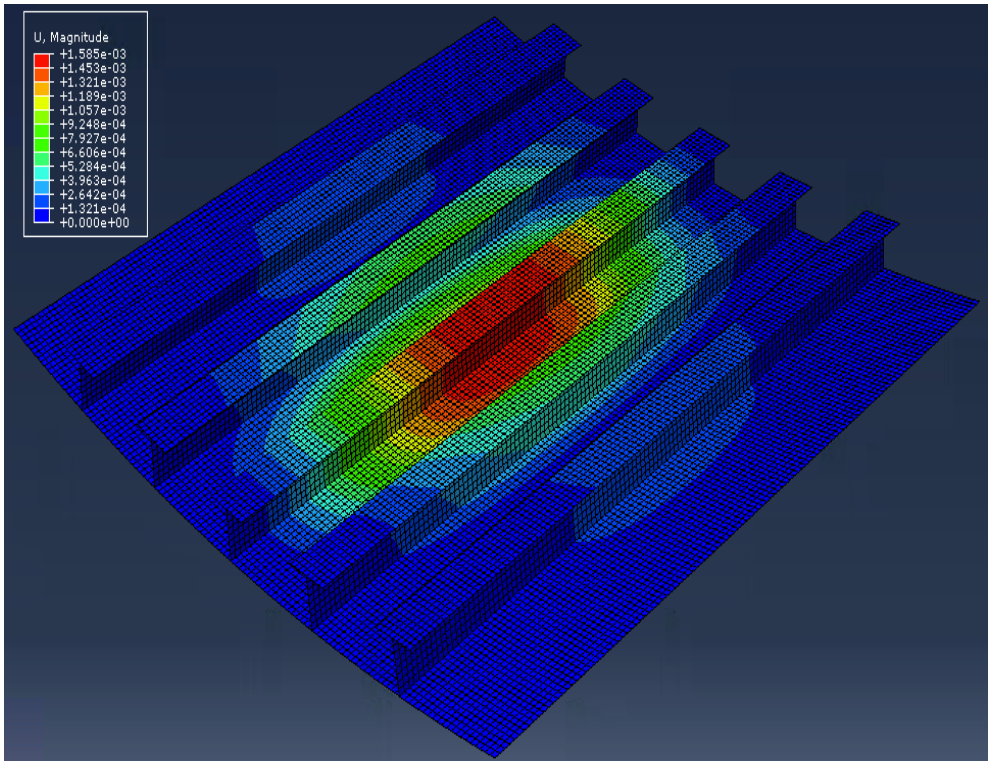

FIGURE 15.15: Displacement for load angles of 45 degrees

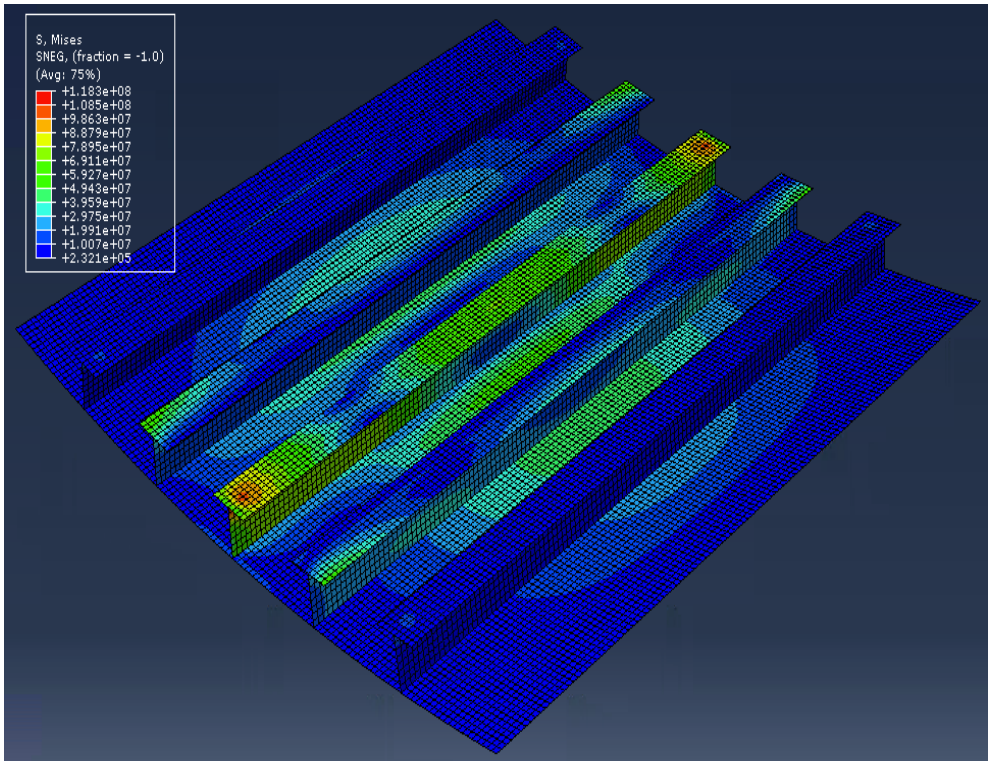

FIGURE 15.16: Stresses for load angles of 45 degrees

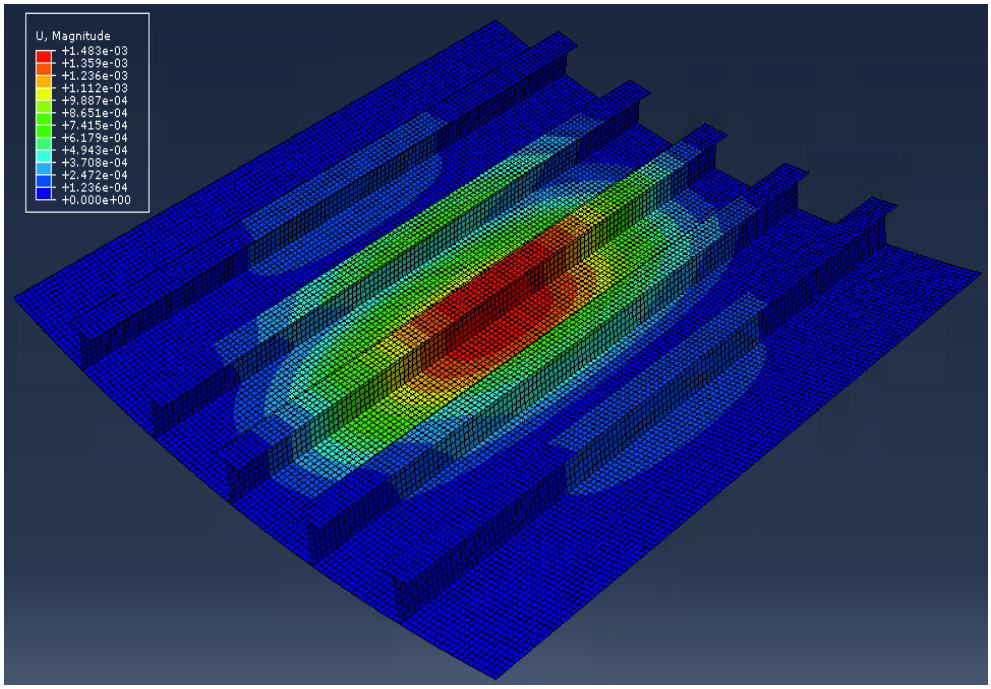

FIGURE 15.17: Displacement for load angles of 75 degrees

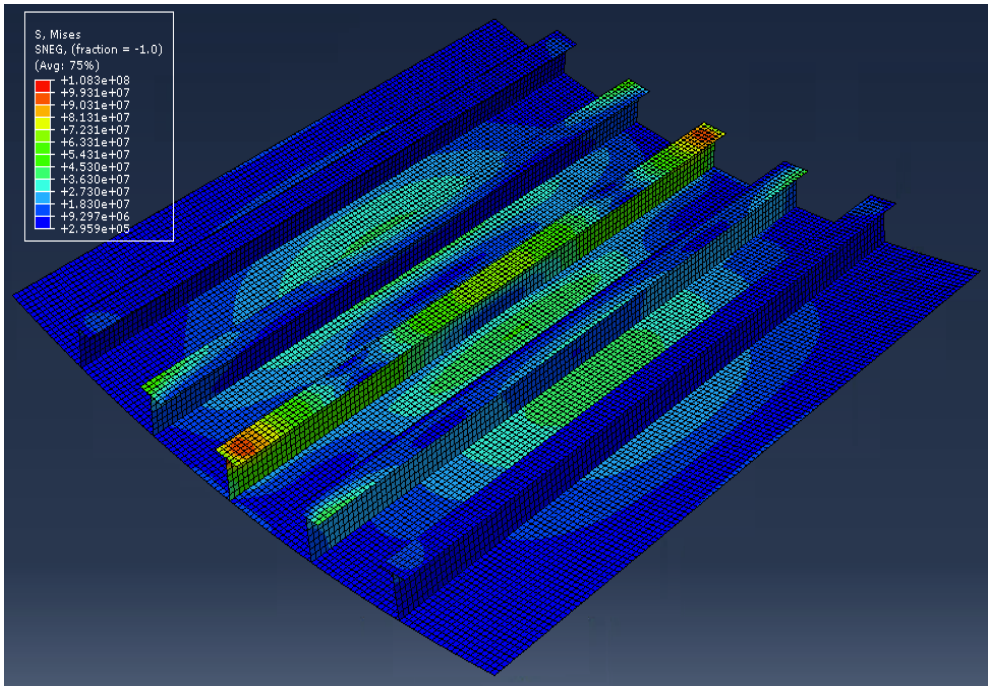

FIGURE 15.18: Stresses for load angles of 75 degrees

From Figure 15.15 and Figure 15.16 the maximum displacement is 1.48 mm and maximum stresses are 108.3 MPa. From Figure 15.17 and Figure 15.18 the max displacement is 1.59 mm and maximum stresses are 118.3 MPa.

15.1.5 Summary

In this parameter study, the plate section has been analyzed using a variety of different values and dimensions for load patch area, stiffeners and load angles. All displacements and Von Mises stresses obtained from these analyzes are presented in Table 15.5.

TABLE 15.5: Displacements and Von Mises stresses found in the parameter study

	Empiric ice pressure		**DNV GL ice pressure**	
Max values	Von Mises	Displacement	Von Mises	Displacement
ORIGINAL VALUES	120.4 MPa	1.55 mm	552.2 MPa	16.70 mm
Contact area 0.32 m	81.6 MPa	1.16 mm	516.0 MPa	9.02 mm
Contact area 0.64 m	155.6 MPa	1.79 mm	580.1 MPa	21.91 mm
Stiffener spacing 0.2 m	111.9 MPa	1.35 mm	533.1 MPa	10.72 mm
Stiffener spacing 0.6 m	140.1 MPa	1.79 mm	589.8 MPa	28.23 mm
No flange	258.0 MPa	1.75 mm	616.4 MPa	23.79 mm
Load angles 75 deg	108.3 MPa	1.48 mm	-	-
Load angles 45 deg	118.3 MPa	1.59 mm	-	-

To see how the new results compare with the results from the original values, this is presented in Table 15.6. For example, one can see that the Von Mises stresses are 214.3% of the original value when removing the flanges from the stiffeners.

TABLE 15.6: Comparing new results versus original results

	Empiric ice pressure		**DNV GL ice pressure**	
Max values	Von Mises	Displacement	Von Mises	Displacement
Original values	100%	100%	100%	100%
Contact area 0.32 m	67.8%	74.8%	93.4%	54.0%
Contact area 0.64 m	129.3%	115.5%	105.1%	131.2%
Stiffener spacing 0.2 m	92.9%	87.1%	96.5%	64.2%
Stiffener spacing 0.6 m	116.4%	115.5%	106.8%	169.0%
No flange	214.3%	112.9%	111.6%	142.5%
Load angles 75 deg	90.0%	95.5%	-	-
Load angles 45 deg	98.3%	102.6%	-	-

15.2 Discussion

In this chapter, a parameter study has been conducted. In this parameter study two different ice pressures were used, one obtained through empiric calculations (0.823 MPa) and one through DNV GL classifications (5.86 MPa). By changing values for load patch area, stiffener dimensions, stiffener spacing and load angles, the different plate responses are found.

In the first part of this chapter, a response analysis for the plate with dimensions as presented in Chapter 14 was conducted. With the pressure from DNV GL being a lot higher than the empirical one, it was expected to cause a bigger impact on the plate. This was also the case. While the empirical pressure gave a displacement of 1.55 mm, the one from DNV GL gave 16.70 mm. For the Von Mises stresses, the maximum value found for the empirical ice pressure was 120.4 MPa and 552.2 MPa for the DNV GL ice pressure.

In the parameter study, the first parameter investigated was the load patch area. In reality, the load patch area will vary constantly, thus it can be interesting to see how changing this change til maximum stresses and displacements of the plate. By decreasing and increasing the contact area length by 33%, new values for the plate response were found. When decreasing the contact are to 0.32 m^2, using DNV GL ice pressure, stresses above yield strength will only occur in the middle stiffener, while the plate behavior will maintain linear. For a increased contact area of 0.64 m^2, larger parts of the plate will experience stresses above the yield strength. For the empirical ice pressure, a 33% decrease/increase in contact are will have a quite linear relation to the max Von Mises stresses, with this value decreasing/increasing roughly 30%.

To investigate the stiffener dimensions, this is done by using stiffeners with and without flanges. To account for the lowered section modulus, the web dimensions have been modified. Flanges are used to prevent local buckling, and removing these should in theory strongly increase the stresses in the stiffeners. This is verified by the analyzes. From Figure D.10, one can see that for the empirical ice pressure the max stresses increase 114.3%. Preventing displacement is mainly accounted for by the stiffener webs, thus the max max displacement only increases 12.9%. In the case where DNV GL ice pressure is used, stresses in the middle stiffener and parts of the plate are above the yield strength, leading to stresses and displacements no longer having the same relation. This is shown in Figure 7.2. The displacement will now increase faster relative to the increase in stresses. Maximum Von Mises stresses increases in this case 11.6%, while displacements increase 42.5%.

Another parameter considered is the stiffener spacing. Through increasing/decreasing these spacings 50%, new analyzes could be perform and new plate responses were obtained. For analyzes with empirical ice pressure, changing the stiffener spacing to 0.2 m caused a 7% and 13% decrease of stresses and displacements, respectively. For a spacing of 0.6 m, this caused roughly 16% increase in both stresses and displacements. In both of these analyzes stresses are below yield. When the DNV GL ice pressure is used, modified stiffener spacing will only have marginal effect on max Von Mises stresses. With updated stiffener spacings, the stresses increase/decrease 6.8% and 3.8%

with spacing of 0.6 m and 0.2 m, respectively. The effect on max displacement is much higher, with an increase of 69% for s=0.6 m and a decrease of 35.8% for s=0.2 m. As mentioned, displacements are mainly accounted for by the stiffener webs. Increasing or decreasing the number of stiffeners in a panel will therefore strongly influence the plates capability to withstand these deflections. In addition, stresses in the panel using this ice pressure are above the yield strength, leading to plastic behavior of the material.

Investigating the load angles were only possible using the empiric pressure. Modifying these values are interesting, as it can represent how the response will vary when investigating different areas of the bow region. By using load angles of 45 degrees, the ice pressure used increased 13%. The change in load angles also led to a modification of the stiffener dimensions. Interestingly, changing these angle led to a slight decrease in maximum Von Mises stress, while the maximum displacement increased marginally. Using load angles of 75 degrees, the pressure decreased approximately 12%. This led to a 10% decrease in max Von Mises stress and roughly 5% in max displacement.

From the parameter study in this chapter, the plate response has been investigated for several scenarios. From the results it is possible to see how the response is affected by changing parameter connected to loading of the plate and plate dimensions. Since uncertainties are connected to some of the chosen values, a parameter study is highly interesting. From this one can see how the different parameters influence the final results, both in terms of stresses and displacements.

Chapter 16

Conclusion

Throughout this master thesis, several topics have been presented and investigated, with focus on ice properties, regulations, loading and resistance. The following conclusion is a summary of the most important aspects in each part of the thesis.

In the first part of this thesis, different types of sea ice and its mechanical and physical properties were presented. The ice thickness is the most important parameter when determining the strength of the ice. The thickness is also directly related to the vessel speed in ice-infested waters. In addition to thickness, density and salinity will strongly influence the strength of ice.

In the second part, ship-ice interactions were presented. In this thesis, only local forces have been investigated. In addition, only the first interaction between ship and ice are accounted for. Further, an idealized load patch is presented, which is set to be constant in the analysis. This is a quite big simplifications, as this in reality will vary as the ship moves. On the basis of thesis assumptions, an empirical ice pressure model is presented.

The next part was a review of the different ice classifications, with the main focus on classifications from IACS and DNV GL. While DNV GL divided their ice classes into geographical areas, IACS focuses entirely on what ice resistance the vessels will be exposed to and for which periods. In this thesis, the focus has primarily been on rules connected to the Arctic region.

The fourth part of this master thesis was related to estimation of ice resistance for ships. Three different semi-empirical formulations for calculation of ice resistance have been reviewed. These models are useful in early estimations of resistance and power requirements, but can not be used as a replacement of model tests. By using the main characteristics from KV Svalbard, the models were compared to each other. The results show that the calculated ice resistance corresponds quite well, especially for low ice thickness and vessel speed.

To further compare these formulations, a parameter study was conducted. The study was done with several combinations of vessel speed and ice thickness. Here, Riska differers from the others, as most of the parameters are included through constants. From the results one can see that some parameters are strongly influenced by speed and thickness, while others are quite independent.

To determine the quality of the empirical resistance calculations, the results were compared with full-scale data from KV Svalbard. The data obtained was of relatively low control, with a big scatter in values for the resistance. In this comparison, only ice thickness and vessel speed were modified, while the other parameters were set to be constant. This is a large simplification, which is also verified from the parameter study. Finding periods with stable ice conditions were challenging.

Given the low quality of the data, it is hard to determine which of the three investigated empirical formulations that predicts resistance better. With no propeller curves, the true propeller efficiency is unknown, giving another source of uncertainty. Using data with higher quality gave more stable ratios, and it would therefore be interesting to have access more data of high quality.

The final part of this thesis was a finite element analysis using Abaqus. Here, a non-linear analysis were performed, which proved to be a good choice. The model was a part of the bow on KV Svalbard. Two different ice pressures were applied, one empirically calculated and one according to DNV GL regulations. Dimensions for plate, load patch area, stiffener dimensions and stiffener spacings were also chosen from DNV GL.

To see how the final response was affected by the different parameters, a parameter study was conducted. The results were quite different using the two different ice pressures. Using the empirical pressure, stresses were below yield strength, leading to, in most cases, a similar effect on both displacement and Von Mises stresses when modifying parameters. Using the ice pressure from DNV GL, maximum stresses are no longer below the yield strength. Here, stresses and displacements no longer will have the same relation, and changes will therefore have a bigger effect on displacements than on stresses.

Chapter 17

Further work

In this chapter, different suggestions to further work is presented. This is divided into two parts, one for the resistance calculations and one for the finite element analysis.

17.1 Resistance

There are a lot of uncertainties connected to the resistance for KV Svalbard. The ice conditions faced were quite varying, with a lot of brash ice. Periods with longer periods of steady level ice conditions would increase the quality of results. When calculating the resistance, the propeller effectivity was set to 90%. There is a lot of uncertainty connected to this, and to ensure better results, the propeller curves should be obtained.

When calculating the resistance from the measurement on KV Svalbard, only ice thickness and vessel speed are set as changeable parameters. It found be interesting to see the results as a function of more than just these two parameters. From the parameter study on the empirical resistance model it is clear that several parameters will strongly influence the resistance, such as flexural strength of ice and temperature.

To verify the quality of the empirical resistance formulation, new raw data from resistance measurements should be obtained. The raw data used in this thesis are of low quality, and it is therefore difficult to conclude. Since both the Riska and Lindqvist model were developed for Baltic conditions, it would be interesting to see how these would compare to full scale results from these areas.

17.2 Finite element analysis

In this analysis, KV Svalbard have been used as a reference, and the model is created as an simplification of this vessel. To get better and more precise results, it would be interesting to conduct the same analysis and parameter study with a real finite element model of KV Svalbard. This would provide more accurate values for dimensions, load angles, curvature and boundaries. Since several parameters used in this analysis are chosen arbitrary, it is hard to determine goodness of the results without access to a model of the actual ship.

Bibliography

[1] ACCESS. *KV Svalbard 2012*. 2012. URL: http://www.access-eu.org/en/publications/access_expeditions/kv_svalbard_2012.html.

[2] AMAP. "Arctic Climate Issues 2011: Changes in Arctic Snow, Water, Ice and Permafrost. 2012". In: *SWIPA 2011 Overview Report. Arctic Monitoring and Assessment Programme (AMAP)* (2011).

[3] AMAP. "Assessment Programme (AMAP). 1998". In: *AMAP assessment report: Arctic pollution issues* (1997).

[4] Kolbein Bell. *An engineering approach to finite element analysis of linear structural mechanics problems*. Akademica Publishing, 2013.

[5] CAE. *Using Stress-Strain Data for a Finite Element Simulation*. 2013. URL: https://caeai.com/blog/using-stress-strain-data-finite-element-simulation.

[6] DNVGL. "Rules for classification of ships: Part 5, Chapter 1-Ships for navigation in ice". In: *Retrieved fro m https://www. dnvgl. com/about/index. html* (2016).

[7] Sandro Erceg and Sören Ehlers. "Semi-empirical level ice resistance prediction methods". In: *Ship Technology Research* 64.1 (2017), pp. 1–14.

[8] D Fequet. "MANICE: manual of standard procedures for observing and reporting ice conditions". In: *Environment Canada* (2005).

[9] Forsvaret. *KV Svalbard*. 2014. URL: https://forsvaret.no/fakta/utstyr/Sjoe/KV-Svalbard.

[10] Herman Holm. "Ice-Induced Loads on Ship Hulls". MA thesis. Institutt for marin teknikk, 2012.

[11] MP Langleben. "Young's modulus for sea ice". In: *Canadian Journal of Physics* 40.1 (1962), pp. 1–8.

[12] B Leira et al. "Ice-load estimation for a ship hull based on continuous response monitoring". In: *Proceedings of the Institution of Mechanical Engineers, Part M: Journal of Engineering for the Maritime Environment* 223.4 (2009), pp. 529–540.

[13] Gustav Lindqvist. "A straightforward method for calculation of ice resistance of ships". In: (1989).

[14] Torgeir Moan. "Finite element modelling and analysis of marine structures". In: *NTNU, September* 45 (2003).

[15] NSIDC. *Salinity and Brine*. 2017. URL: https://nsidc.org/cryosphere/seaice/characteristics/brine_salinity.html.

[16] Polar Portal. *Sea ice extent and thickness*. 2017. URL: http://polarportal.dk/en/havisen-i-arktis/nbsp/sea-ice-extent/.

[17] Kaj Riska. "Design of ice breaking ships". In: *Course material NTNU* (2011).

[18] Kaj Riska. "Lecure notes in Ship design for ice, NTNU". In: (2017).

[19] Kaj Riska. *Performance of merchant vessels in ice in the Baltic*. Sjöfartsverket, 1997.

[20] Kaj Riska and Jorma Kämäräinen. "A review of ice loading and the evolution of the finnish-swedish ice class rules". In: *Proceedings of the SNAME Annual Meeting and Expo. November*. 2011, pp. 16–18.

[21] Svein Sævik. "Lecture notes in TMR4305 Advanced structural analysis, NTNU". In: (2017).

[22] Torstein Skår. "Ice induced resistance of ship hulls: A comparison of resistance estimated from measurements and analytical formulations". MA thesis. Norges teknisk-naturvitenskapelige universitet, Fakultet for ingeniørvitenskap og teknologi, Institutt for marin teknikk, 2011.

[23] Solidworks. *Stress-Strain Relation for Linear Material*. 2013. URL: http://help.solidworks.com/2013/english/SolidWorks/cosmosxpresshelp/c_stress-strain_relation_for_linear_material.htm.

[24] Bendik Johnsen Stephan. "Ice Loading On Ship Hull-Ice Specimen Testing and Stress Analysis of Local Plate Fields in the Bow Region." MA thesis. NTNU, 2017.

[25] Abdillah Suyuthi, Bernt J Leira, and Kaj Riska. "Full scale measurement on level ice resistance of icebreaker". In: *ASME 2011 30th International Conference on Ocean, Offshore and Arctic Engineering*. American Society of Mechanical Engineers. 2011, pp. 983–989.

[26] OK Teien. *Spesifikasjon 5-så rutine*. 2014. URL: http://docplayer.me/39846805-Spesifikasjon-5-ars-rutine-kv-svalbard.html.

[27] Ingvill Bryn Thorsen. "Estimation and computation of ice-resistance for ship hulls". MA thesis. Institutt for marin teknikk, 2012.

[28] GW Timco and WF Weeks. "A review of the engineering properties of sea ice". In: *Cold regions science and technology* 60.2 (2010), pp. 107–129.

[29] Jukka Tuhkuri. "Ice ridge formation". In: (2014).

Appendix A

Empirical model comparison

Plots for empirical resistance formulations with the same input values.

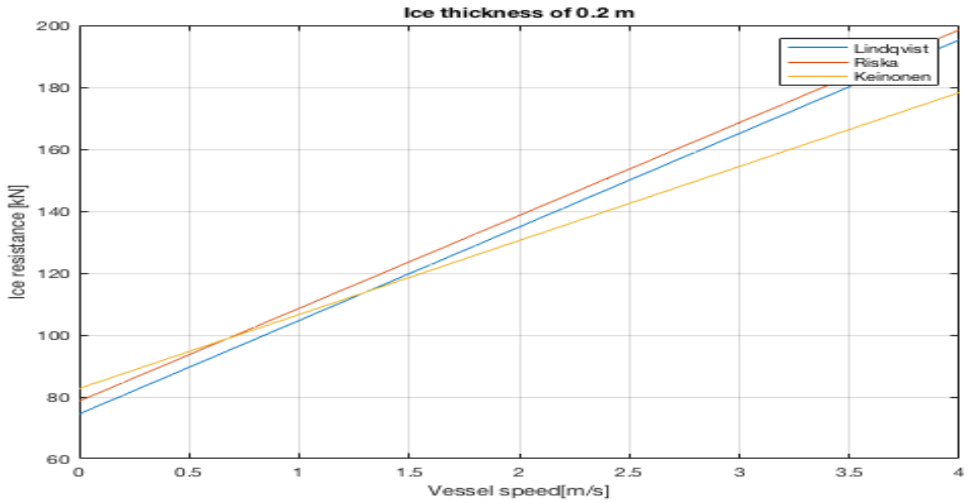

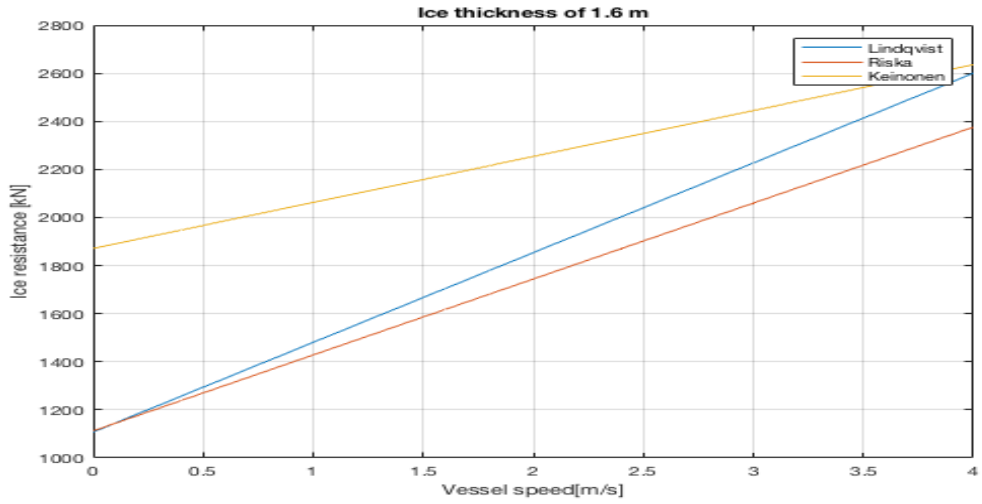

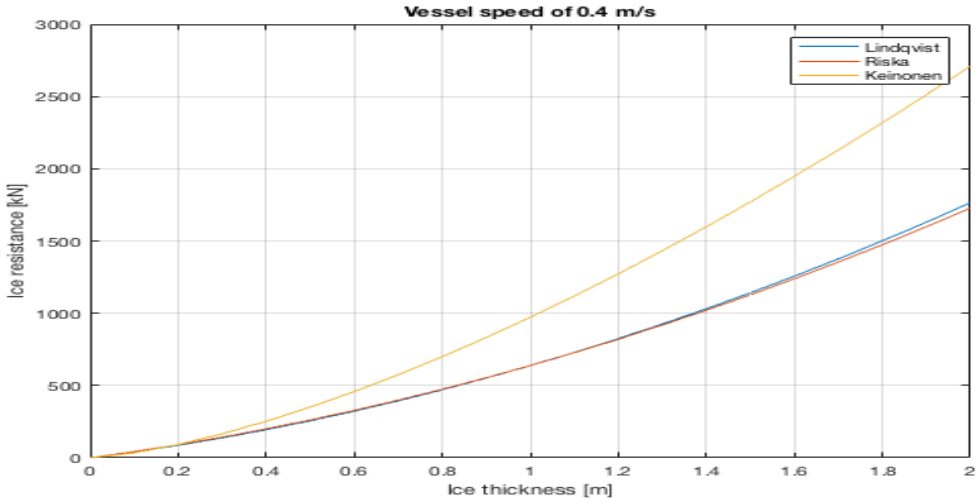
Vessel speed of 0.4 m/s
Lindqvist
Riska
Keinonen
Ice resistance [kN]
Ice thickness [m]
0
500
1000
1500
2000
2500
3000
0.2
0.4
0.6
0.8
1
1.2
1.4
1.6
1.8
2

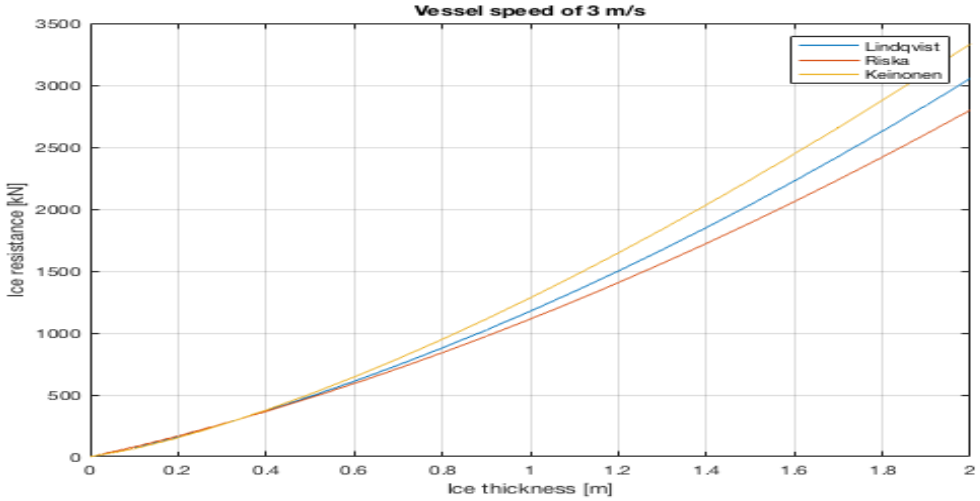
Vessel speed of 3 m/s
Lindqvist
Riska
Keinonen
Ice resistance [kN]
Ice thickness [m]
0
500
1000
1500
2000
2500
3000
3500
0.2
0.4
0.6
0.8
1
1.2
1.4
1.6
1.8
2

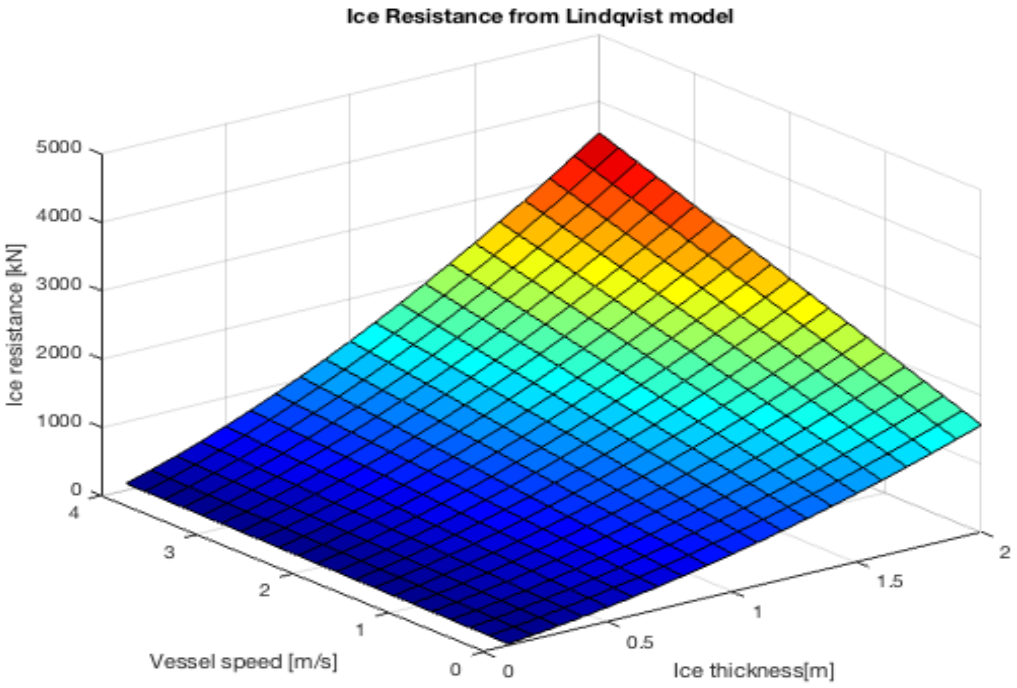
Ice Resistance from Lindqvist model
Ice resistance [kN]
5000
4000
3000
2000
1000
0
4
3
2
1
0
Vessel speed [m/s]
0
0.5
1
1.5
2
Ice thickness[m]

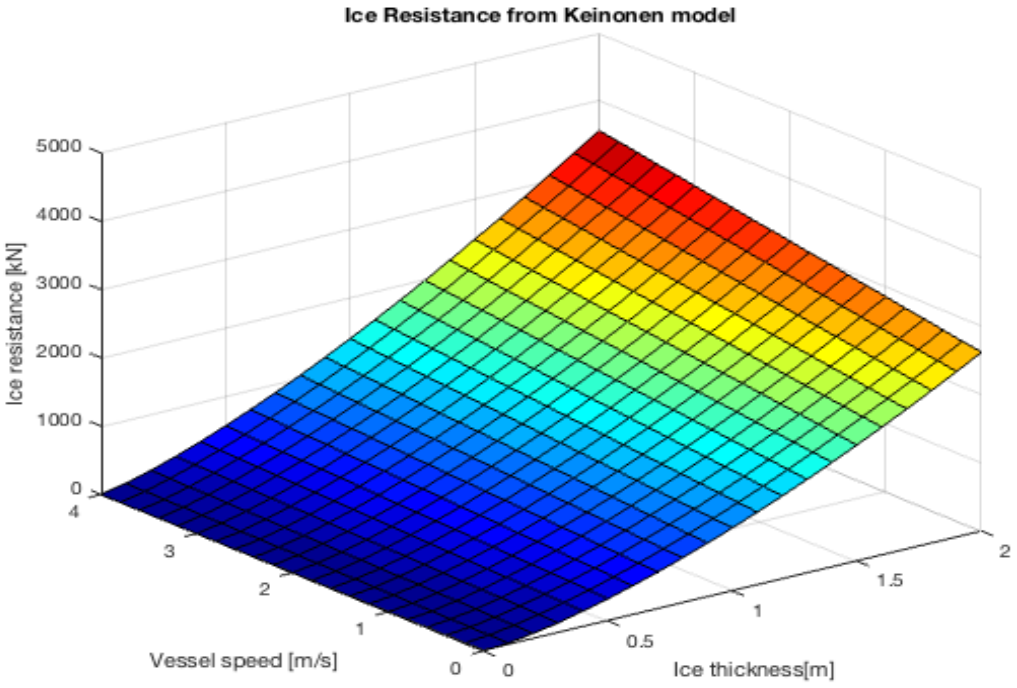
Ice Resistance from Keinonen model
Ice resistance [kN]
5000
4000
3000
2000
1000
0
4
3
2
1
0
Vessel speed [m/s]
0
0.5
1
1.5
2
Ice thickness[m]

Appendix B

Sensitivity plots - combinations of ice thickness and vessel speed

B.1 Length of bow

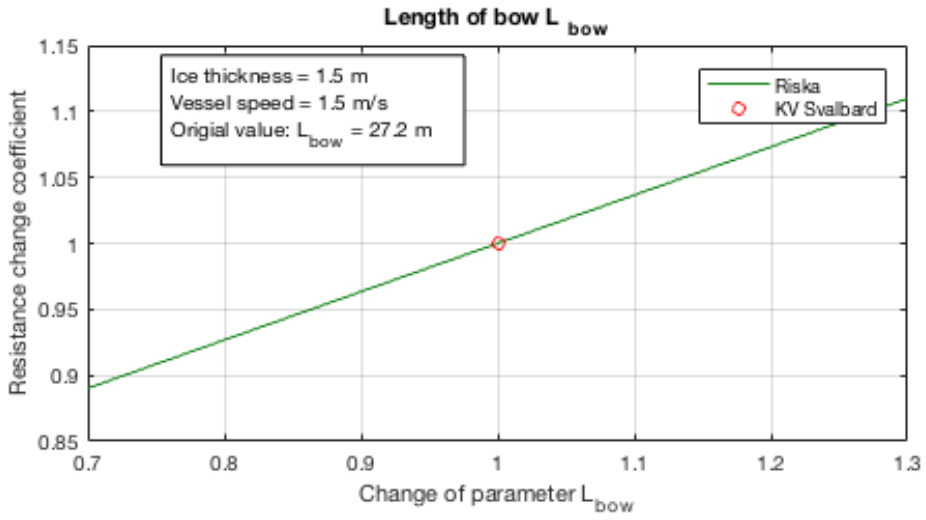

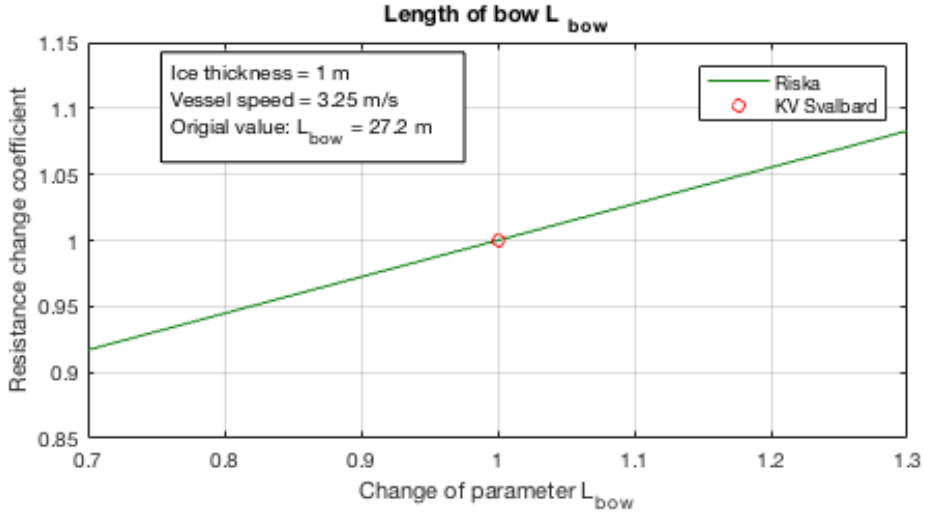

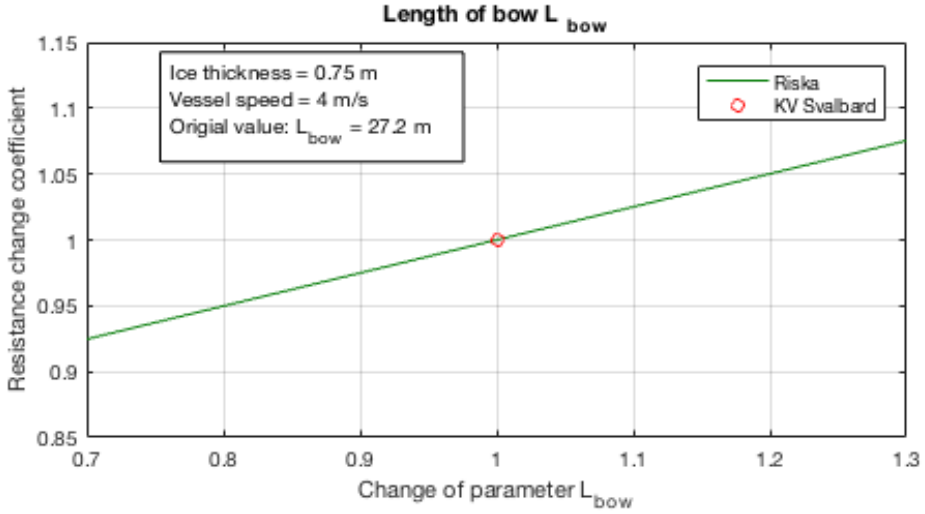

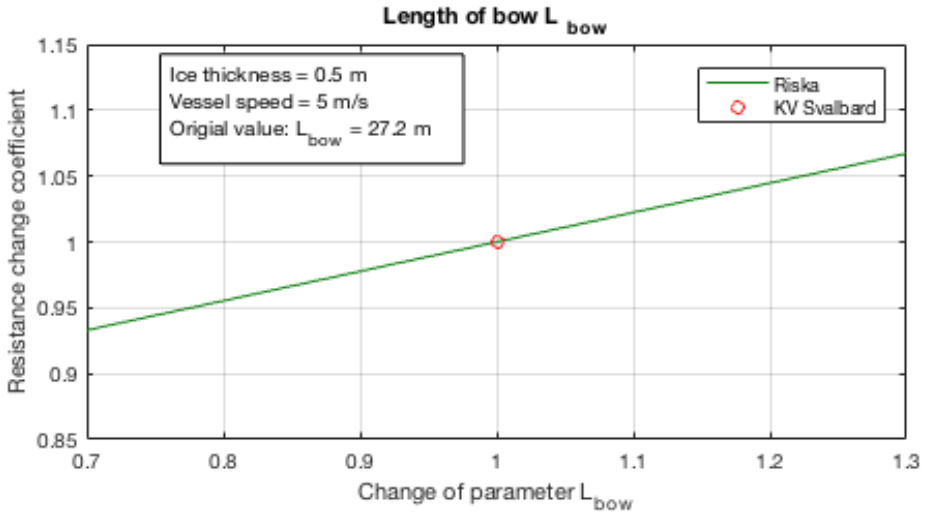

B.2 Length of parallel mid-body

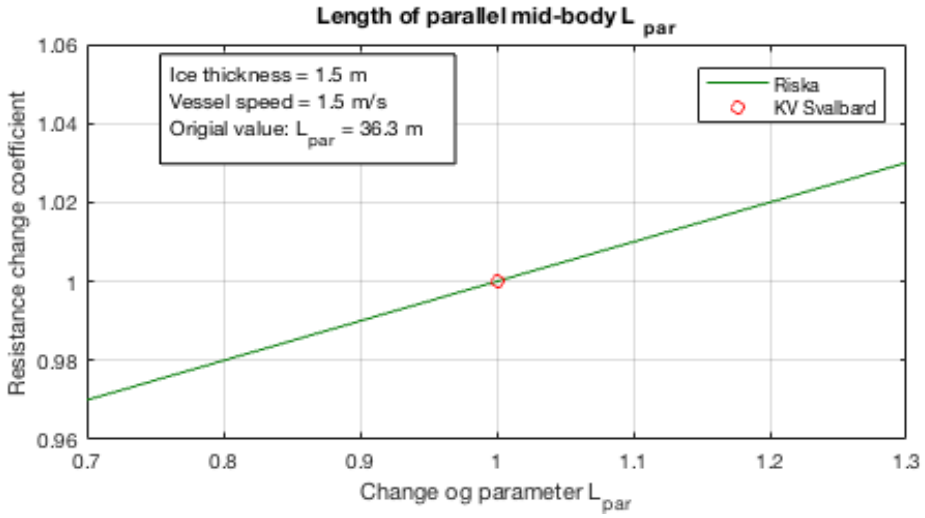

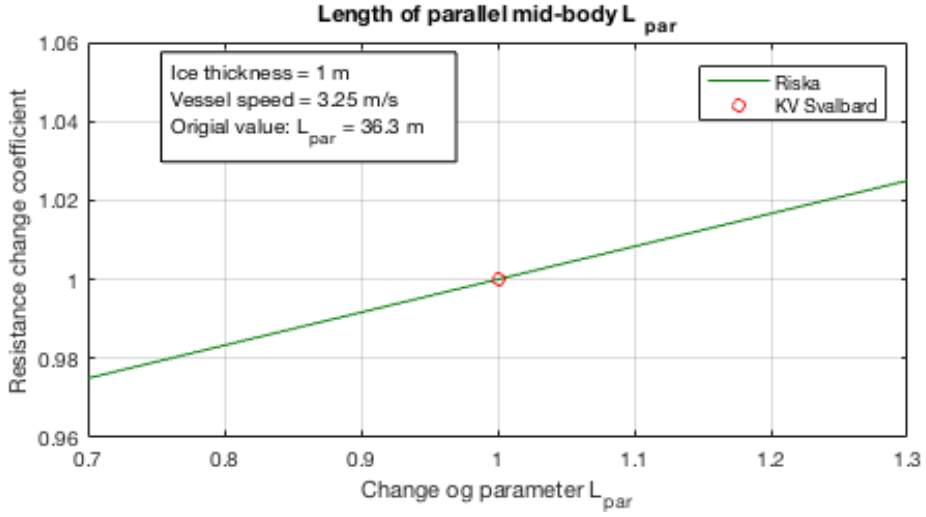
Length of parallel mid-body L par
Ice thickness = 1 m
Vessel speed = 3.25 m/s
Origial value: L par = 36.3 m
Riska
KV Svalbard
Resistance change coefficient
Change og parameter L par
1.06
1.04
1.02
1
0.98
0.96
0.7
0.8
0.9
1
1.1
1.2
1.3

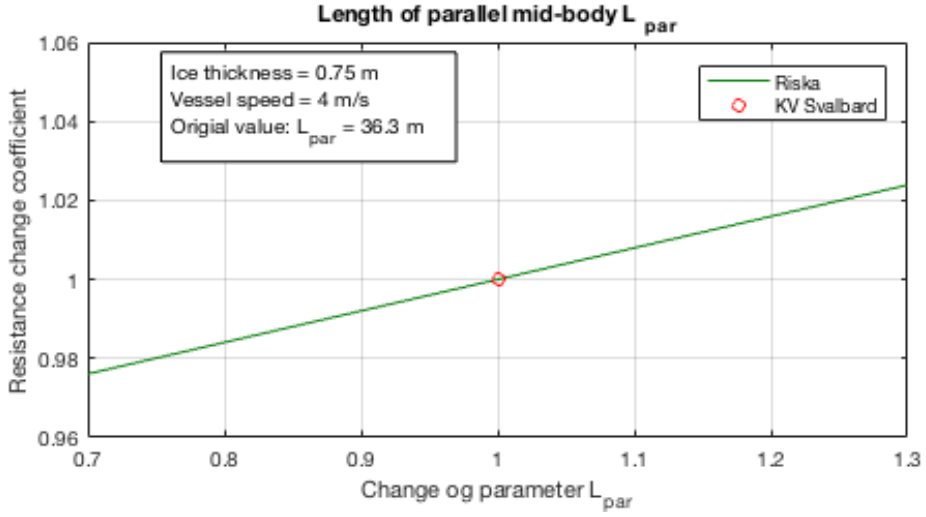
Length of parallel mid-body L par
Ice thickness = 0.75 m
Vessel speed = 4 m/s
Origial value: L par = 36.3 m
Riska
KV Svalbard
Resistance change coefficient
Change og parameter L par
1.06
1.04
1.02
1
0.98
0.96
0.7
0.8
0.9
1
1.1
1.2
1.3

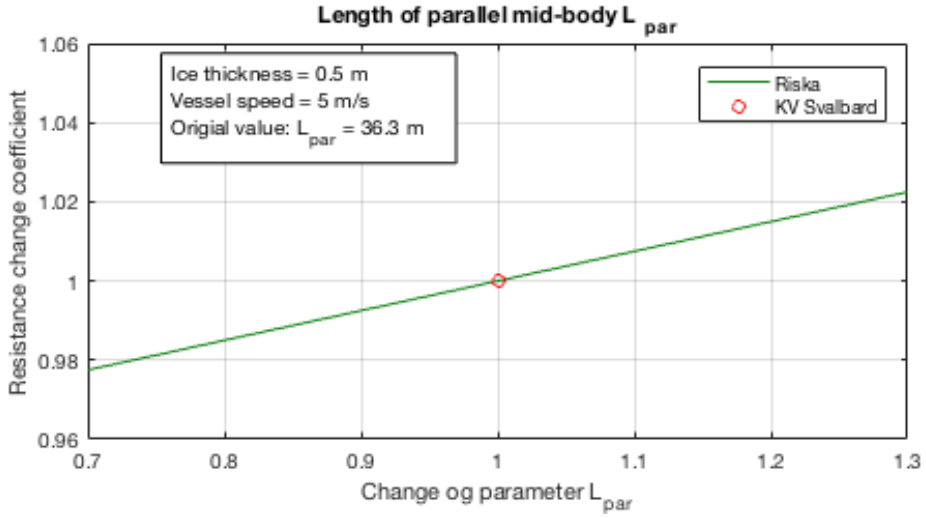
Length of parallel mid-body L par
Ice thickness = 0.5 m
Vessel speed = 5 m/s
Origial value: L par = 36.3 m
Riska
KV Svalbard
Resistance change coefficient
Change og parameter L par
1.06
1.04
1.02
1
0.98
0.96
0.7
0.8
0.9
1
1.1
1.2
1.3

B.3 Water line entrance angle

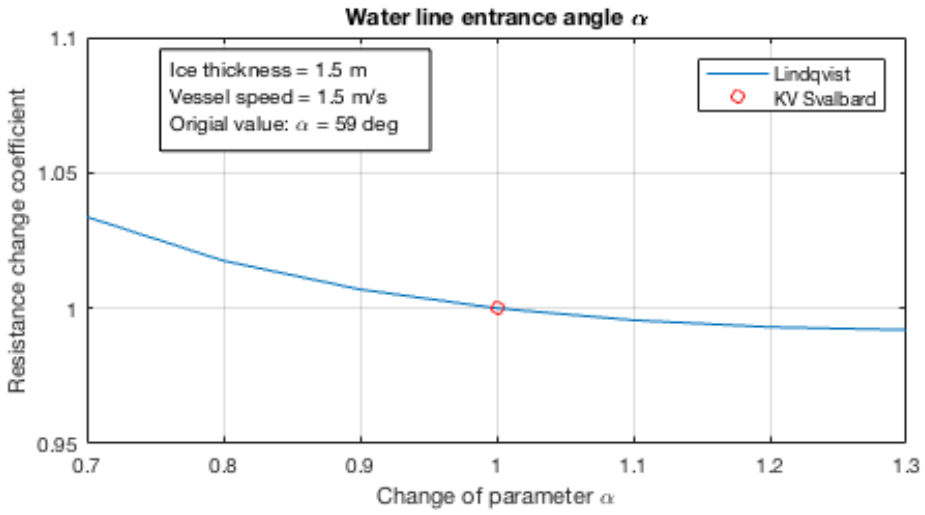

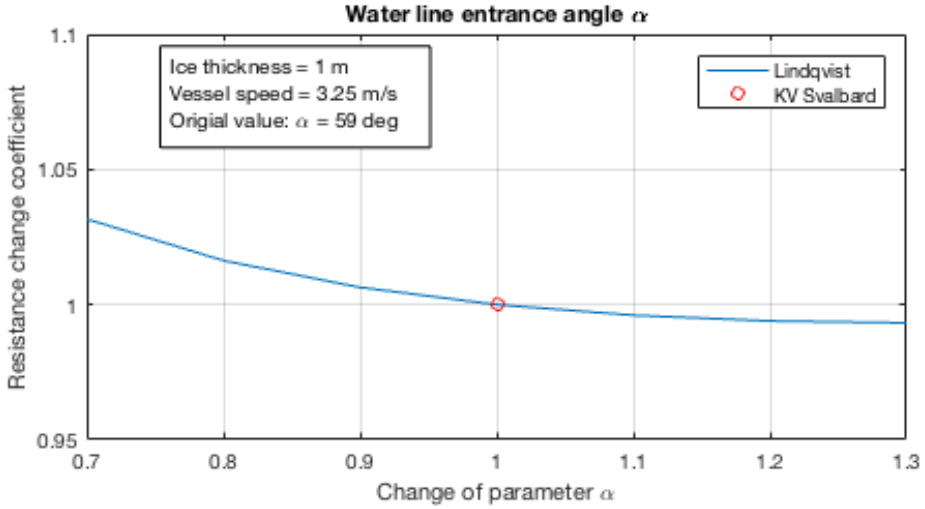

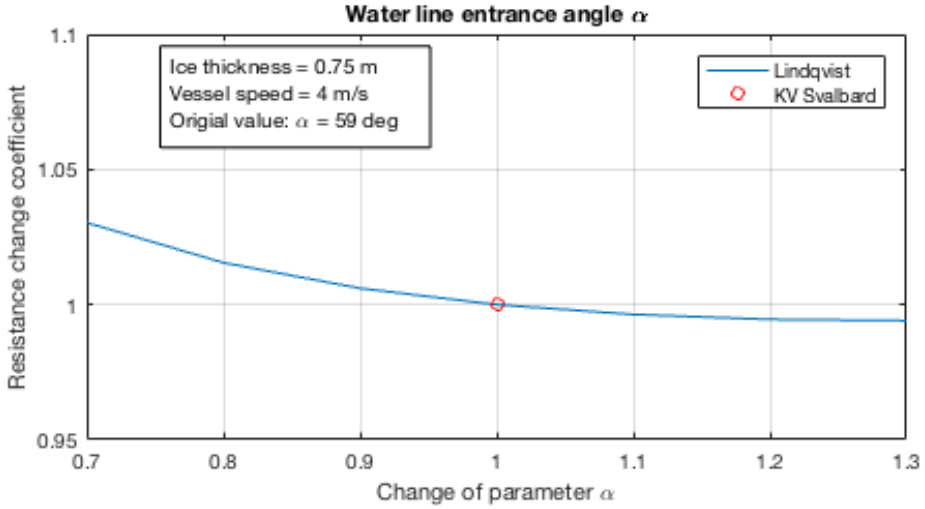

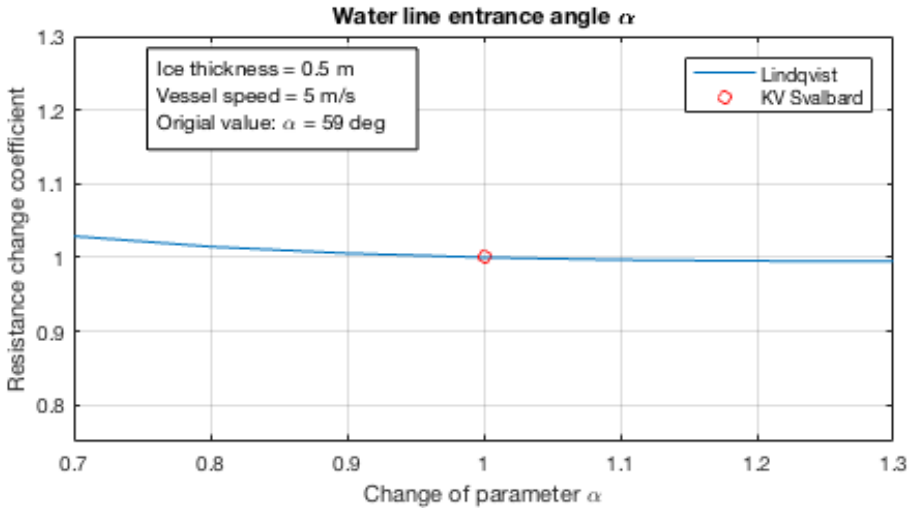

B.4 Buttock angle

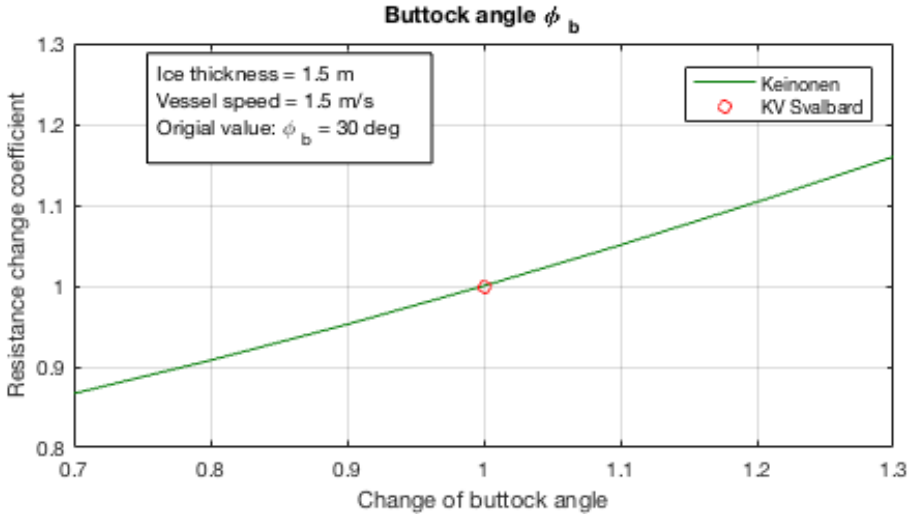

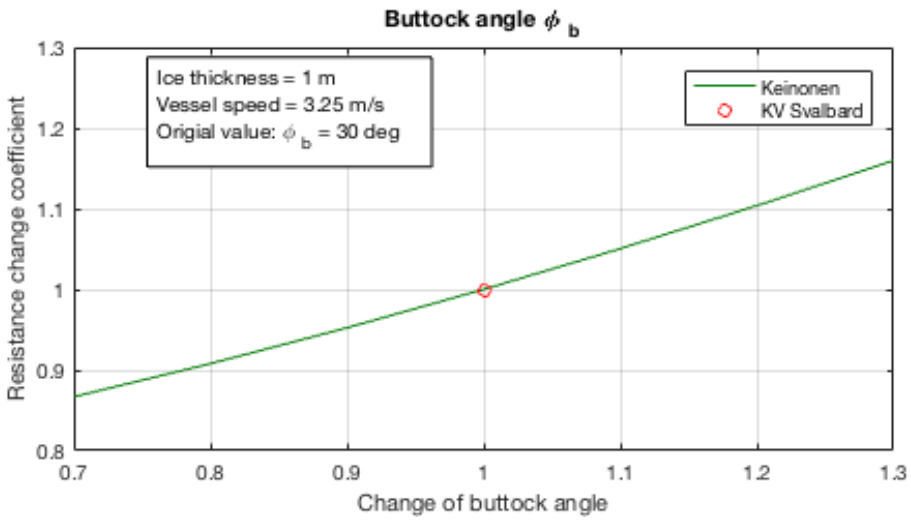

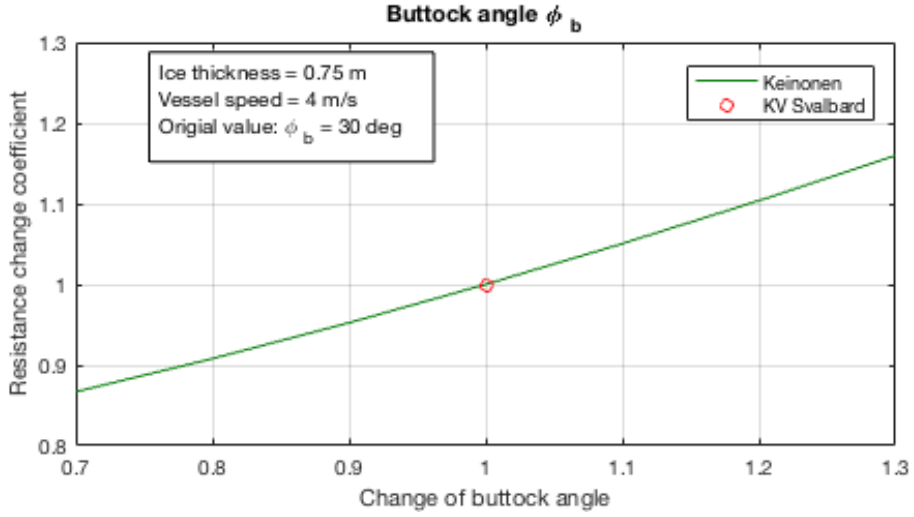

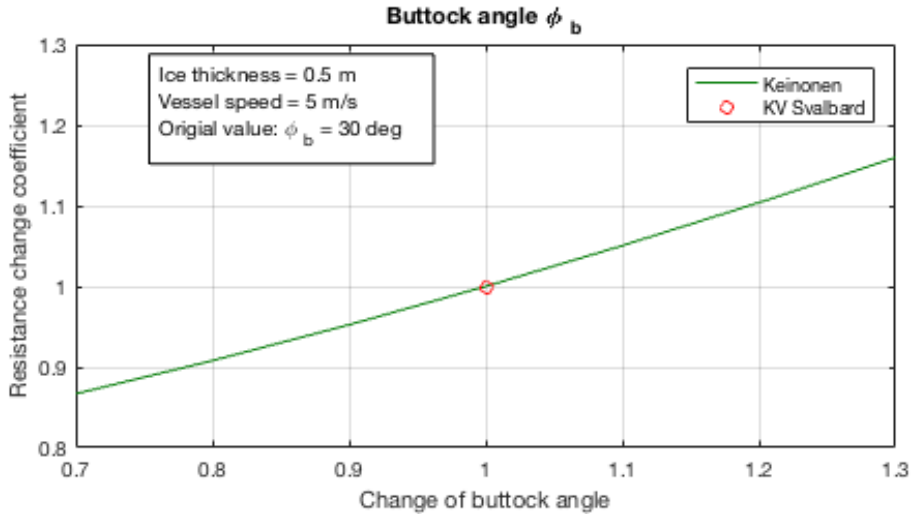

B.5 Stem angle

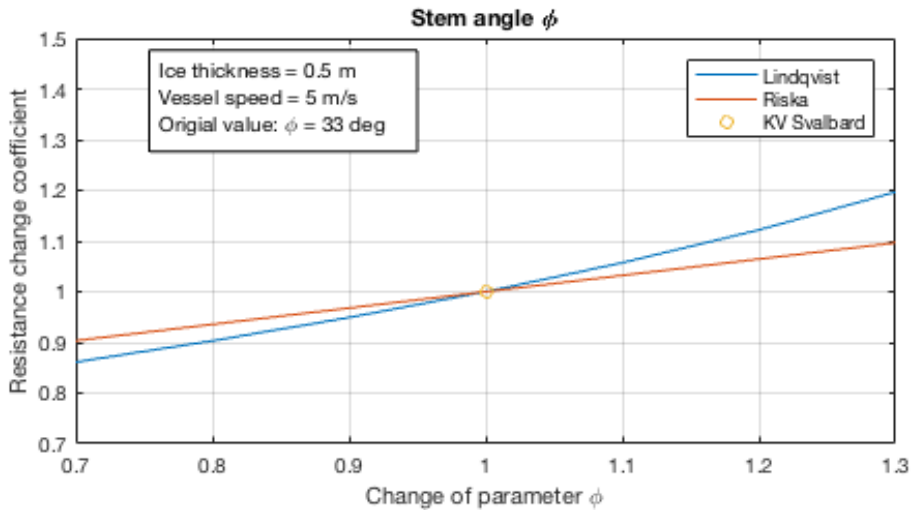

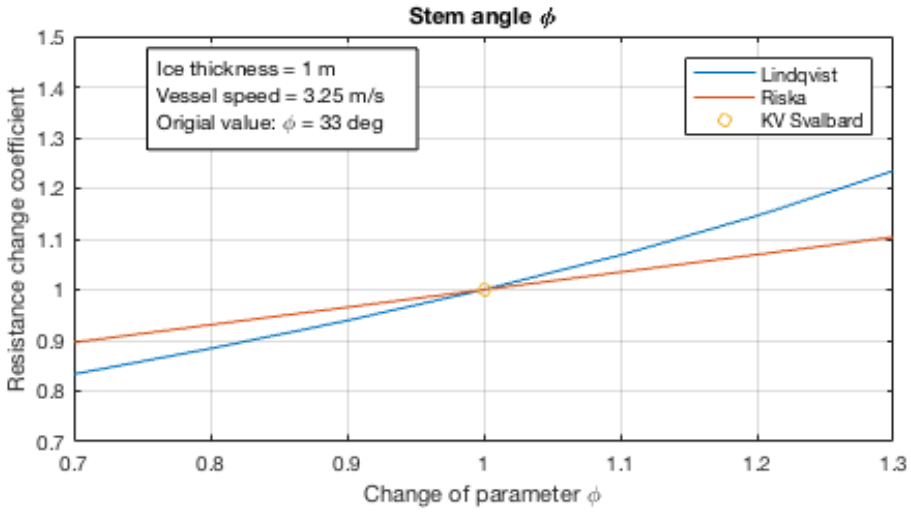
Stem angle ϕ
Ice thickness = 1 m
Vessel speed = 3.25 m/s
Origial value: ϕ = 33 deg
Lindqvist
Riska
KV Svalbard
Resistance change coefficient
Change of parameter ϕ
0.7
0.8
0.9
1
1.1
1.2
1.3
1.4
1.5

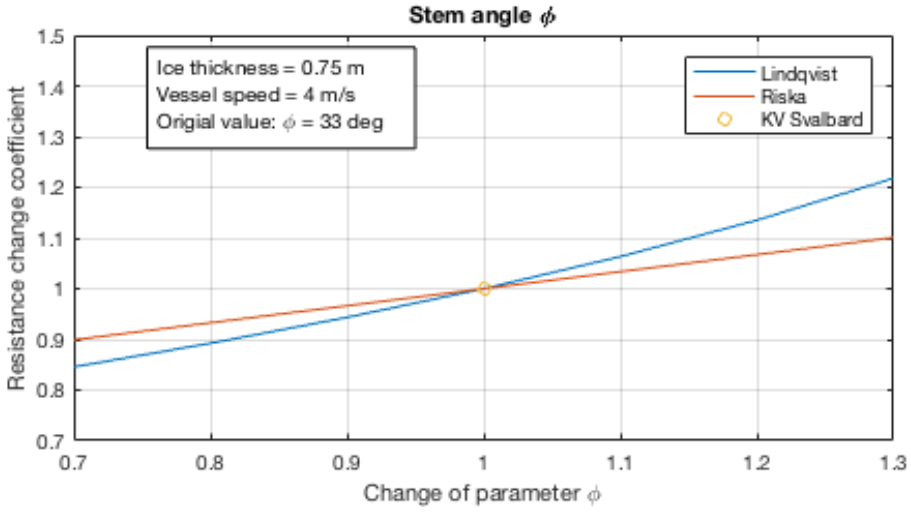
Stem angle ϕ
Ice thickness = 0.75 m
Vessel speed = 4 m/s
Origial value: ϕ = 33 deg
Lindqvist
Riska
KV Svalbard
Resistance change coefficient
Change of parameter ϕ
0.7
0.8
0.9
1
1.1
1.2
1.3
1.4
1.5

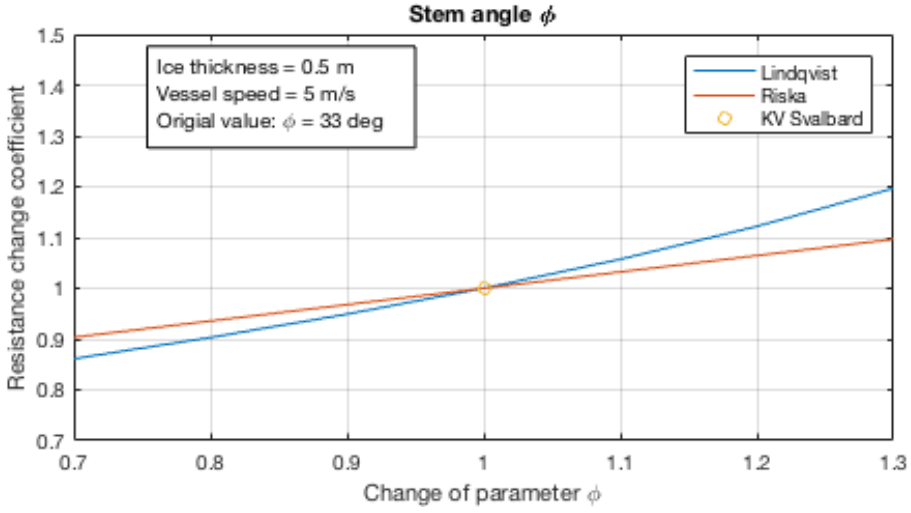
Stem angle ϕ
Ice thickness = 0.5 m
Vessel speed = 5 m/s
Origial value: ϕ = 33 deg
Lindqvist
Riska
KV Svalbard
Resistance change coefficient
Change of parameter ϕ
0.7
0.8
0.9
1
1.1
1.2
1.3
1.4
1.5

B.6 Flexural strength

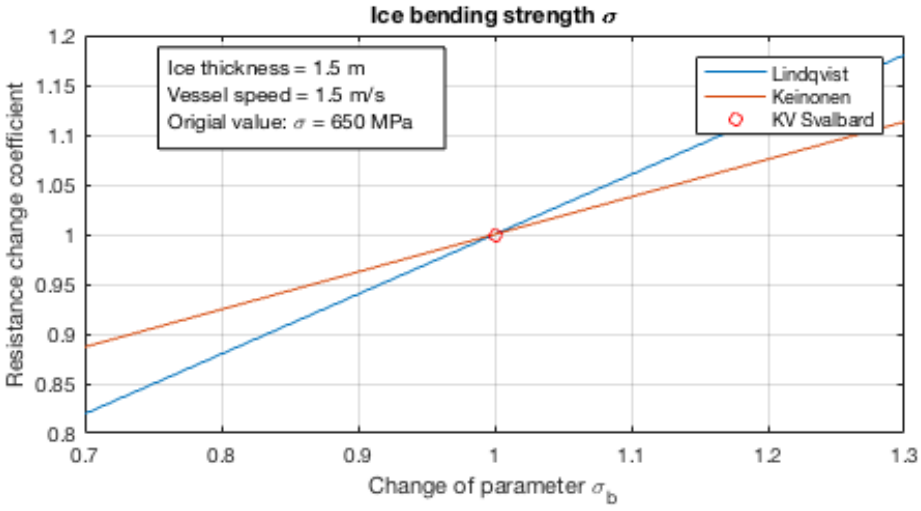

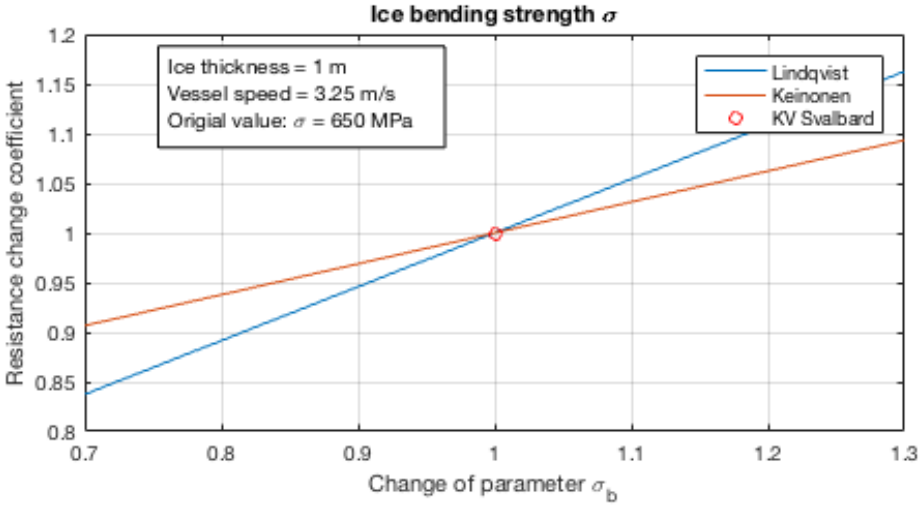

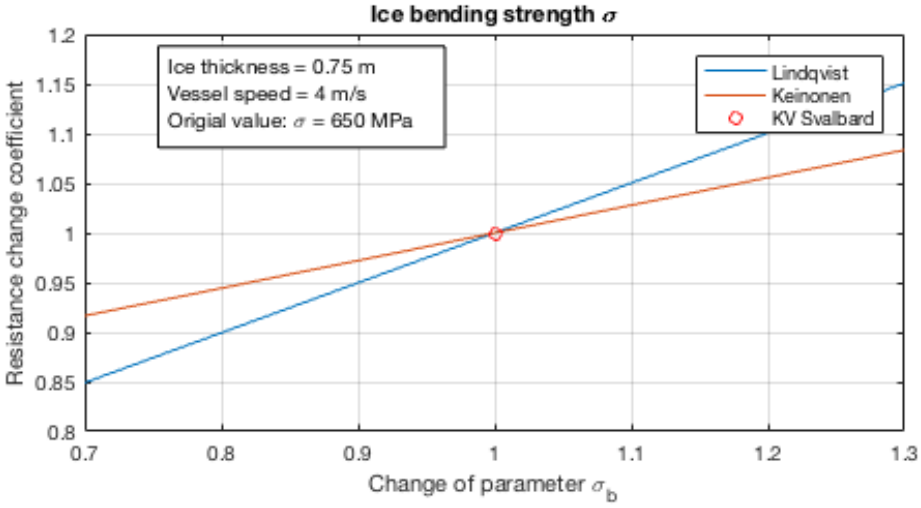

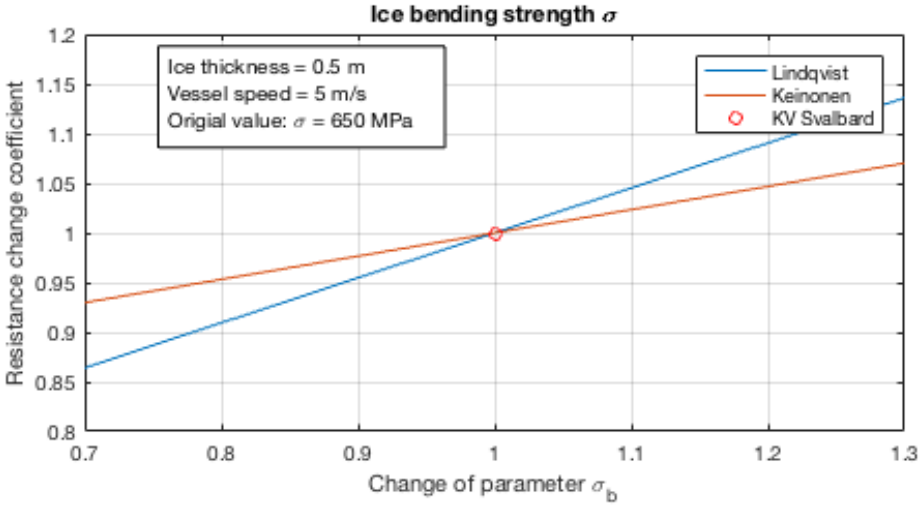

B.7 Hull-ice friction coefficient

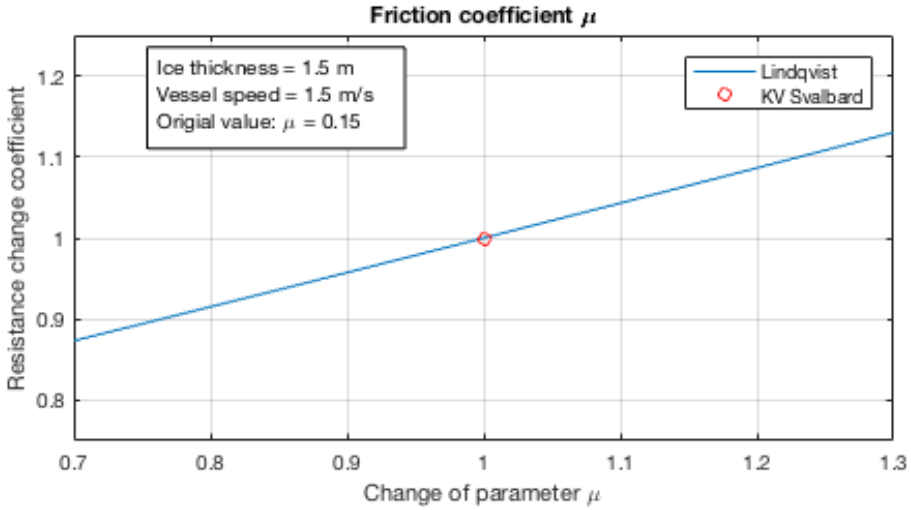

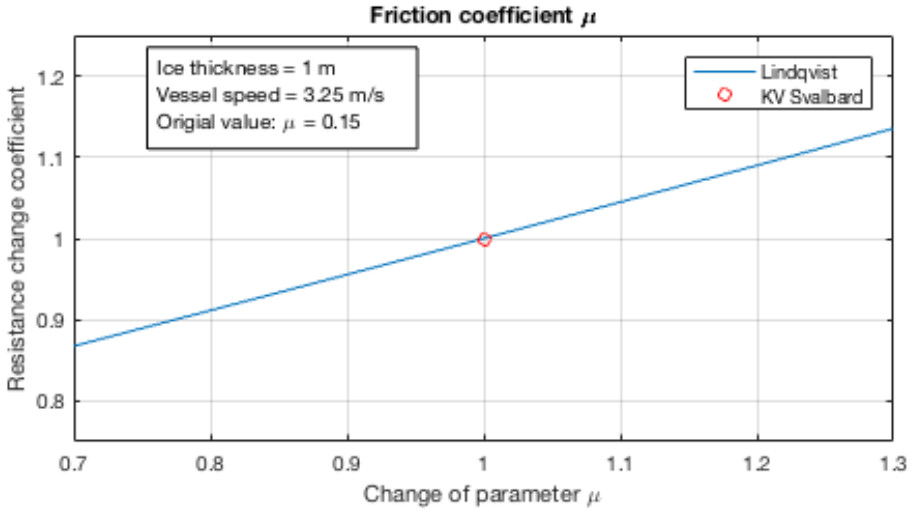

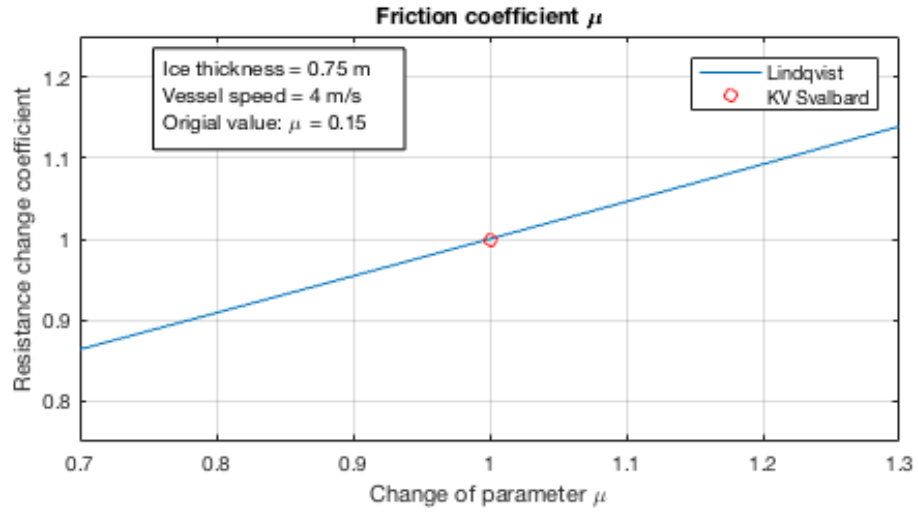

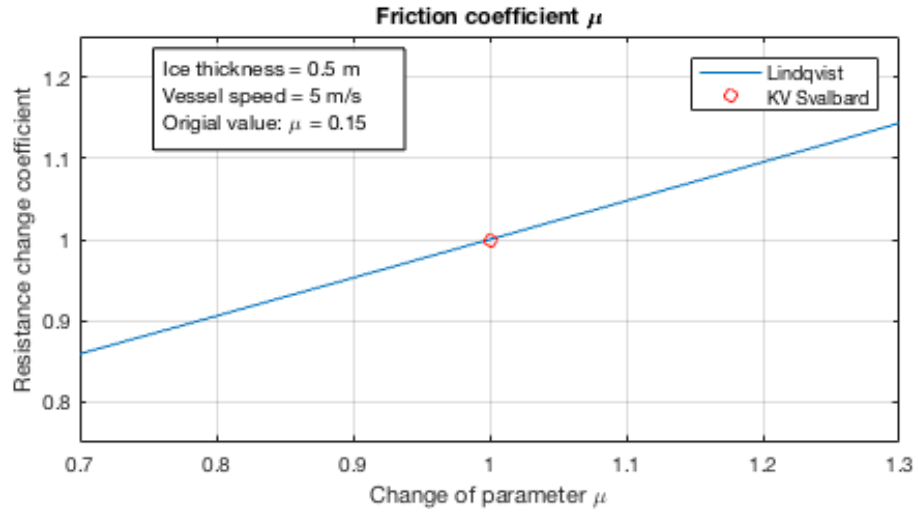

B.8 Temperature

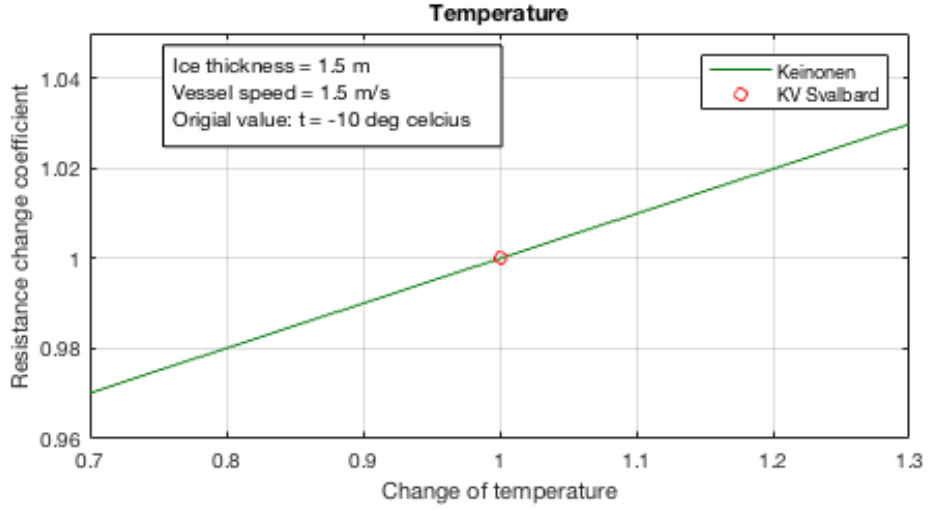

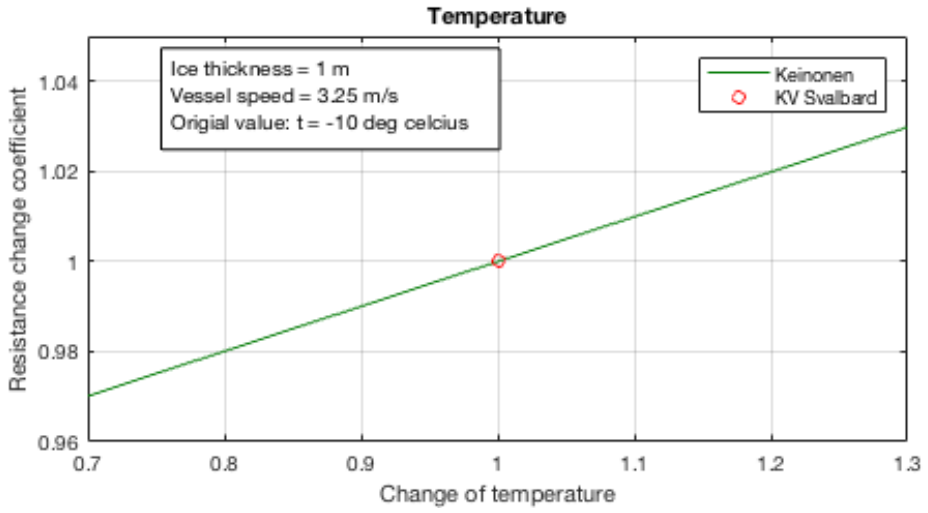
Temperature
Ice thickness = 1 m
Vessel speed = 3.25 m/s
Origial value: t = -10 deg celcius
Keinonen
KV Svalbard
Resistance change coefficient
1.04
1.02
1
0.98
0.96
0.7
0.8
0.9
1
1.1
1.2
1.3
Change of temperature

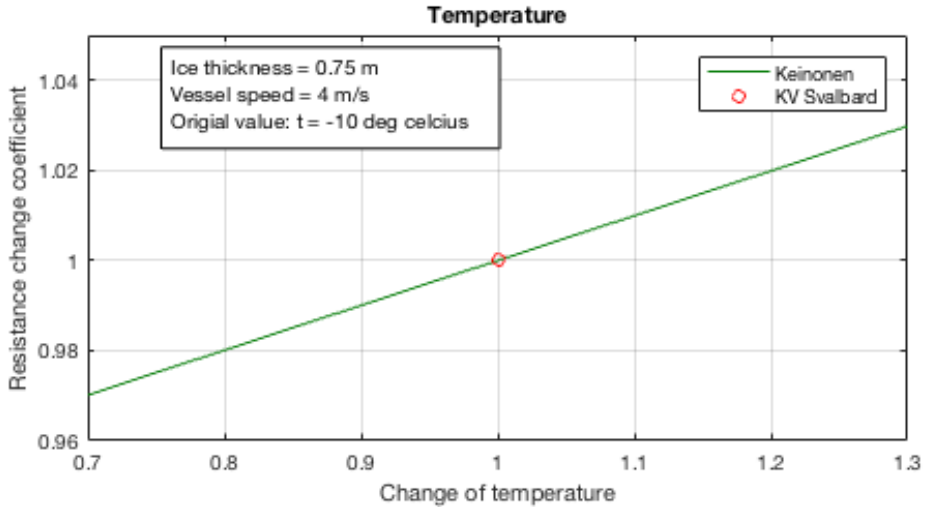
Temperature
Ice thickness = 0.75 m
Vessel speed = 4 m/s
Origial value: t = -10 deg celcius
Keinonen
KV Svalbard
Resistance change coefficient
1.04
1.02
1
0.98
0.96
0.7
0.8
0.9
1
1.1
1.2
1.3
Change of temperature

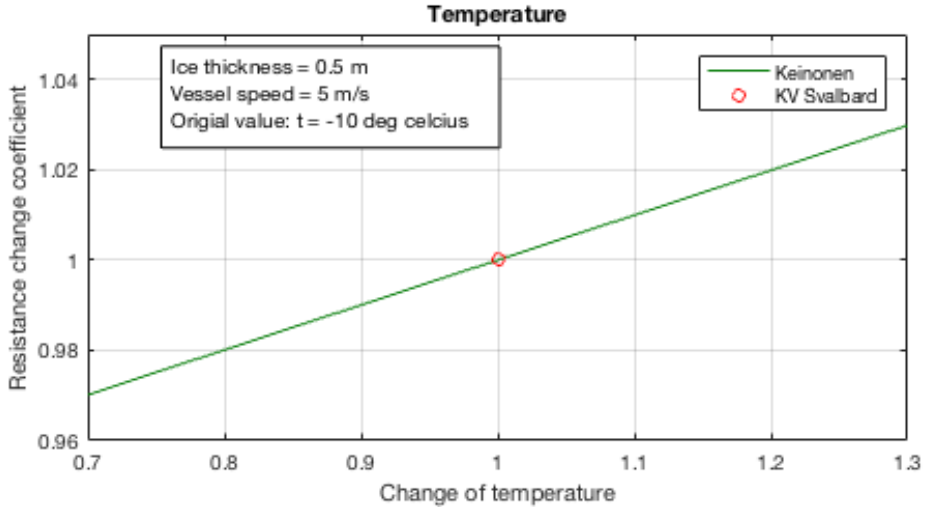
Temperature
Ice thickness = 0.5 m
Vessel speed = 5 m/s
Origial value: t = -10 deg celcius
Keinonen
KV Svalbard
Resistance change coefficient
1.04
1.02
1
0.98
0.96
0.7
0.8
0.9
1
1.1
1.2
1.3
Change of temperature

Appendix C

Ice resistance

C.1 Additional figures

This chapter contains additional figures for the surface ratios. All plots in this section has a propeller efficiency of 0.9.

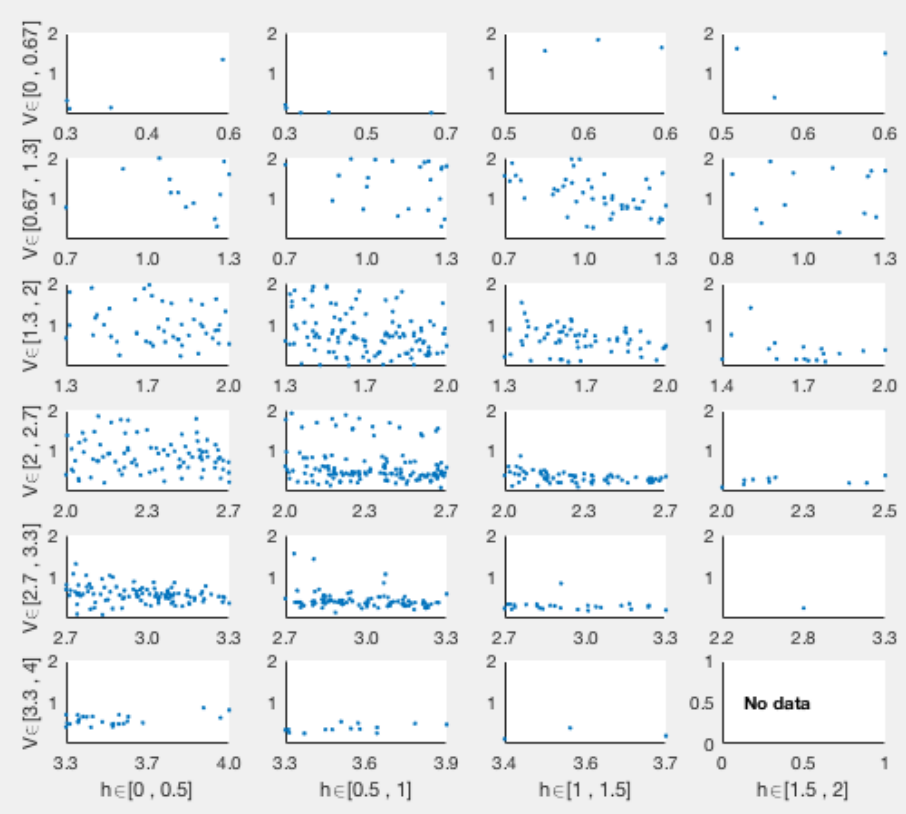

FIGURE C.1: Lindqvist vs measured resistance for varying vessel speed

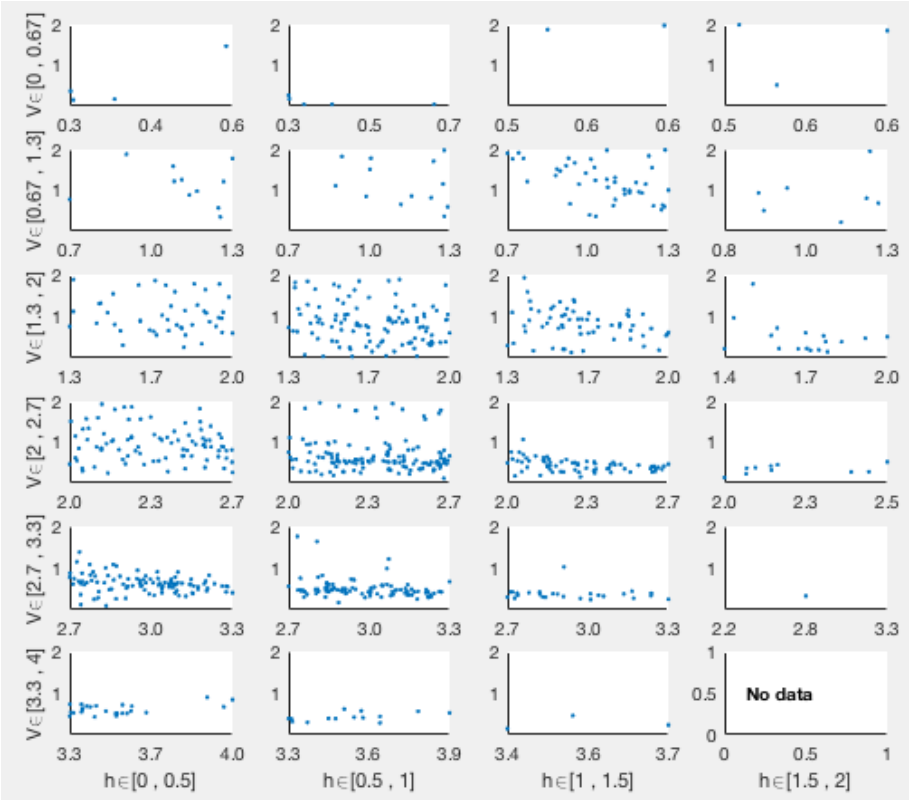

FIGURE C.2: Riska vs measured resistance for varying vessel speed

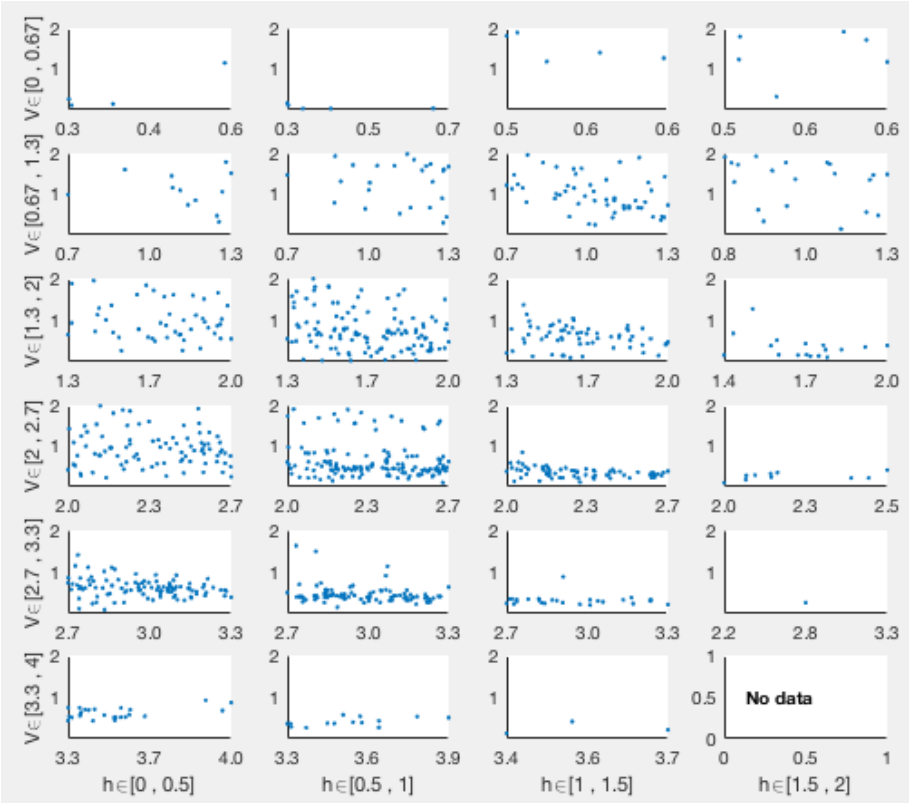

FIGURE C.3: Keinonen vs measured resistance for varying vessel speed

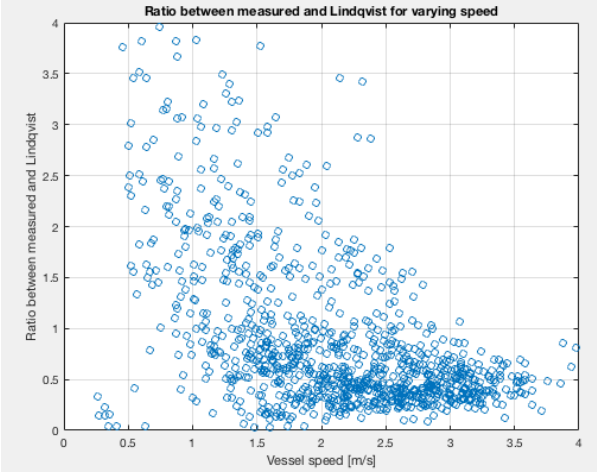

FIGURE C.4: Varying vessel speed

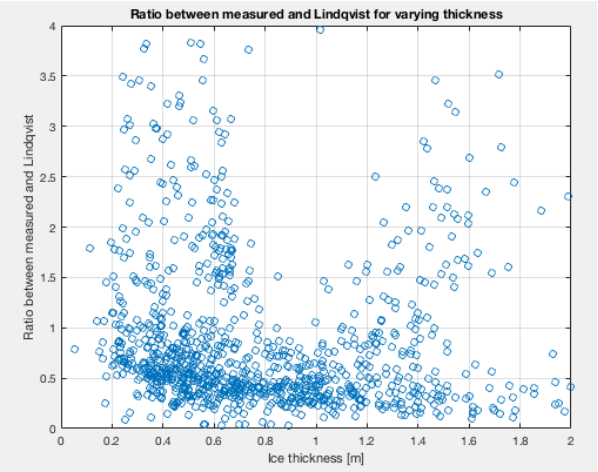

FIGURE C.5: Varying ice thickness

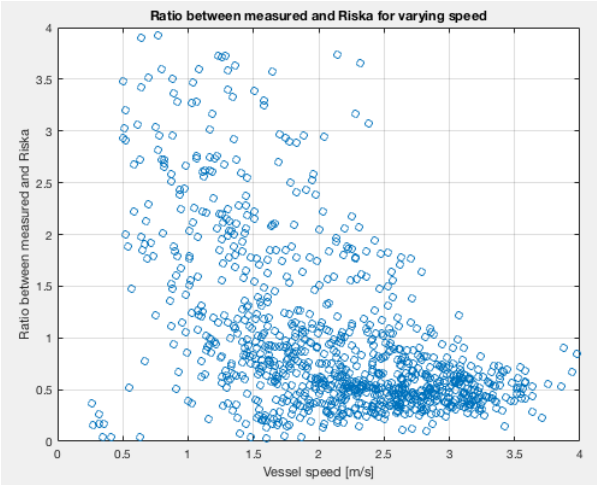

FIGURE C.6: Varying vessel speed

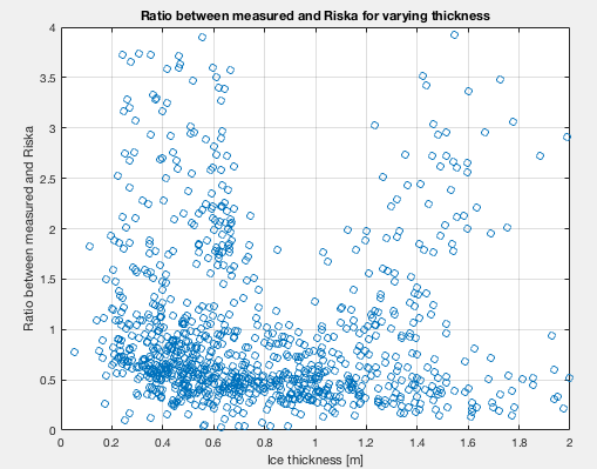

FIGURE C.7: Varying ice thickness

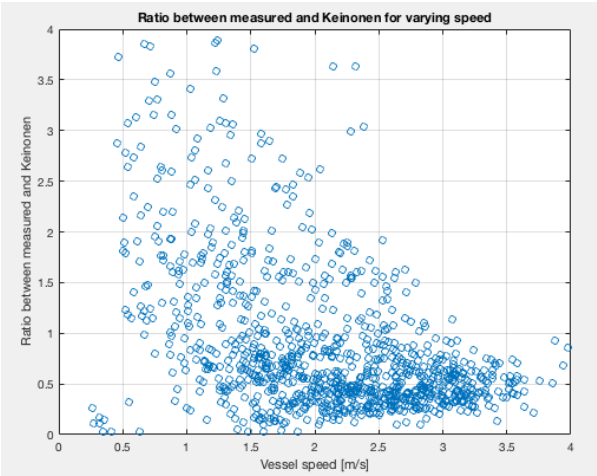

FIGURE C.8: Varying vessel speed

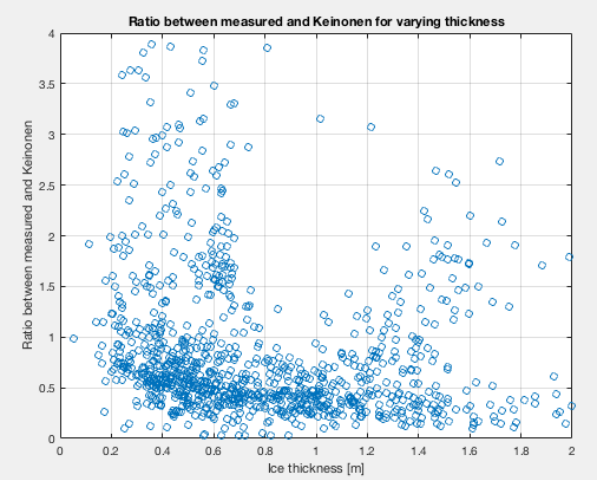

FIGURE C.9: Varying ice thickness

C.2 Data from Suyuthi

This section includes additional figures using higher quality data from Suyuthi. The following figures show different ratios for a varying ice thickness

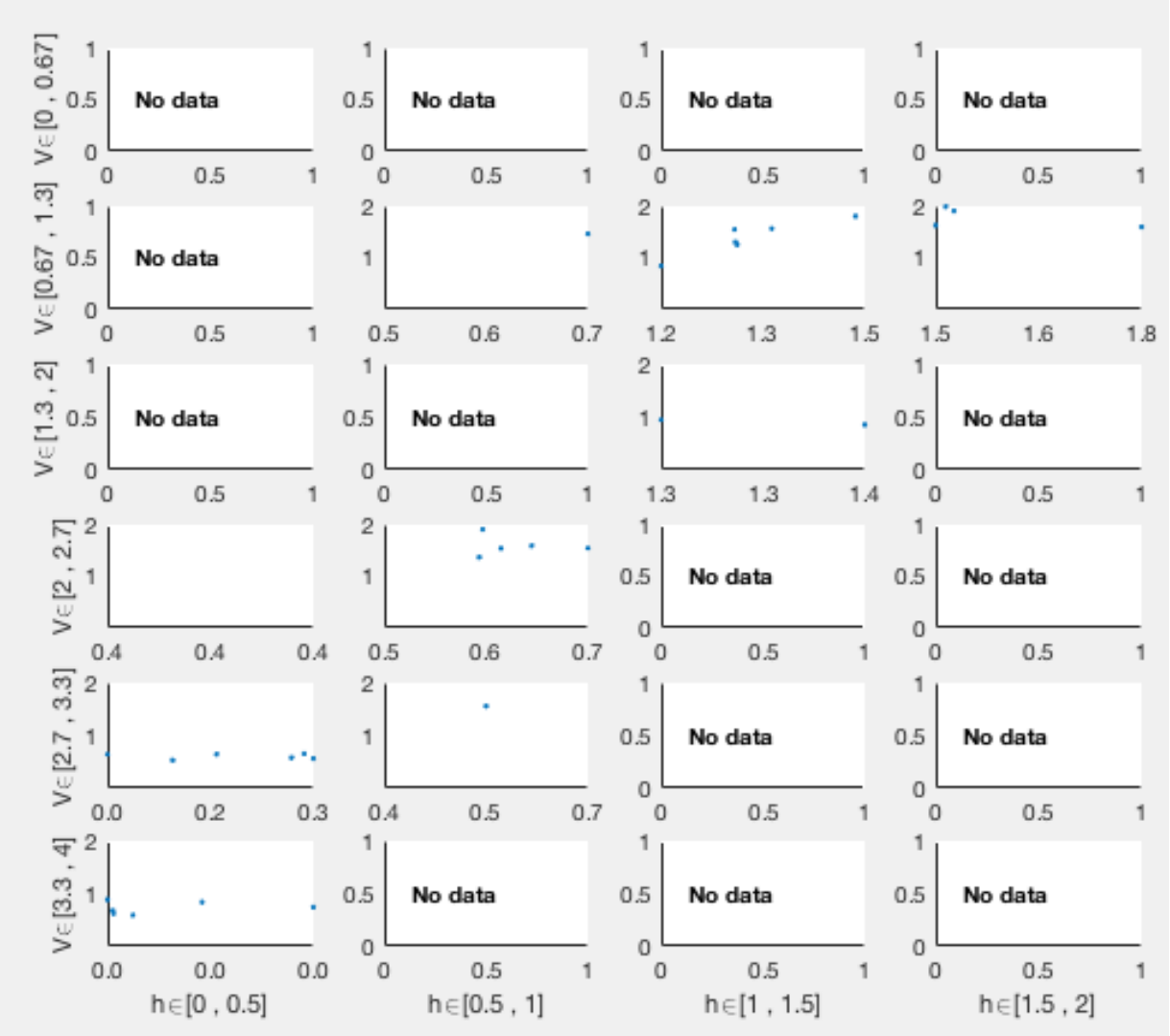

FIGURE C.10: default

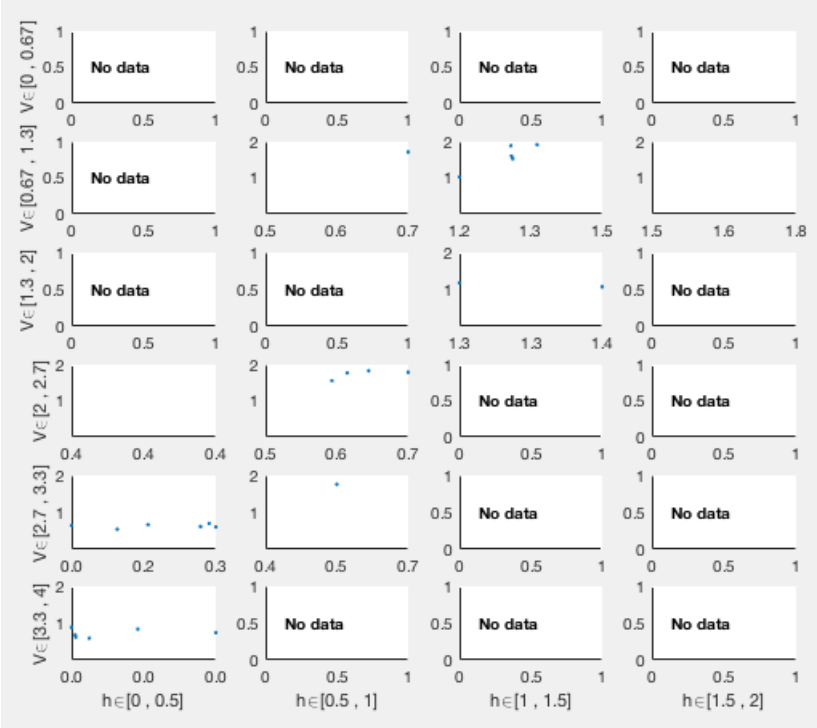

FIGURE C.11: default

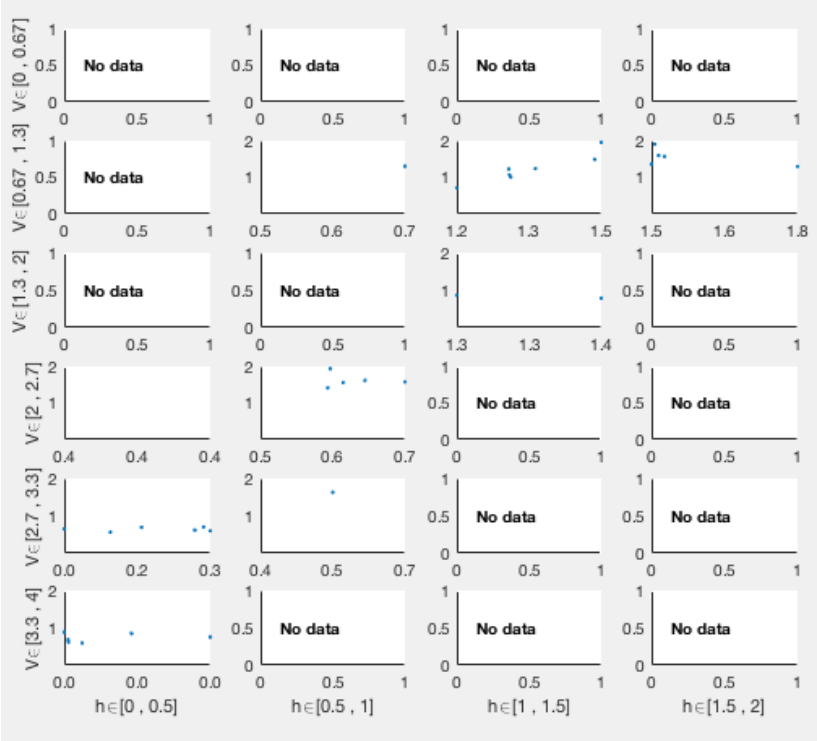

FIGURE C.12: default

C.3 100% propeller efficiency using data from Skaar

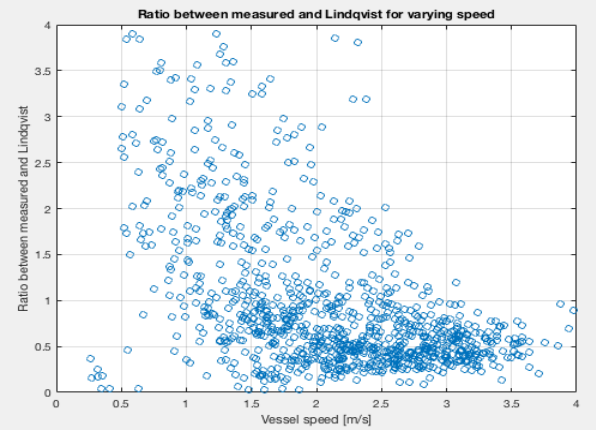

FIGURE C.13: Varying vessel speed

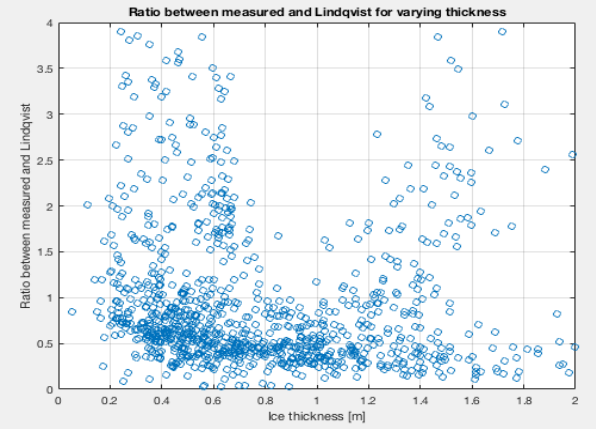

FIGURE C.14: Varying ice thickness

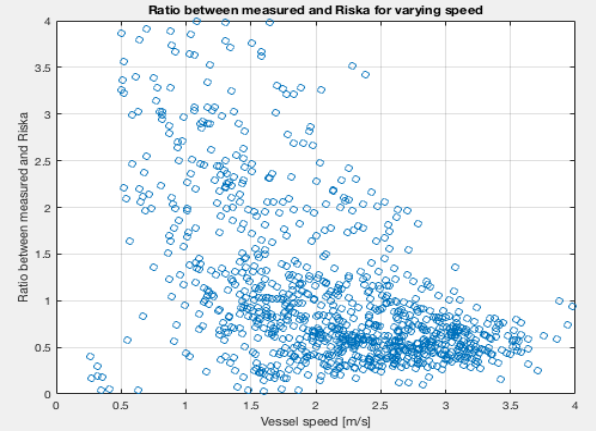

FIGURE C.15: Varying vessel speed

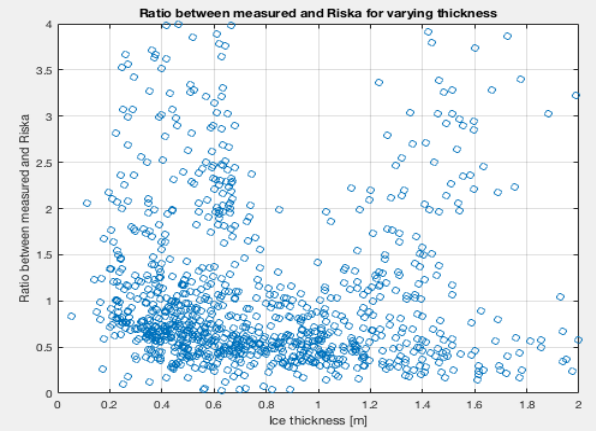

FIGURE C.16: Varying ice thickness

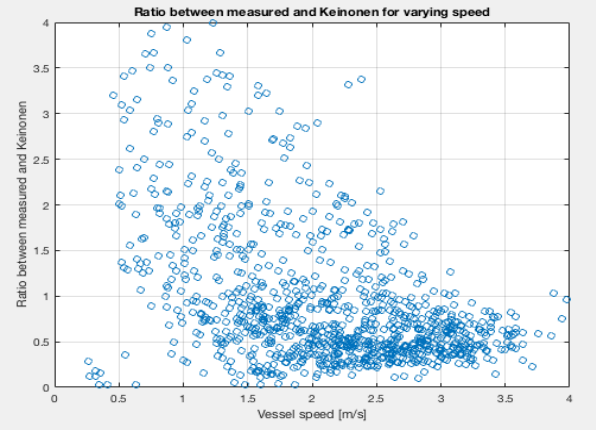

FIGURE C.17: Varying vessel speed

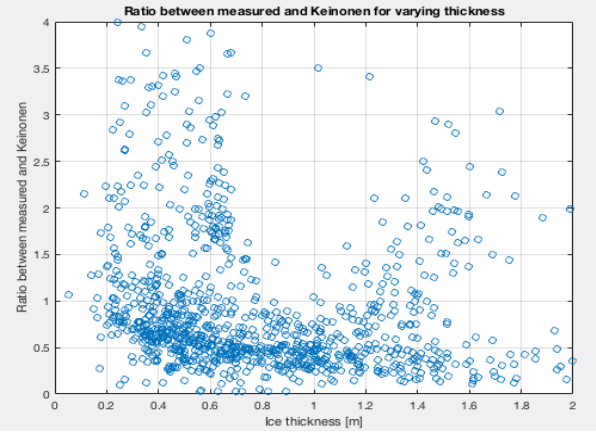

FIGURE C.18: Varying ice thickness

C.4 80% propeller efficiency using data from Skaar

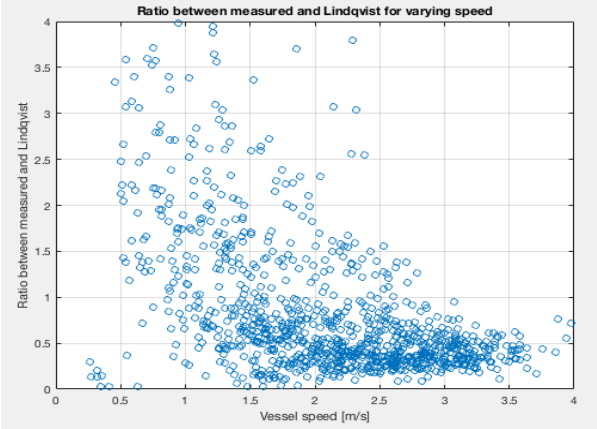

FIGURE C.19: Varying vessel speed

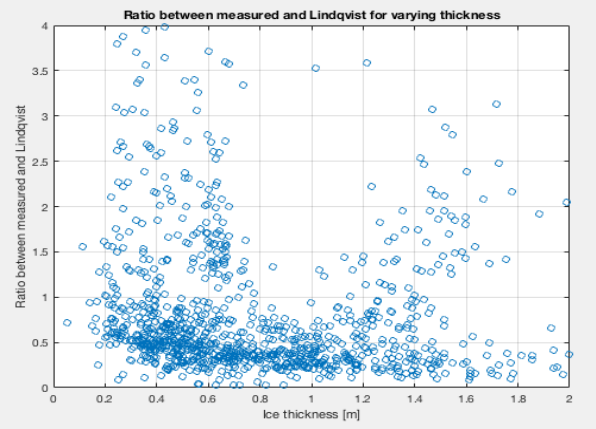

FIGURE C.20: Varying ice thickness

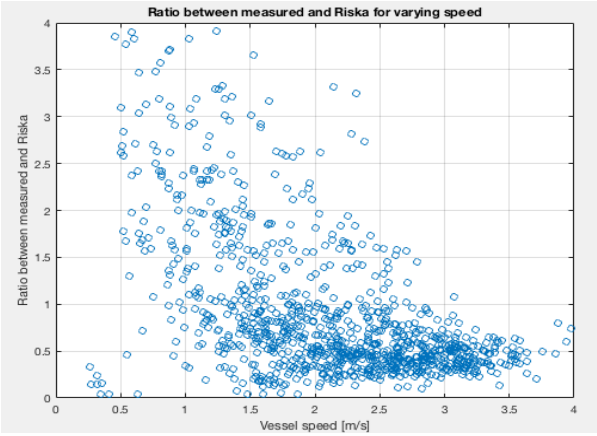

FIGURE C.21: Varying vessel speed

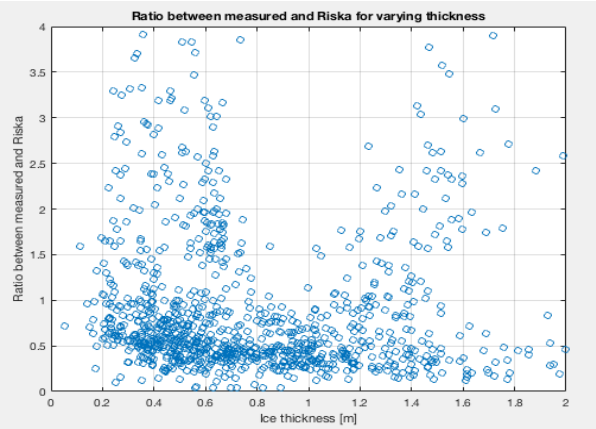

FIGURE C.22: Varying ice thickness

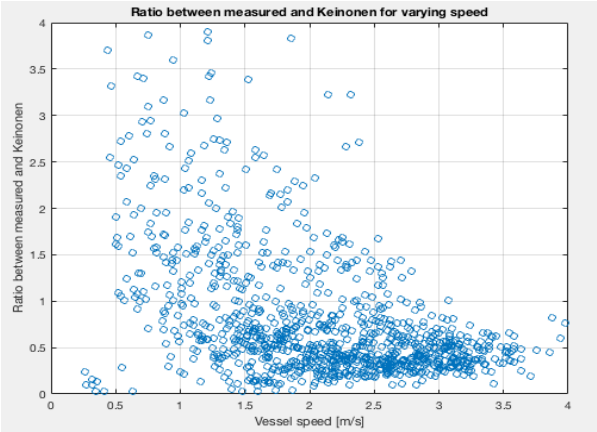

FIGURE C.23: Varying vessel speed

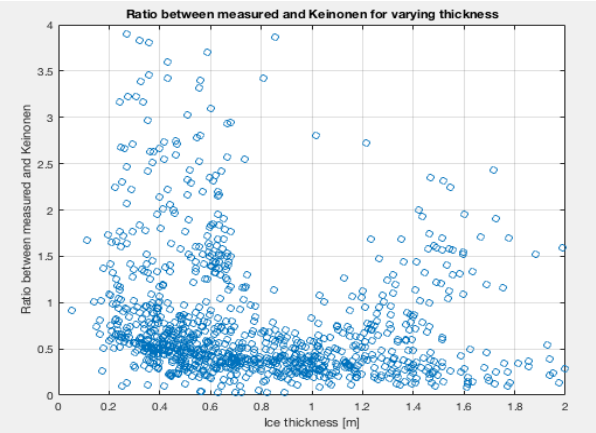

FIGURE C.24: Varying ice thickness

C.5 70% propeller efficiency using data from Skaar

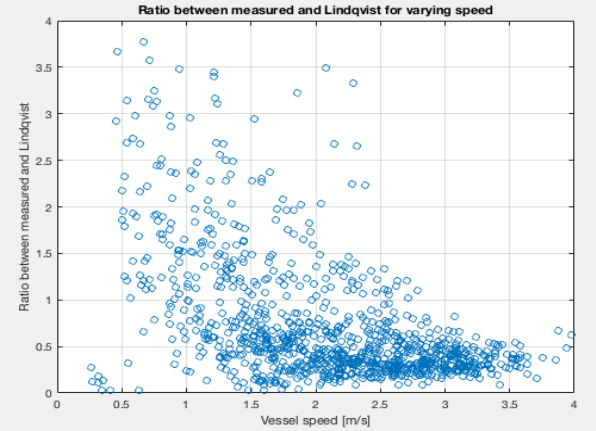

FIGURE C.25: Varying vessel speed

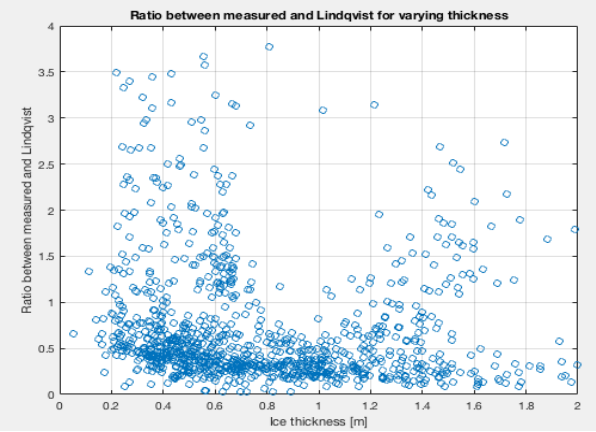

FIGURE C.26: Varying ice thickness

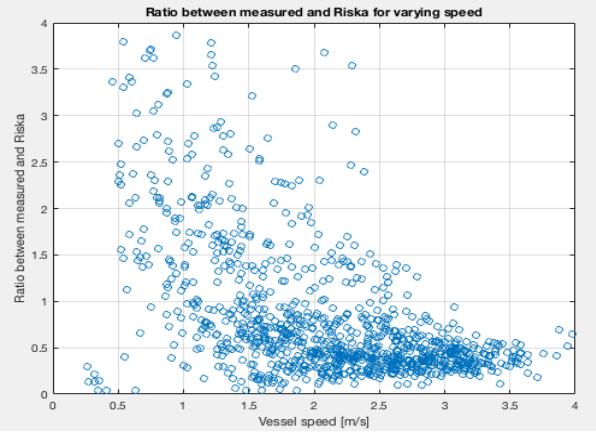

FIGURE C.27: Varying vessel speed

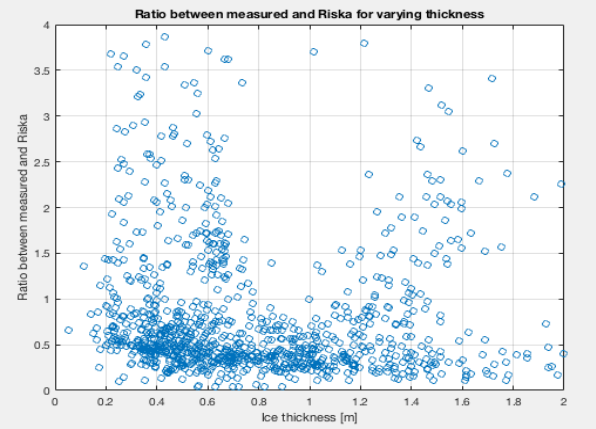

FIGURE C.28: Varying ice thickness

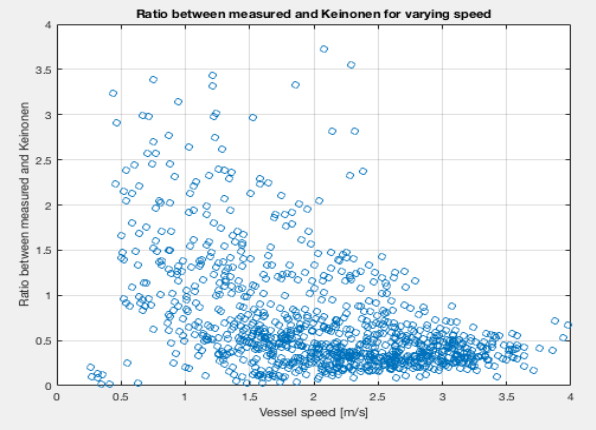

FIGURE C.29: Varying vessel speed

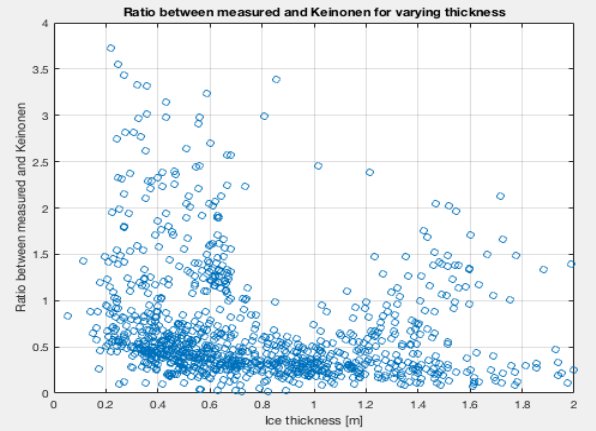

FIGURE C.30: Varying ice thickness

Appendix D

Finite Element Analysis

This chapter contains additional plots from the parameter study conducted in Chapter 15.

D.1 Original analysis

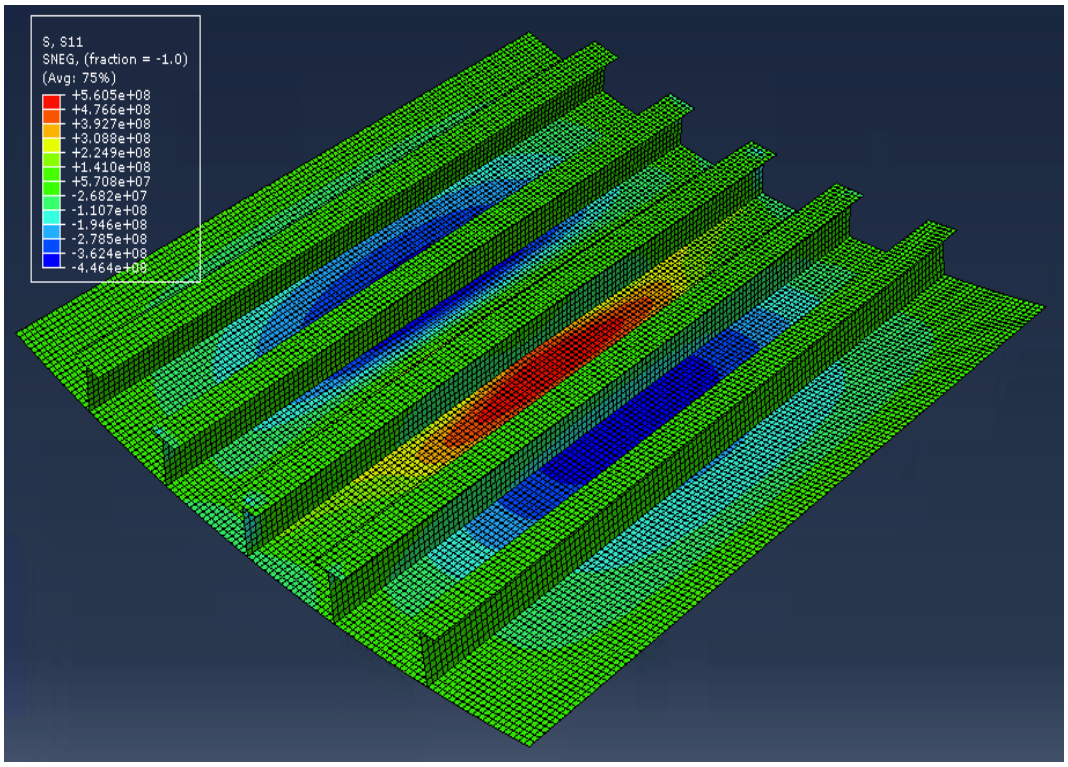

FIGURE D.1: Stresses in x-direction with ice pressure according to DNV GL regulations

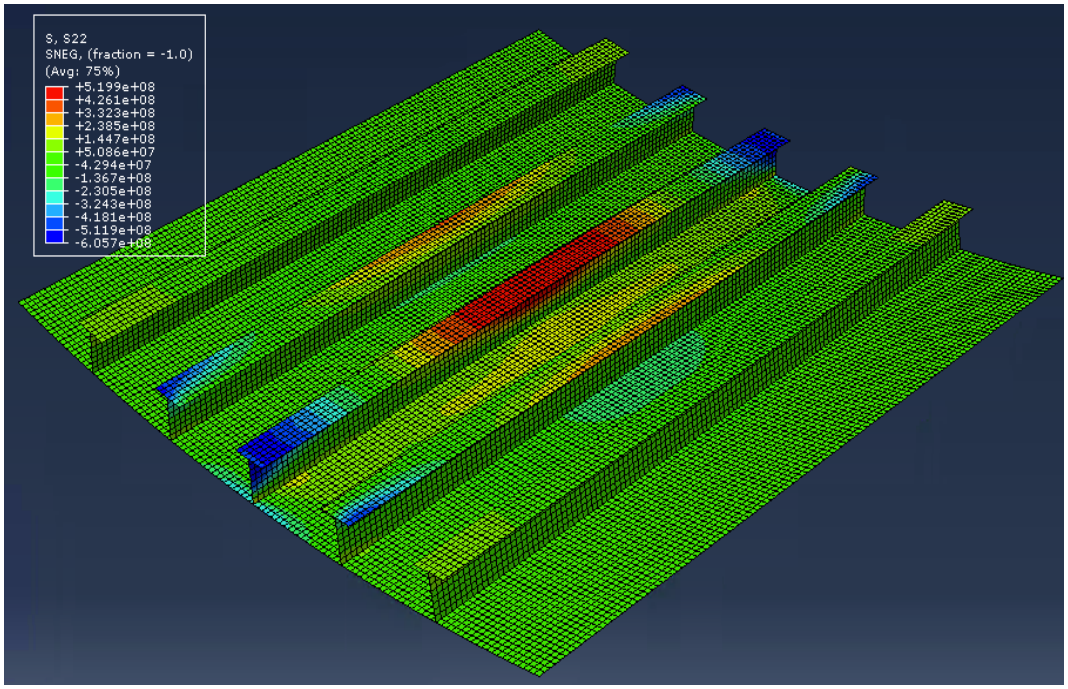

FIGURE D.2: Stresses in z-direction with ice pressure according to DNV GL regulations

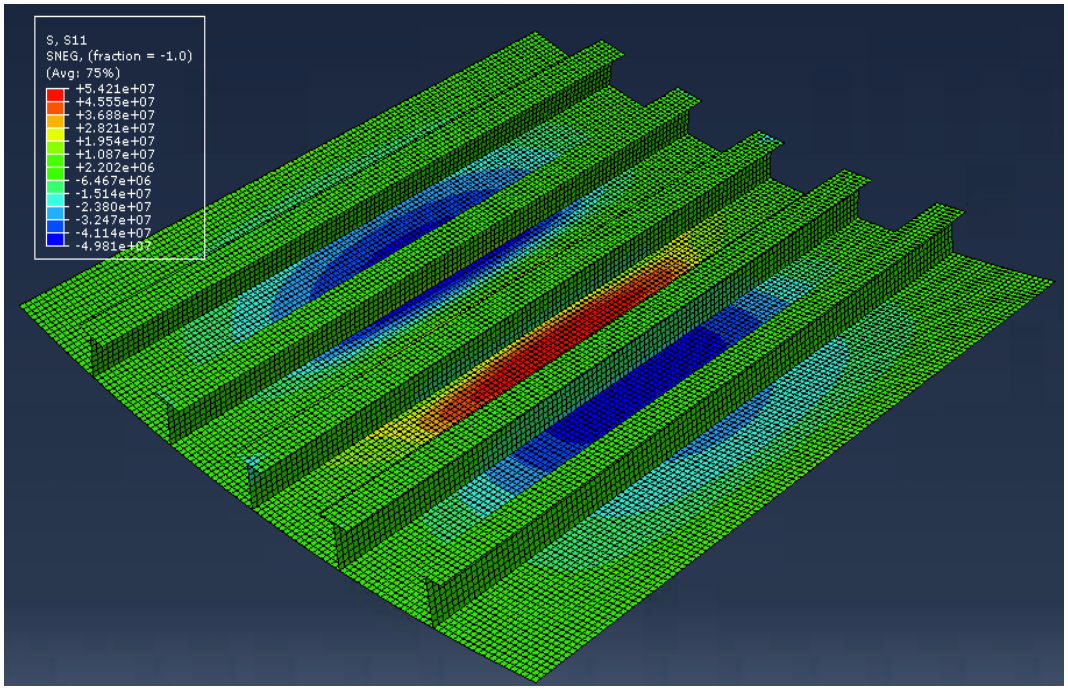

FIGURE D.3: Stresses in x-direction with ice pressure according to empiric calculations

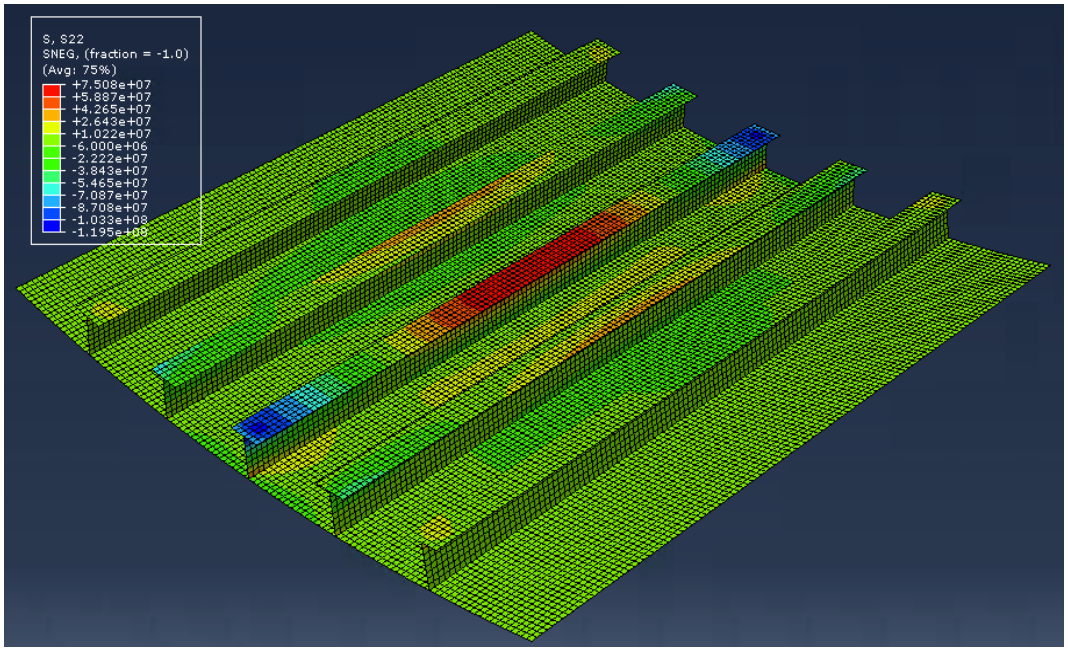

FIGURE D.4: Stresses in z-direction with ice pressure according to empiric calculations

D.2 Load patch area

The following plots shows plate response when using the empirically calculated ice pressure.

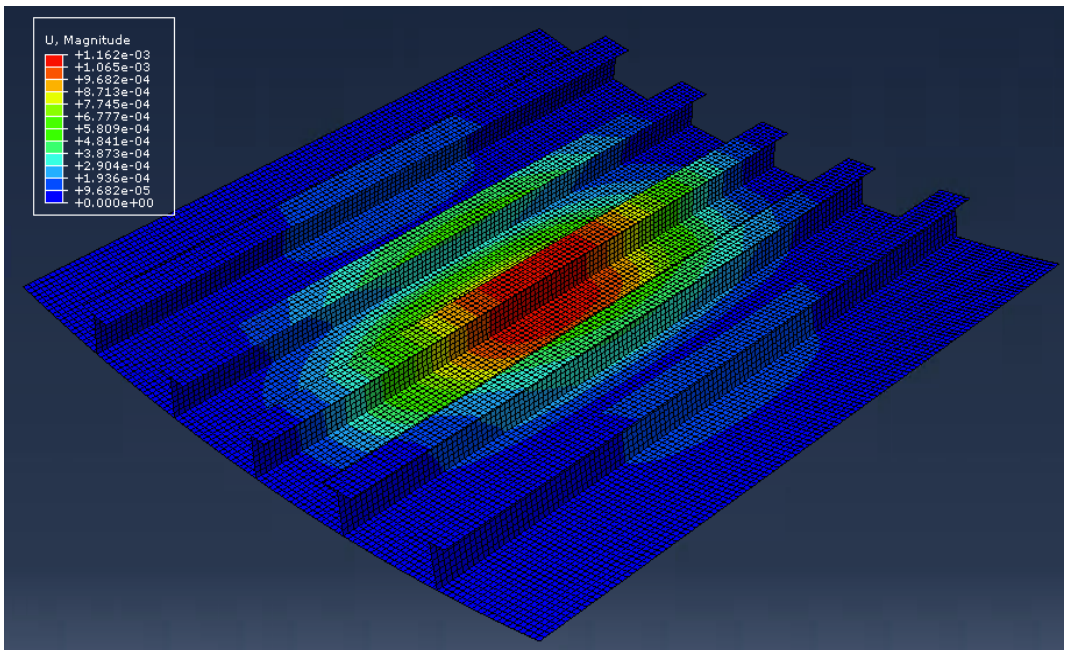

FIGURE D.5: Displacement for a contact area of 0.32 m^2

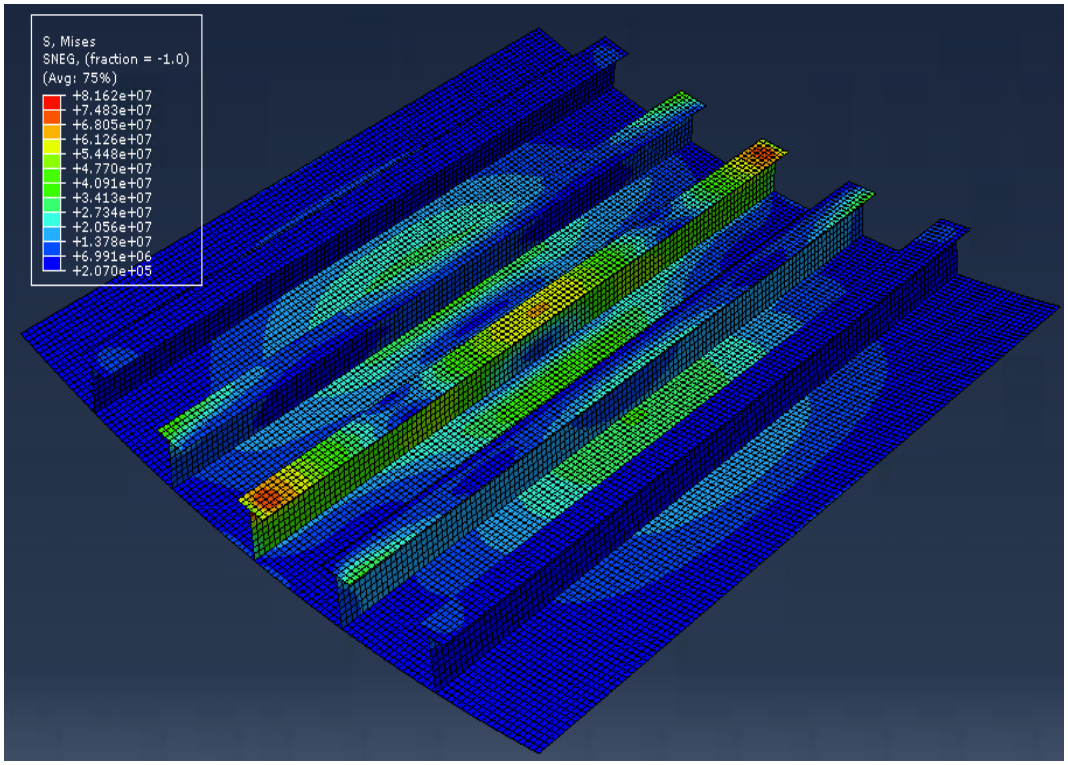

FIGURE D.6: Stresses for a contact area of 0.32 m^2

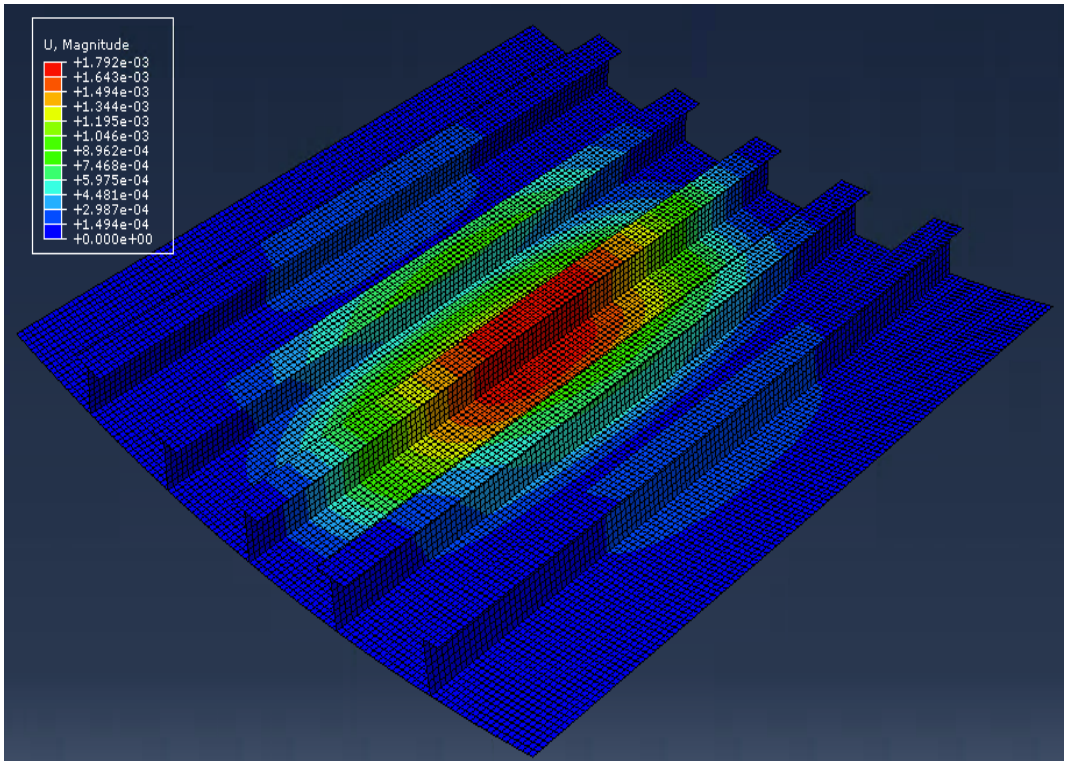

FIGURE D.7: Displacement for a contact area of 0.64 m^2

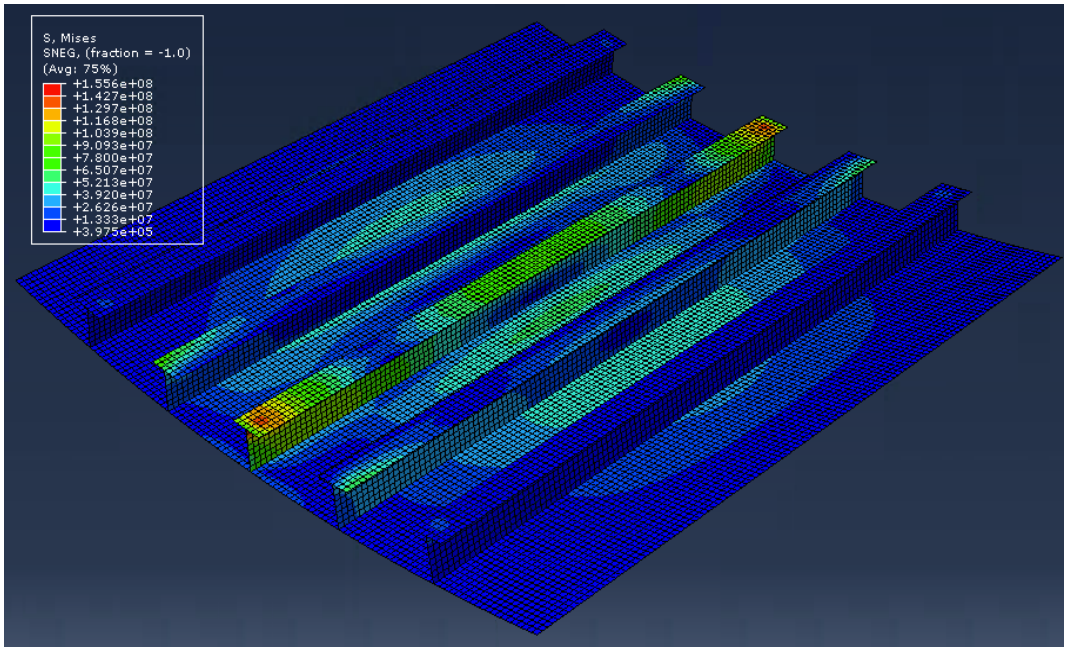

FIGURE D.8: Stresses for a contact area of 0.64 m^2

D.3 Stiffener dimensions

The following plots shows plate response when using the empirically calculated ice pressure.

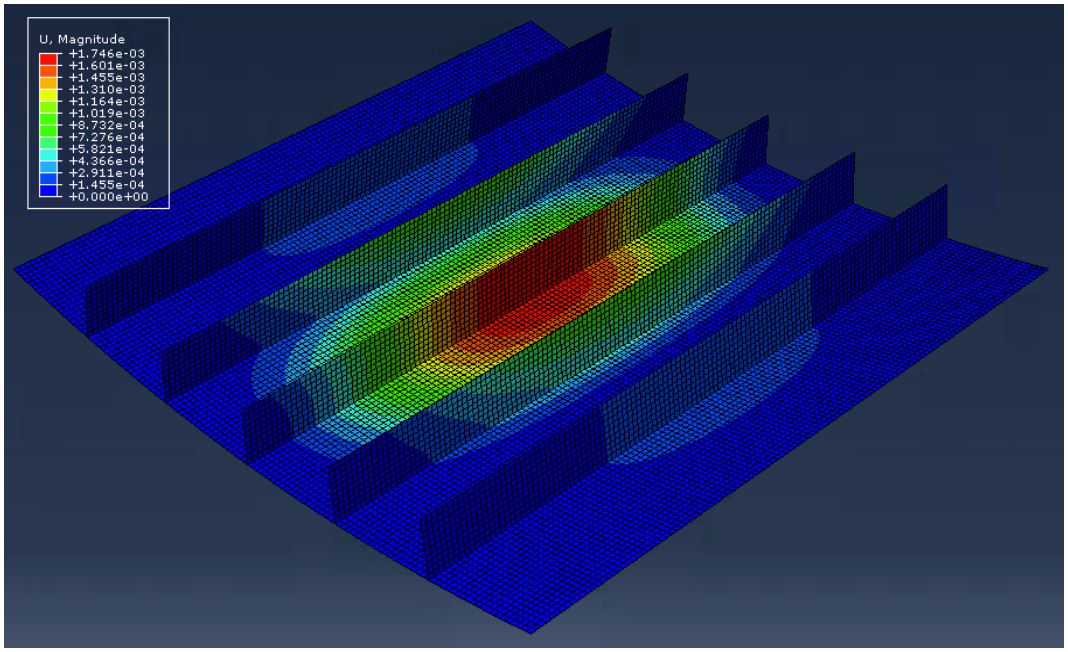

FIGURE D.9: Displacements without flanges

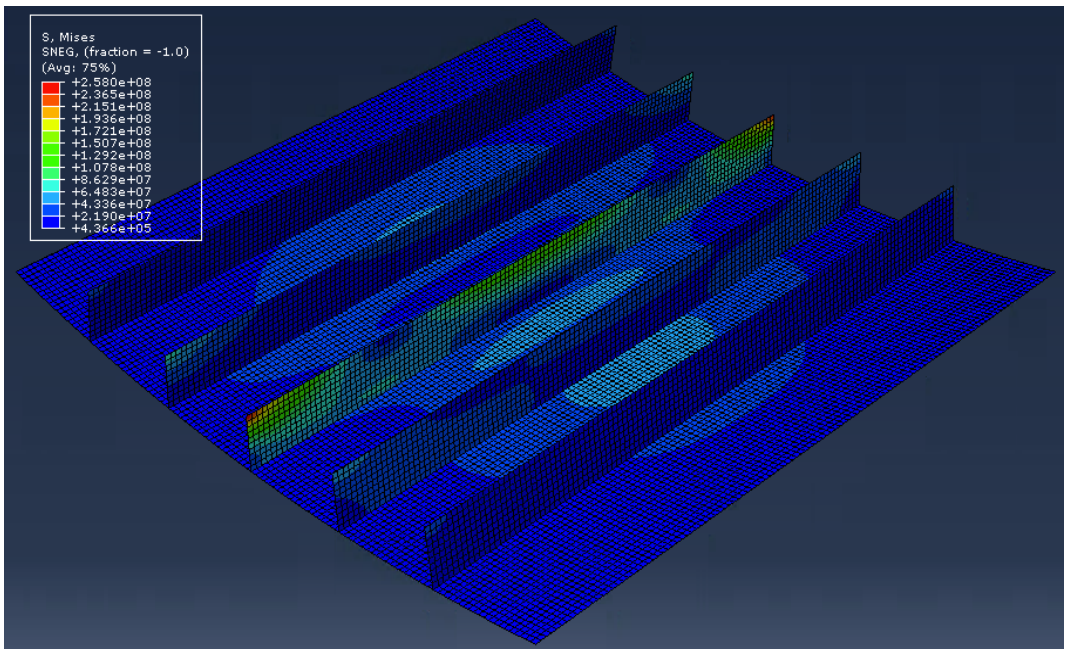

FIGURE D.10: Stresses without flanges

D.4 Stiffener spacing

The following plots shows plate response when using the empirically calculated ice pressure.

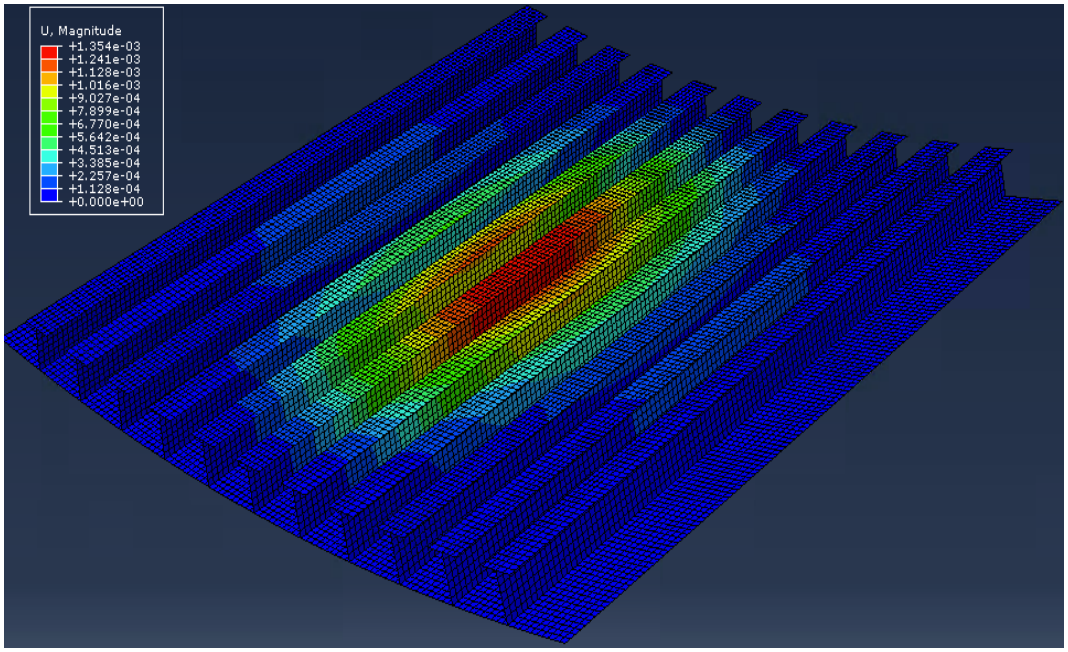

FIGURE D.11: Displacement for a stiffener spacing of 0.2 m

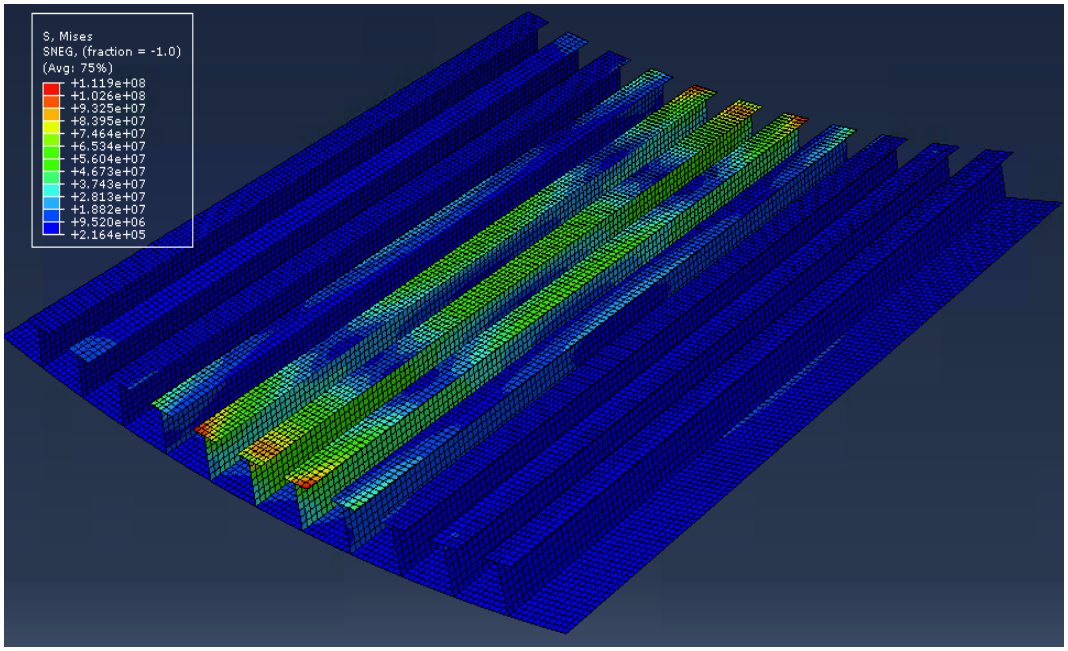

FIGURE D.12: Stresses for a stiffener spacing of 0.2 m

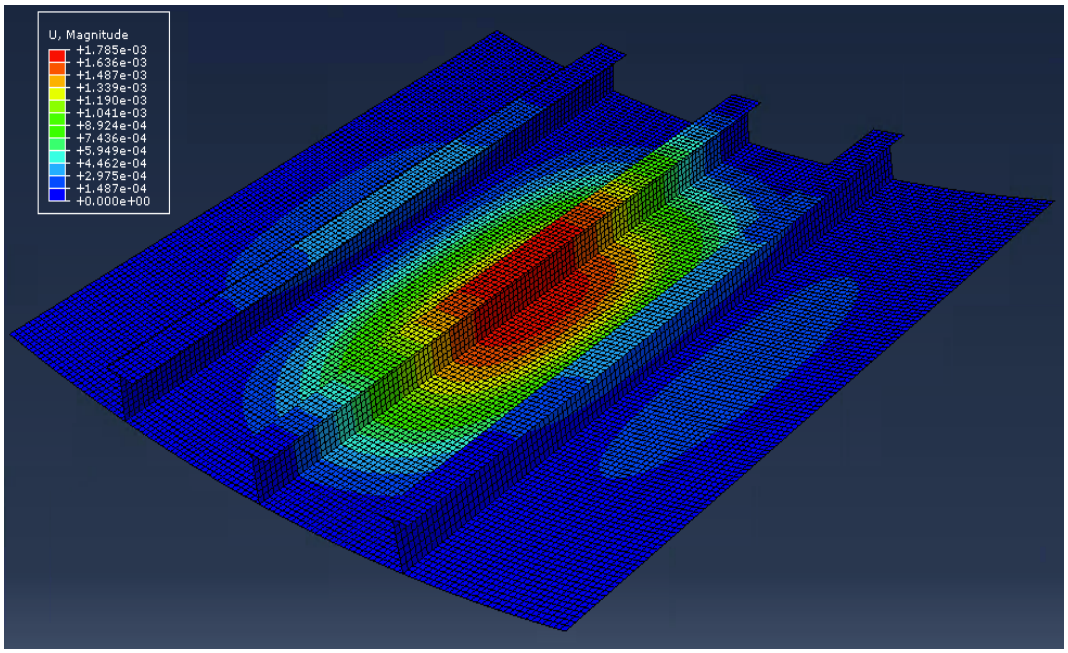

FIGURE D.13: Displacement for a stiffener spacing of 0.6 m

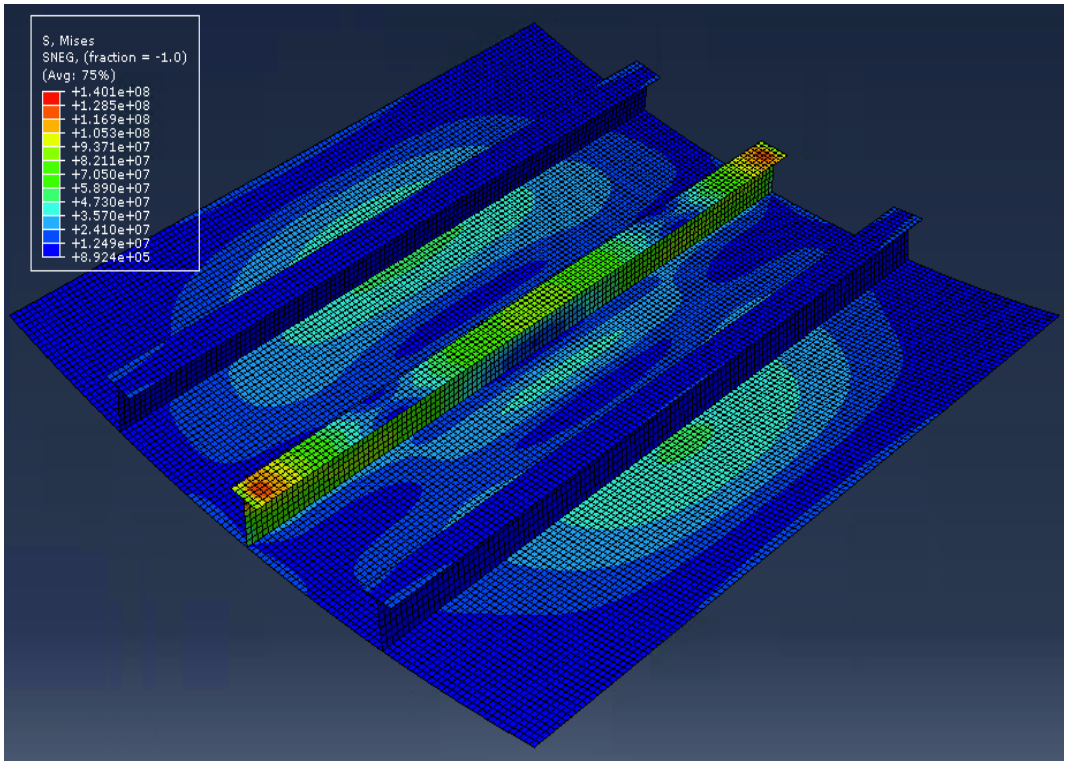

FIGURE D.14: Stresses for a stiffener spacing of 0.6 m